



**University of Kerbala
College of Science
Department of Chemistry**

Synthesis of Hybrid Organic-Inorganic Polyoxometalates-based Materials for Optoelectronic Applications

A Thesis

**Submitted to the Council of the College of Science/University of Kerbala in
Partial Fulfillment of Requirements for the Master Degree in Chemistry**

Written by

**Mariam Khaleel Jalil
B.Sc. in Chemistry (2017) /University of Kerbala**

Supervised by

**Prof. Dr.
Adnan Ibrahim Mohammed**

**Asst. Prof. Dr.
Ahmed Hadi Al Yasari**

2023 A.D

1445 H.D

بِسْمِ اللَّهِ الرَّحْمَنِ الرَّحِيمِ

يَرْفَعُ اللَّهُ الَّذِينَ آمَنُوا مِنْكُمْ وَالَّذِينَ أُوتُوا الْعِلْمَ دَرَجَاتٍ
وَاللَّهُ بِمَا تَعْمَلُونَ خَبِيرٌ

صدقَ اللهُ العَليُّ العَظِيمُ

سورة المجادلة : آية 11

Supervisor Certification

We certify that this thesis was prepared by “**Mariam Khaleel Jalil**” my Supervision at the Chemistry Department, College of Science, University of Kerbala, as a partial requirements for the master degree of science in chemistry.

Signature:



Name: **Dr. Adnan Ibrahim Mohammed**

Title: Professor

Address: University of Kerbala,

College of Science,

Department of Chemistry

Date:

(Member & Supervisor)

Signature:



Name: **Dr. Ahmed Hadi Al-Yasari**

Title: Assistant Professor

Address: University of Kerbala,

College of Science,

Department of Chemistry

Date:

(Member & Supervisor)

In view of the available recommendations by the Supervisor, I forward this thesis for debate by the examining committee

Signature:



Name: **Dr. Luma M. Ahmed**

Title: Professor

Head of Chemistry Department, College
of Science

Date:

Examination Committee Certification

We certify that we have read this thesis entitled “**Synthesis of Hybrid Organic-Inorganic Polyoxometalates-based Materials for Optoelectronic Applications**” As the examining committee, examined the student “**Mariam Khaleel Jalil**” on its contents, and that in our opinion, it is adequate for the partial fulfillment of the requirements for the master degree of science in chemistry.

Signature:

Name: **Dr. Rahman Tama Haiwal**

Title: Professor

Address: University of Kerbala, College of Science,
Department of Chemistry

Date:

(Chairman)

Signature:

Name: **Dr. liqaa Hussein Khadium**

Title: Professor

Address: University of Kufa, College of
education for Girls, Department of Chemistry

Date:

(Member)

Signature:

Name: **Dr. Ola Mahdi Abd Ali**

Title: Assistant Professor

Address: University of Kerbala, College of
Education for Pure Science, Department of
Chemistry

Date:

(Member)

Signature:

Name: **Dr. Adnan Ibrahim Mohammed**

Title: Professor

Address: University of Kerbala, College of
Science, Department of Chemistry

Date:

(Member & Supervisor)

Signature:

Name: **Dr. Ahmed Hadi Al Yasari**

Title: Assistant Professor

Address: University of Kerbala, College of Science,
Department of Chemistry

Date:

(Member & Supervisor)

Approved by the council of the College of Science

Signature:

Name: **Dr. Hassan Jameel Jawad Al-Fatlawy**

Title: Professor

Address: Dean of College of Science, University of Kerbala

Date:

Dedication To
Fatima al-Zahra, her father, her
husband and her sons, peace be
upon them

Acknowledgments

I thank God very much for his success and for helping me complete my thesis.

I also offer the highest verses of thanks and gratitude to **Prof. Dr. Adnan I. Mohammed** who kindly accepted the supervision of my master's thesis, and **Asst. Prof. Dr. Ahmed Hadi Al Yasari**, who gave me his precious time and see of information and his extensive experience constituted a great addition to the research work. So his guidance and advice were the beacon that I used in him throughout my research work. I ask God Almighty to reward him with the best reward.

My beloved father, my dear mother, my husband, and my companion I cannot forget your support of me and what you have given me. You have all my love, and no matter how many words of gratitude I say to you, I will never give you what you deserve.

I also extend my sincere thanks to the faculty members and colleagues who helped me at University of Kerbala, College of Science, and Department of Chemistry.

I would also like to thank all members of the examining committee for accepting to discuss my master's thesis.

Abstract

In this work, a series of new organic-inorganic polyoxometalates-based (POMs) hybrid dyes were designed and synthesized as donor- π bridge-acceptor systems where it can be used as a sensitizer/or co-sensitizers in Dyes Sensitized Solar Cells (DSSCs). Initially, we have theoretically, by using a combination of density functional theory (DFT) and time-dependent density functional theory (TDDFT) calculations, and systematically studied new chromophores in which hexamolybdate Lindqvist-type derivatives electron acceptors are connected via phenylimido groups to organic electron donors such as **acrdine-imido-hexamolybdate (1)**, **acrdine-9-phynylactylene-imido-hexamolybdate (2)**, **aminoanthracene-imido-hexamolybdate (3)**, **2-amino-3-carboxylanthracene-imido-hexamolybdate (4)**, **anthracene-imido-hexamolybdate (5)**, **anthraquinone-imido-Hexamolybdate (6)**, **aminoanthraquinone-imido-hexamolybdate (7)**, **bromophenyl-imido-hexamolybdate (8)**. The energy levels of frontier molecular orbitals, absorption spectra with electronic transition characters, and photovoltaic parameters of dyes **1-4** were systematically evaluated. It is found that the HOMO energy levels of dyes **1-4** are more negative than the redox of I/I_3^- and the LUMO energy levels are higher than the conduction band of TiO_2 , suggesting that these dyes to match the requirements of n-type DSSCs. The HOMO levels decrease in the order **4 > 3 > 2 > 1**, and the LUMO levels also decrease in the order **4 > 3 > 2 > 1**. Based on TD-DFT calculations, all systems **1-4** have absorption bands in visible region ranges from 420 to ~494 nm, with relatively high oscillator strengths despite system **4**, where **1** (POM-acridine system) has the largest maximum absorption wavelength λ_{max} of 494 nm with $f_{os} = 0.8657$ and $\Delta r = 3.66 \text{ \AA}$. These results confirm the suitability of all the studied dyes for n-type DSSCs. The investigated dyes could be introduced as an active co-absorbent as well as main dye.

All dyes showed remarkable reorganization energy for electron transport (λ_e) and hence increased electron transfer rate. Due to the strong absorption in the visible region, as well as high light harvesting efficiency (LHE), dye regeneration efficiency (DRE), and electron injection efficiency (Φ_{inj}), dyes **2** and **3** are the most promising candidates for high performance DSSC materials.

The promising DFT results have motivated us to explore the experimental synthesis of these dyes using DCC coupling protocol. Dyes **1,5,6,7** and **8** were characterized by FTIR, ^1H NMR, and UV-Vis. The computed absorption spectrum for **1** is in a good agreement with the preliminary experimental results. Interestingly, introducing π -linker in dye **2** is blue shifted by 54 nm in λ_{max} and an increase in f_{os} by a factor of ≈ 2.1 and Δr by a factor of ~ 2 compared to dye **1**.

Table of Contents

NO.	Subject	Page
	Acknowledgments	I
	Abstract	II
	List of Contents	IV
	List of Tables	VI
	List of Figures	VII
	List of Schemes	IX
	List of Equations	IX
	List of Abbreviations	IX
Chapter One		
Introduction		
1.1	Organic Photonics	1
1.2	Optoelectronic Materials	1
1.2.1	Organic Optoelectronic Materials	2
1.3	Hybrid Organic-Inorganic Materials	4
1.3.1	Advantage of Hybrid Organic-Inorganic Materials	6
1.4	Historical background of the Solar Cells	7
1.4.1	Dye Sensitized Solar Cells (DSSCs)	8
1.4.1.1	Components in DSSCs	9
1.4.1.2	Type of DSSCs	10

1.4.1.2.1	p-type DSSCs	10
1.4.1.2.2	n-type DSSCs	11
1.5	Design and Functioning of Chromophores	11
1.6	Polyoxometalates (POMs)	14
1.6.1	Structure and Types for POMs	17
1.6.1.1	Lindqvist-type for POMs	20
1.6.1.2	Organo-imido-hexamolybdate	21
1.6.2	POMs in DSSCs	25
1.8	An overview of dyes in DSSCs	26
1.7	Aims of the study	30
Chapter Two		
Experimental Part		
2.1	Materials	31
2.2	Instrumentation	32
2.3	Methods	32
2.4	Synthesis of Lindqvist-POM and derivatives	33
2.4.1	Synthesis of $[(C_4H_9)_4N]_2[Mo_6O_{19}](A)$	33
2.4.2	Synthesis of $[(C_4H_9)_4N]_2[Mo_6O_{18}N_2C_{13}H_8]$ (1)	34
2.4.3	Synthesis of $[(C_4H_9)_4N]_2[Mo_6O_{18}NC_{14}H_9]$ (5)	35
2.4.4	Synthesis of $[(C_4H_9)_4N]_2[Mo_6O_{20}NC_{14}H_7]$ (6)	36

2.4.5	Synthesis of $[(C_4H_9)_4N]_2[Mo_6O_{20}N_2C_{14}H_8]$ (7)	37
2.4.6	Synthesis of $[(C_4H_9)_4N]_2[Mo_6O_{18}NC_6H_4Br]$ (8)	38
Chapter Three		
Theory and Computational Methods		
3.1	Theoretical Background about quantum mechanics	39
3.1.1	Quantum mechanics theories of calculations	39
3.1.2	Approximation via Born-Oppenheimer	40
3.1.3	Hartree-Fock (HF)	41
3.2	Density Functional Theory (DFT)	42
3.2.1	Concept of Basis Set	43
3.3	DSSCs Theoretical background	44
3.4	Computational details	45
Chapter Four		
Results and Discussions		
4.1	Part I: - Theoretical design & Investigation	48
4.1.1	Molecular Geometric Structure	48
4.1.3	Electronic Structure of derivatives 1 to 4	50
4.1.4	Electronic Absorption Spectra and Molecular Orbitals	51
4.1.5	Photovoltaic Performance	61
4.2	Part II: - Experimental results & Discussion	63
4.2.1	General Synthesis	63

4.2.2	Characterization of the synthesized compounds using FT-IR spectrum	64
4.2.2.1	Compound (A)	64
4.2.2.2	Characterization of the synthesized compounds	65
4.2.2.2.1	Compound (1)	65
4.2.2.2.2	Compound (5)	67
4.2.2.2.3	Compound (6)	68
4.2.2.2.4	Compound (7)	70
4.2.2.2.5	Compound (8)	71
4.2.3	(¹ H NMR) characterization	73
4.2.4	Electronic Spectroscopy	78
Conclusions		82
Future works		83
References		84

List of Tables

NO.	Subject	Page
2.1	Chemicals and their commercial sources	31
2.2	Instrumentation used and their details	32
4.1	Optimized structure of derivatives 1 to 4	49
4.2	Calculated geometrical parameters for 1-4	50
4.3	Calculated maximum absorption wavelength (λ_{\max}), oscillator strength (f_{os}), electronic transition energy (E_{\max}), and the percentage MO contribution.	55

4.4	Calculated photovoltaic parameters	62
4.5	UV-Vis absorption data for compounds 1,6 and 7 in acetonitrile at room temperature	79

List of Figures

NO.	Subject	Page
1.1	Some of Organic dyes & Polymers	1
1.2	Some of Organic Optoelectronic materials	3
1.3	Examples of Organic-inorganic hybrid materials	4
1.4	Components in DSSCs	9
1.5	Structure of Organic dye with push-pull system	12
1.6	Some of π -bridge groups	12
1.7	Some of donor and acceptor groups	13
1.8	Diagrams of various POM geometric structures	15
1.9	Structure of hexamolybdate	17
1.10	Structure of POM-Types	18
1.11	Structure of some coupling reagents	22
1.12	The donors that were used by Peng and Wer's team, Maatta	23
1.13	Structure of N3 and N719	28
1.13	Some of inorganic dye	28
2.1	Structure of Compound (A)	33
2.2	Synthesis of Compound (1)	34
2.3	Synthesis of Compound (5)	35
2.4	Synthesis of Compound (6)	36
2.5	Synthesis of Compound (7)	37

2.6	Synthesis of Compound (8)	38
4.1	Structure of Lindqvist-POMs derivatives	47
4.2	UV-Vis Computational Calculations for compound (1)	52
4.3	UV-Vis Computational Calculations for compound (2)	53
4.4	UV-Vis Computational Calculations for compound (3)	53
4.5	UV-Vis Computational Calculations for compound (4)	54
4.6	Representation showing the changes in HOMO and LUMO energies caused by varying the electron donor strength for compounds 1-4 .	57
4.7	Excitation-induced charge density difference ($\Delta\rho$) for compounds 1-4 in their main excited states (isovalue = 0.0002 au; green and blue corresponds to positive and negative $\Delta\rho$, respectively. Upon excitation, transfer of the induced electron occurs from blue to green).	62
4.8	FT-IR spectrum of Compound (A)	64
4.9	FT-IR spectrum for 9-aminoacrdine (donor)	66
4.10	FT-IR spectrum for Compound (1)	66
4.11	FT-IR spectrum for 2-aminoanthracene (donor)	67
4.12	FT-IR spectrum for Compound (5)	68
4.13	FT-IR spectrum for 2-aminoanthraquinone (donor)	69
4.14	FT-IR spectrum for Compound (6)	69
4.15	FT-IR spectrum for 2,6-Diaminoanthraquinone (donor)	70
4.16	FT-IR spectrum for Compound (7)	71
4.17	FT-IR spectrum for 4-bromoaniline (donor)	72
4.18	FT-IR spectrum for Compound (8)	72
4.19	^1H NMR for Compound (1)	73

4.20	¹ H NMR for 9-aminoacrdine (donor)	74
4.21	¹ H NMR for Compound (6)	75
4.22	¹ H NMR for 2-aminoanthraquinone (donor)	76
4.23	¹ H NMR for Compound (7)	77
4.24	¹ H NMR for 2,6-Diaminoanthraquinone (donor)	78
4.25	UV-Vis spectra of compounds (1) in acetonitrile	80
4.26	UV-Vis spectra of compounds (6) in acetonitrile	80
4.27	UV-Vis spectra of compounds (7) in acetonitrile	81

List of Schemes

NO.	Subject	Page
1.1	Synthesis of Organo-imido Lindqvist derivatives.	23
1.2	Proposed mechanism for reaction hexamolybdate with primary amine	24
4.1	Calculated HOMO and LUMO energy levels for dyes 1-4	51
4.2	Synthesis of novel Organo-imido Lindqvist POMs.	63

List of Equation

NO.	Subject	Page
2.1	Synthesis of Compound (A)	33

List of Abbreviations

Symbol	Definition
---------------	-------------------

Abs.	Absolute
BS	Basis sets
CB	Conductive Band
CRE	Charge Recombination Efficiency
DSSCs	Dye-sensitized Solar Cells
DFT	Density functional theory
DCC	<i>N, N</i> -Dicyclohexyl Carbodiimide
DMSO	Dimethyl sulfoxide
DRE	Dye Regeneration Efficiency
EES	Electrochemical Energy Storage
EO	Electro-Optic Materials
E_{\max}	Maximum electronic transition Energy
FT-IR	Fourier Transform Infrared
Ff	Fill Factor
f_{os}	Oscillator Strength
HOMO	High energy occupied molecular orbitals
HJE	Hole-Injection Efficiency
HF	Hartree-Fock
HPC	High Performance Computing Cluster
ICT	Intramolecular Charge Transfer
J_{sc}	Short Circuit Current
LMCT	Ligand to metal charge-transfer
LUMO	Low energy unoccupied molecular orbitals

LHE	Light-Harvesting Efficiency
LPCT	ligand-to-POM Charge Transfer
MLCT	Metal to ligand charge-transfer
MOS	Metal-Oxide Semiconductors
MOs	Molecular Orbitals
OLEDs	Organic light emitting diodes
OPVs	Organic Photovoltaic cells
POMs	Polyoxometalates
PMMA	Poly Methyl Methacrylate
PR	Photorefractive
PV	Photo Voltaic
PEC	Photoelectrochemical
PCE	Power Conversion Efficiency
P_{\max}	Maximum Power
P_{in}	input Power
p-SC	p-type Solar Cell
QC	Quantum chemistry
TD-DFT	Time-Dependent Density Functional Theory
T_e	electrons' kinetic energy
Uv-vis.	Ultra Violet Visible
VOCs	Volatile organic compounds
V_{oc}	Open-Circuit Voltage
V_{ee}	electron-electron repulsion
V_{ne}	electron-nuclear attraction

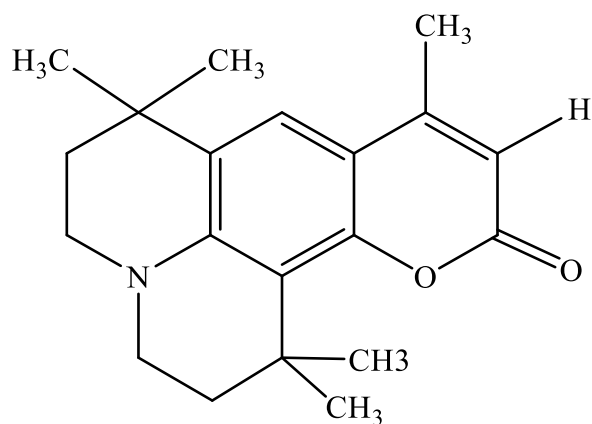
XCFs	exchange – Correlation Functionals
λ_{\max}	Maximum Wavelength

Chapter One

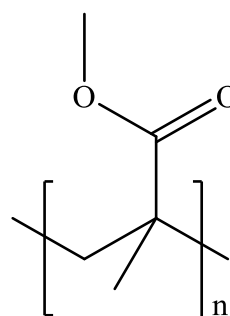
Introduction

1.1 Organic photonics

Organic photonics are very broad topic that deals with the production, transmission, detection, and processing of light using organic materials. Organic dyes, organic polymers, and organic-inorganic compounds for photonics applications (Fig. 1.1) are some of the most fundamental components of organic photonics.^[1]



Coumarin 102 tetramethyl



Poly(methyl methacrylate)(PMMA)

Figure 1.1 Some of Organic dyes & Polymers

Organic materials have several benefits, including low cost, simple processing, environmental friendliness, and the ability to be carefully tuned to get desired qualities. The optical quality of the materials is crucial for photonic applications.^[2]

1.2 Optoelectronic Materials

The world's overall energy consumption is currently rising, with fossil fuels accounting for a disproportionately large portion of it globally.^[3] However, given the sharply rising demand for energy and the need for human society to continue to expand sustainably, fossil fuels' limited storage capacity and their intrinsic CO₂ generation are insufficient to meet these demands.^[4] As a result, with the growing

focus on developing carbon-neutral energy sources to replace fossil fuels, sunlight holds enormous promise for meeting the world's energy needs by turning it into a variety of different energies.^[3,5] Photovoltaics (PV), a proven solar energy utilization technology that has drawn a lot of interest and offers direct energy production in the form of electricity for beneficial uses. With the recent advancement of perovskite materials, PV has also grown massively.^[8,9] Meanwhile, photo(electro)catalysis offers a technique for converting sunlight to create fuel that is combustible (H₂, CO, NH₃, etc.).^[10,11] For the production of recyclable, clean, and long-lasting hydrogen, photoelectrochemical (PEC) water-splitting technology which is a form of artificial photosynthesis, is also of great interest. However, further applications of photogenerated electricity and fuels require the combination of independent devices (renewable batteries, regenerative fuel cells, etc.) with the purpose of achieving high reliability and efficient solar energy consumption. Rechargeable batteries provide a tremendous amount of potential for the application of solar energy with practical feasibility^[12,13] notably with the accelerating development of electrochemical energy storage (EES) technologies and PV systems.^[14]

1.2.1 Organic optoelectronic materials

Organic electronic materials (optics) have attracted a lot of attention, mainly owing to their ease of use in solar cells, sensors, light-emitting diodes, photorefractive devices, thin-film transistors, and many other items.^[15] Derivatives of anthracene,^[15] anthraquinone^[16] and Acridine^[17-19] (Fig. 1.2) have been studied for their optical and electrical characteristics for the first time in the 1910s. They have been well known for over a century.^[20]

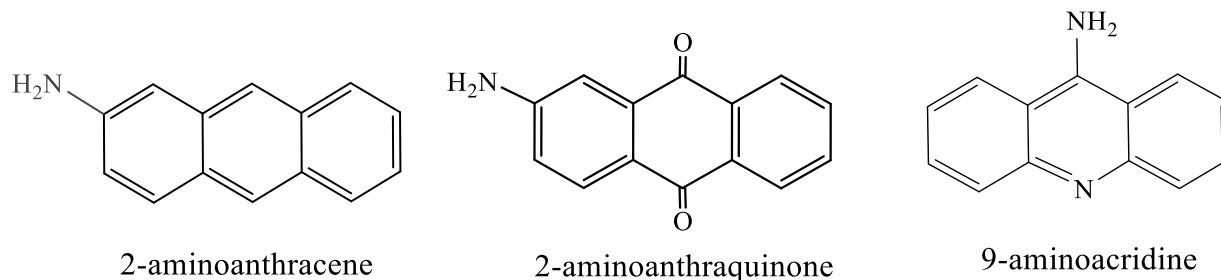


Figure 1.2 Some of Organic optoelectronic materials

On the other hand, the discovery of conducting polymers and electroluminescence in molecular crystals increased interest in these materials in the 1960s and 1970s.^[21] But during the past 20 years, there has been noticeable rise in interest in organic (opto)electronics due to important developments in design and purification of materials that have greatly enhanced the performance of the materials. Due to its use in optoelectronic and electrical devices including organic thin-film transistors, Organic light-emitting diodes (OLEDs), sensors, photorefractive (PR) devices, solar cells, and many others, organic materials are currently receiving a lot of attention. A particular area of technological interest is the production of low-cost thin films that can be processed on flexible substrates and/or expanding surfaces.^[15]

The interconversion of signals between the electrical and photonic domains is a crucial aspect of photonic/electronic integration. In this situation, electro-optics proves beneficial. In order to allow for the interaction of photon and electron electrical fields, electro-optic (EO) materials must have charge distributions that are highly hyperpolarizable (easily influenced by electric fields). The best option for converting information from an electrical signal to a photonic signal must be able to have an electro-optic material. By a charge distribution that is easily perturbed by small electric field potentials (ideally, millivolt electric field potentials to reduce power consumption) and a very quick (ideally, femtosecond (fs)) response to time-

varying electrical fields. These qualities are what have made organic EO materials popular. The phase relaxation period, which is generally often in the order of 10 fs, is the fundamental reaction time of conjugated π -electron systems.^[22]

1.3 Hybrid Organic-Inorganic Materials

The most comprehensive explanation of hybrid is as the following: Having two molecules that have been molecularly joined creates a hybrid material. Typically, one of these chemicals is organic in nature, and the other is inorganic (Fig. 1.3).

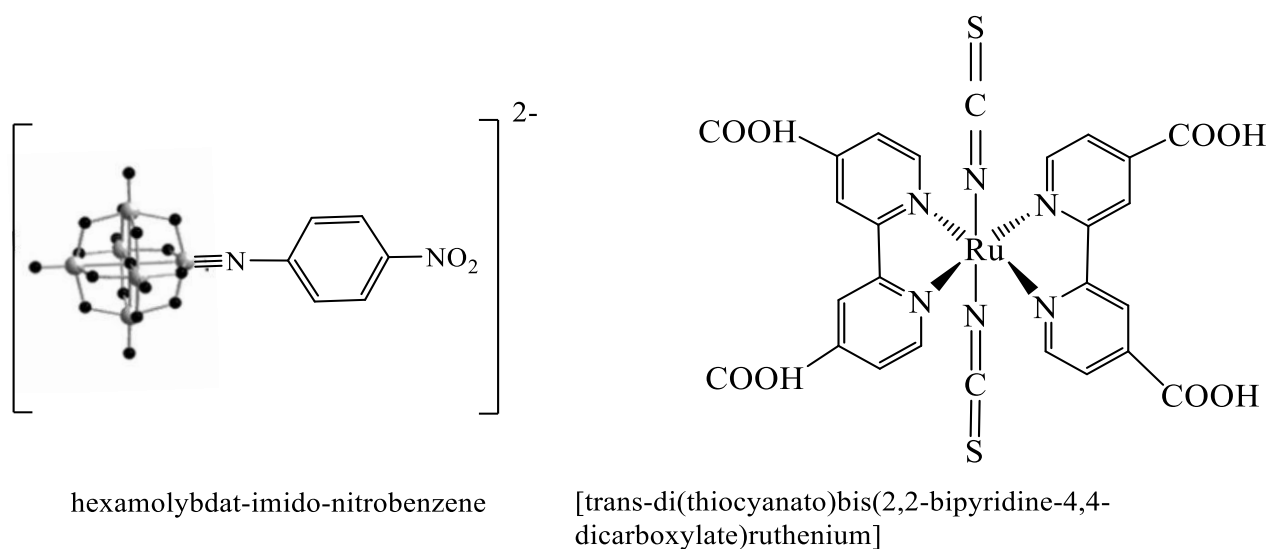


Figure 1.3 Example of organic-inorganic hybrid materials^[23,24]

Hybrid materials classified as class I exhibit only insignificant interactions between the two moieties, like Hydrogen bonds, Van der Waals contacts, or minuscule electrostatic interactions. Materials classified as class II hybrids exhibit significant chemical interactions between the two constituents.

Because chemical connections gradually get stronger, it is evident that there is a constant shift between weak and strong contacts. For example, hydrogen bonds are unquestionably stronger than weak coordinative bonds. In addition to features of

bonding, structure features can be used to differentiate between different hybrid materials such as a functional group in an organic moiety allowing connection to an inorganic network.

A significant class of materials in terms of technology is electrochemically active hybrid materials, which have a wide variety of uses.^[25–28] The electrochemical and physical properties of the resulting hybrid can be tailored to meet the requirements of specific electrochemical applications by chemically combining various crystalline, amorphous, liquid, solid, organic and inorganic components.^[29–31] The synergistic interactions between these physical and electrochemical features usually result in hybrid materials that are very beneficial. Since they are crucial to comprehending how these materials are applied to real-world issues, the fundamental mechanisms of electrical and ionic conductivity in these types of materials have been discussed.^[32]

An important class of hybrid materials that has potential applications in a number of areas, such as the encapsulation and controlled release of active substances as well as their use as fillers for the paint and coating industries, are organic/inorganic hybrid particles with diameters ranging from ten nanometers to several hundred nanometers. The basic physicochemical pathways or polymerization procedures used in synthetic approaches include. In contrast to the chemical approach, the physicochemical method includes a combination of prepared macro molecules and/or nanoparticles with particle templates, which forms the mineral and organic phases in situ in the presence of organic or inorganic particles, respectively. It will also be taken into consideration how organic and inorganic precursors react simultaneously to form single-phase hybrid nanoparticles.^[32] The properties of organic and inorganic particles depend on their morphology and the spatial arrangement of the various phases, which in turn are governed by the synthetic

process and the experimental conditions. These factors are in addition to the chemical nature of the organic and inorganic components should be taken into account.

1.3.1 Advantages of Organic-Inorganic Hybrid Materials

The ability of inorganic-organic hybrids to favourably blend the sometimes-disparate features in one material of organic and inorganic components is their most evident benefit. This field is particularly creative since it offers the ability to create an almost infinite number of modern materials with a wide range of known and undiscovered properties. This is made possible by the numerous combinations of components that are conceivable. The potential to develop multifunctional materials is another driving force in the field of hybrid materials. The production of hybrid materials is arguably the most fascinating aspect that makes this material class appealing for many applications. Due to their high organic content or the formation of crosslinked inorganic networks from small molecular precursors, just like in polymerization reactions, hybrid materials exhibit more polymer-like handling than pure solid state inorganic materials, which frequently require a high temperature treatment for their processing. As a result, both in bulk and in films, these materials may be molded in any way. Even while from an economic standpoint, bulk hybrid materials can only now compete with traditional inorganic or organic materials in very few areas, such as the biomaterials industry, the potential of their processing as thin films can lead to, for instance, the potential of processing biomaterials as thin films might result in the enhancement of cheaper materials' properties with a straightforward surface treatment, such as scratch-resistant coatings.^[32] One of the most potential long-term approaches for organic optoelectronics is to combine the best properties of organic and inorganic materials in high-performance optoelectronic devices.^[33,34] For instance, the performance of inverted organic

photovoltaic cells (OPVs) has been improved and adjustable energy level matching between the inorganic electrode and organic active layers has been made possible by the use of inorganic oxides (Al_2O_3 , CeO_2).^[35] In tandem cells combining polymer: fullerene and amorphous silicon (a-Si:H) or organic semiconductors cells, which each exhibited PCEs of 8% in a single-junction device, Kim et al.^[36] Reported PCEs of up to 10.5%. The efficiency of various organic–inorganic hybrids, with PCEs of up to 13–14%, in photorefractive (PR) devices and solar cells.^[15]

1.4 Historical background of the solar cells

Solar cells, commonly referred to as photovoltaic cells, are a form of a green energy source that use the photovoltaic method to turn sunlight into electricity.^[37,38] They contain a semiconductor material, which when exposed to sunlight, absorbs it and releases electrons that may be trapped and utilized to produce energy.

There are several types of solar cells, including older silicon-based inorganic cells and more modern polymer- or small-molecule-based organic cells. On the other hand, organic solar cells are created by applying thin covering of photovoltaic material onto a backing material, such glass or a polymeric substance. They are also more adaptable because they may be created in a range of sizes and forms. However, compared to conventional inorganic cells, organic solar cells now have lower efficiency rates and shorter lives.^[39]

When French physicist Edmond Becquerel discovered the photovoltaic effect via the electrolytic cell in 1839, the first description of photovoltaic technology was initiated. Adam and Day carried out the initial studies on selenium-based solid-state photocells in London in 1876. It took more than 50 years to develop the earliest solar photocells, which had an efficiency of only a little over 1%.^[40] Since the first Si-based p-n junction designed to convert sunlight into electrical energy was invented in the 1950s, research on solar cells and photoelectric (PE) modules has been

intensive. The development of photovoltaic solar cells then began its modern age in 1954. The first silicon-based photovoltaic device was created by Calvin Fuller, Daryl Chapin, and Gerald Pearson of Bell Telephone Laboratories in the US. Originally known as a solar battery, the device is now known as a solar cell.^[4] This device had an initial energy conversion efficiency of 6% and used the basic p-n junction ideas that were discovered in the early 1950s. However, it had increased to 11% by 1957 and 14% by 1960.^[41]

1.4.1 Dye Sensitized Solar Cells (DSSCs)

A crystalline silicon wafer coated in several chemicals to enable power production is the basis of a solar cell. The quantity of electrons separates n-type solar cells from p-type solar cells. Boron is used in p-type cells because it has one fewer electron than silicon, which results in a positively charged cell. Phosphorus, which is negatively charged and has one additional electron than silicon, is a component of an n-type solar cell. Solar energy shows enormous potential for resolving the energy shortfall brought on by the use of fossil fuels since it is clean, ecologically benign, and renewable.^[6] The collection and storage of solar energy for use in forming and transforming readily available chemical feedstock and electric power through the artificial photosynthesis process and solar cell devices is an efficient method for effectively using visible and/or solar light.^[42] Lasers, Stimulated Emission, and Photoluminescence Organic dyes are good light-emitting materials with little reabsorption because of their high photoluminescence quantum yield and Stokes shift, this is the difference in energy between the absorption and emission maxima. There are dyes for a wide variety of wavelengths, from the UV to the near-IR. The tuning range for each dye is just a few tens of nanometers because of the wide emission spectrum.^[2] However, most light-absorbers have a number of drawbacks, which notably restrict their practical applicability. These drawbacks include being

made of noble metals or unstable organic dyes and absorbing only a little amount of visible light. Therefore, the development of low-cost, reliable, and related to models of molecular light-absorbers with a wide photoabsorption spectrum is crucial for optimizing the conversion of solar energy.^[43] It was therefore replaced by simpler models. An illustration of this is the use of dyes, where a variety of photosensitizers, involving artificial and natural dyes, have been researched for DSSCs.^[44] Organic and mineral dyes are two different types of synthetic dyes. While organometallic dyes consist of a group of organic chromophores, transition metals form organometallic dyes (Fig 1.4).

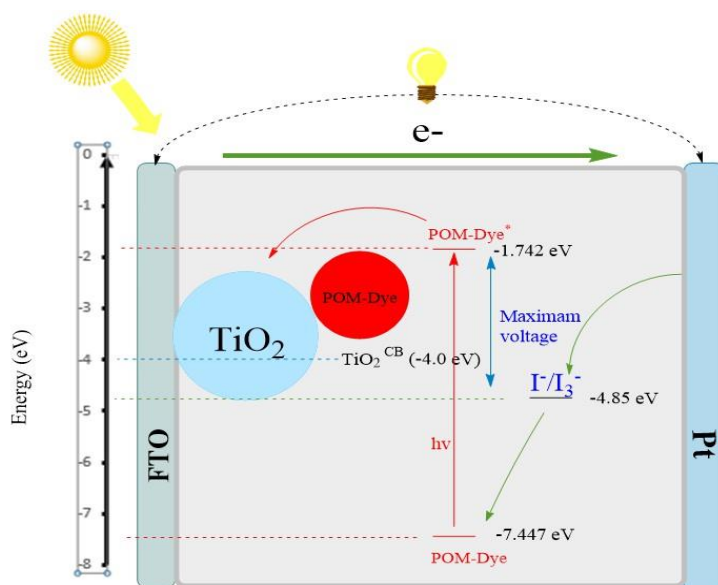


Figure 1.4 Components in DSSCs

1.4.1.1 Components of DSSCs

A DSSC has four sections: an electrolyte, a photosensitizer (dye), a photoanode, and a counter electrode. The general traits of these components are covered in the following sections.

1.4.1.2 Types of DSSCs

Classification of DSSCs based on semiconductors into two types :- ^[45]

1.4.1.2.1 p-Types DSSCs

A p-DSSC works on the idea that excitation of the sensitizer (S) creates its excited state (S^*), which decays by introducing a hole into the valence band of the p-type semiconductor (p-SC), creating the charge separated state $S^-/p-SC^+$. The reduced sensitizer is then reacted with a redox mediator (the couple M/M^+), which returns the sensitizer to its ground state and moves the electron to the counter electrode (CE), where it is supplied to the external electric circuit. The relative rates of these processes regulate each step's effectiveness, which has a direct bearing on the device's total effectiveness.

The power conversion efficiency of a solar cell (η) is the maximum power (P_{max}) from three terms: the short circuit photocurrent density (J_{SC}), the open-circuit photovoltage (V_{OC}), and the fill factor (ff) divided by the input sunlight power (P_{in}) show in Eq. (1.1).

$$\eta = \frac{P_{max}}{P_{in}} = \frac{J_{SC} \cdot V_{OC} \cdot ff}{P_{in}} \dots \dots \dots (1.1)$$

Every term should be maximized. When compared to the similar values in a traditional n-DSSC, the typical values for all three of the aforementioned components are low in a typical p-DSSC.^[46] The best NiO p-DSSC exhibits a $J_{SC} = 5.35 \text{ mA/cm}^2$, a $V_{OC} = 218 \text{ mV}$ and $ff = 0.35$, which yields an η of 0.41%.^[47]

The ratio of free electrons to holes in ZnO should be the same for intrinsic semiconductor materials. However, for the majority of semiconductors, the concentration of electrons and holes cannot be maintained at the same level due to flaws and impurities in the crystal. Most of carriers in p-type semiconductors are holes. The crystal flaws cause the extra holes in intrinsic p-type materials.^[48]

1.4.1.2.2 n-Type DSSCs

For the conversion of solar energy, dye-sensitized solar cells are very promising. In this system, an adsorbed layer of photosensitizing dye molecules modifies an electrically conducting, mesoporous semiconducting anode (usually TiO_2). The introduction of an electron into the TiO_2 's conduction band (CB) occurs as a result of photoexcitation of the dye molecule. The electron then travels to the cathode through an external connection. A species in the electrolyte (usually the redox system I^-/I_3^-) reduces the photooxidized dye Molecule. The I^- are oxidized in this instance to I_3^- , which diffuses to the cathode. The electrons that have gone via an external circuit and been photoexcited diminish I_3^- at the cathode.^[49] The output power by illumination is equal to the difference between the Fermi level (The highest energy level that an electron can occupy at the absolute zero temperature is known as the Fermi Level. The Fermi level lies between the valence band and conduction band because at absolute zero temperature, the electrons are all in the lowest energy state) of the electron in the solid and the redox potential of the solution redox couple. In general, electricity production does not involve long-term chemical change.^[50] While p-type cells are currently used in the majority of solar panels, some high-end solar panels use n-type cells to increase their efficiency. Also, higher efficiency carries a higher cost. More power per square foot, fewer modules, less space, reduced hardware costs, and less labor are all benefits of this technology.

1.5 Design and functioning of Chromophores.

The push-pull structural moiety of the dye is frequently developed around the general form D- π -A (Fig. 1.5).

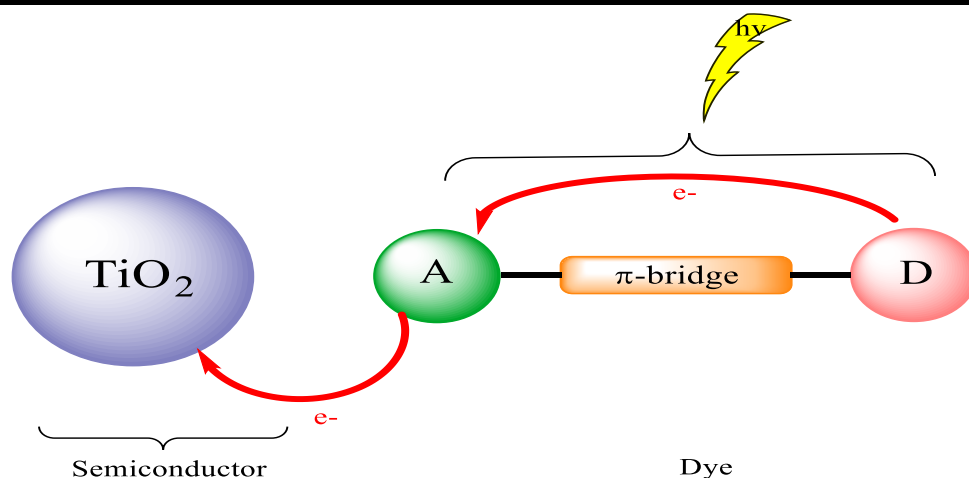


Figure 1.5 Structure of organic dye with push-pull system

Where D is an electron donor group coupled to an electron acceptor group A by a conjugated moiety (π -bridge)^[51]. During photoexcitation, the electron density shifts from the dye molecule's donor (where the HOMO is localized) to electron acceptor (where the LUMO is localized) section, causing electron injection into the conduction band of the nanocrystal line semiconductor (TiO_2). The ability of the donor and acceptor components to provide and absorb electrons, as well as the electrical properties of the used π -bridge, are all crucial factors in the sensitization process. The π -bridge conjugated component is composed of a range of chemical groups, such as coumarin, phenoxazine, and polythiophene, (Fig. 1.6) while the donor groups involve dialkylamine, diphenylamine, and triphenylamine.^[52]

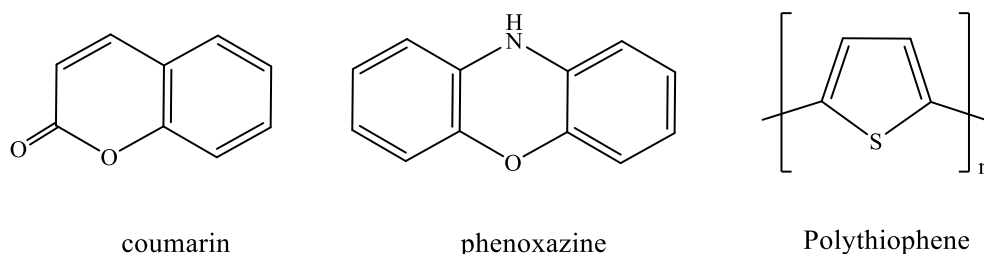
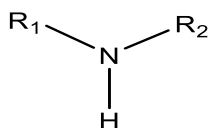


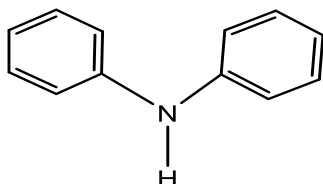
Figure 1.6 Some of π -bridge groups

On the TiO₂ surface, carboxylic acid, rhodanine-3-acetic acid, and cyanoacrylic acid moieties are frequently used as anchoring groups (Fig. 1.7).^[53–55]

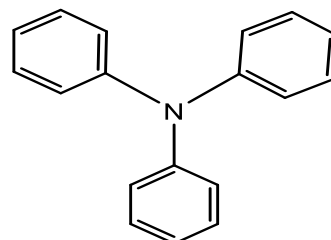
(a) Donor groups



Dialkylamine

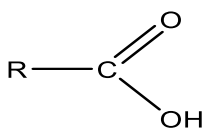


Diphenylamine

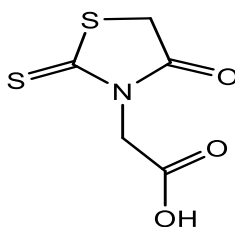


Triphenylamine

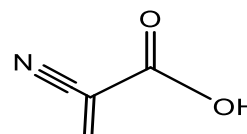
(b) Anchor groups



Carboxylic acid



Rhodanine-3-acetic acid



Cyanoacrylic acid

Figure 1.7 Some of donor and acceptor groups

It is suggested that a useful dye for applications of dye-sensitized solar cells should have the following requirement:

- a) Light from the visible and near-infrared spectrums should be absorbed by the dye.^[56]
- b) The metal oxides that will be adsorbed on the semiconductor layer and dye must have a strong affinity for one another. Response groups like phosphates and carboxylates are added in order to form ester bonds with the metal oxide. The absorbed photons and electrons are directly interposed into

the conduction band (CB) of the metal oxides as a result of this stimulation of the LUMO, or lowest unoccupied molecular orbital.

c) The energy levels of the dyes, the metal oxide and electrolyte must be compatible ((LUMO) dye > (CB) metal oxide; (HOMO) dye < (HOMO) electrolyte); HOMO stands for highest occupied molecular orbital).

d) To minimize the excited state's nonradioactive drop to the ground state, avoid dye aggregation.^[57]

e) The dye must be long-stable chemically, thermally, and light stable, which is now the main obstacle to commercialization.^[58]

1.6 Polyoxometalates (POMs)

POM shows a class of molecular materials that great potential applications for a variety of energy-related. POMs have an unusual capacity to govern redox processes in energy conversion and storage as a result of their "special" structure. Their many redox active sites, which are produced by the intricate, three-dimensional cluster of metal-oxide ions connected by oxygen atoms, are one example of their astounding abilities. Therefore, POMs are considered as a unique class of inorganic redox active materials made up of many metal-oxide ions connected by oxygen atoms to form nanoclusters in a structured three-dimensional framework. Given their size and extremely high surface to bulk ratio, they can be thought of as an oxide quantum dot type. They possess outstanding electrochemical properties due to their quick and highly reversible redox activity; they can accept multielectron. The reason for doing more study into POMs for use in energy materials and other related applications is supported by these interesting properties.^[59] POMs, particularly with an amino group to produce organonitrogenous derivatives of POMs, is an effective method for

enlarging their structural diversity and enhancing their characteristics for a variety of applications.^[60]

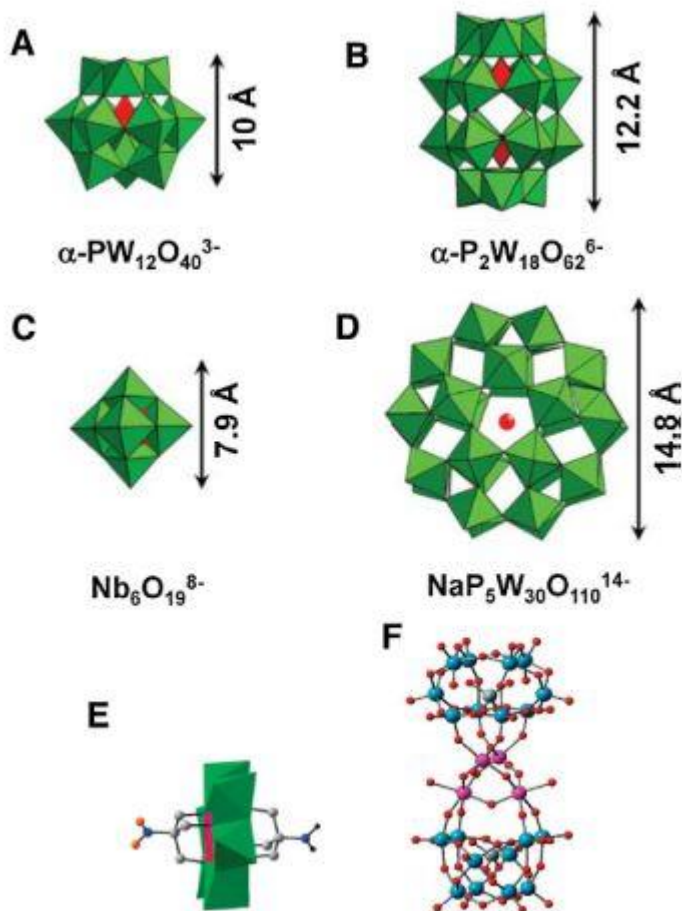


Figure 1.8 Diagrams of various POM geometric structures. (a) Keggin structure; (b) Dawson structure; (c) Lindqvist structure and (d) Preyssler structure incorporating Na^+ (red) viewed approximately down the molecular C_5 axis (e) Anderson structure (f) The “sandwich” anion $[\text{Ru}_4(\mu\text{-O})_4(\mu\text{-OH})_2(\text{H}_2\text{O})_4(\text{Y-SiW}_{10}\text{O}_{36})_2]^{10-}$, showing Ru(IV) centres (lilac) sandwiched between two $\{\text{SiW}_{10}\text{O}_{36}\}$ fragments.^[61]

POMs are unique transition metal-oxide groups that come in a range of forms, sizes, and compositions (Fig. 1.8), as well as physical and chemical characteristics. Due to the many redox processes that could be influenced by the characteristics of the transition metal, the hetero-atom, and the solvent medium, or the pH, POMs exhibit

an electrochemical diversity that is really astonishing.^[62] Thus, POMs are particularly appealing as building blocks for more sophisticated materials, from molecular up to extended ones, because of their adaptable electrochemical characteristics.^[63] Development of very effective, ecologically friendly, and energy-saving cell materials for DSSCs are urgently needed due to the world's growing energy demands and problems. POMs are intriguing candidates for usage in various DSSC components because of their redox, superior photosensitivity, and catalytic characteristics, in addition to their relative stability.^[64] By replacing a terminal oxide group with an imido group formed from a primary amine molecule, POMs can be tailored leading to functionalized hybrid materials.^[65] Recently, a lot of research has concentrated on the creation of structure-controlled hybrid materials combining organic molecules with POMs.^[66] Countless structures of POMs have now been synthesized and described. Currently, POMs are a vast class of polynuclear metal-oxygen clusters that are typically generated by Mo, W, or V as well as combinations of these elements.^[67] They might be used in a variety of industries, including chemical analysis, medicine, and catalysis, among others. Over 700 communications (publications and patents) in the family of POMs were recorded in 1996, according to Katsoulis' collection.^[68]

Due to its potential uses in a variety of areas, such as drug-delivery systems, switchable electronics, and multifunctional materials, dynamically reversible self-assembly, POMs have attracted growing interest. POMs are capable of being applied in catalysis, optics, magnetics, biomedicine, and energy materials due to the abundance of metal elements and the variety of frameworks that give them required physical and chemical characteristics. In addition, POMs, a class of functional inorganic materials, can operate as intriguing building blocks for self-assembly, particularly when modified by organic moieties.^[69] A broad range of assembly

morphologies have been acquired thanks to the synergistic interaction of organic parts with inorganic clusters.^[70]

1.6.1 Structures and Types for POMs

According to its composition and structure, POMs may be divided into a number of groups; Isopolyoxometalates (Polyhedral) representations of some common POMs structures $[M_6O_{19}]^{n-}$.

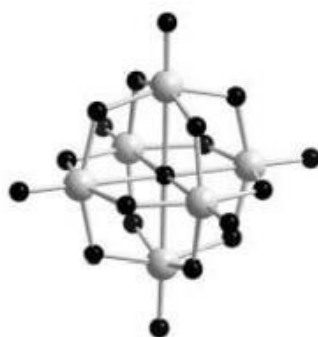


Figure 1.9 Structure of **hexamolybdate**

Hexamolybdate (Lindqvist-structure)^[71] is a type of polyoxometalates that have the generic formula $[M_mO_y]^{n-}$ and solely comprise a transition metal and oxygen, shown in (Fig. 1.9). Hetero-POMs are a subclass of compounds that include just a few extra elements, namely $[X_xM_mO_y]^{n-}$ (X = heteroelement, x lower than m) such as $[XM_{12}O_{40}]^{n-}$ -(Keggin-structure), $[X_2M_{18}O_{62}]^{n-}$ (Dawson-structure) etc. as shown in (Fig. 1.10).

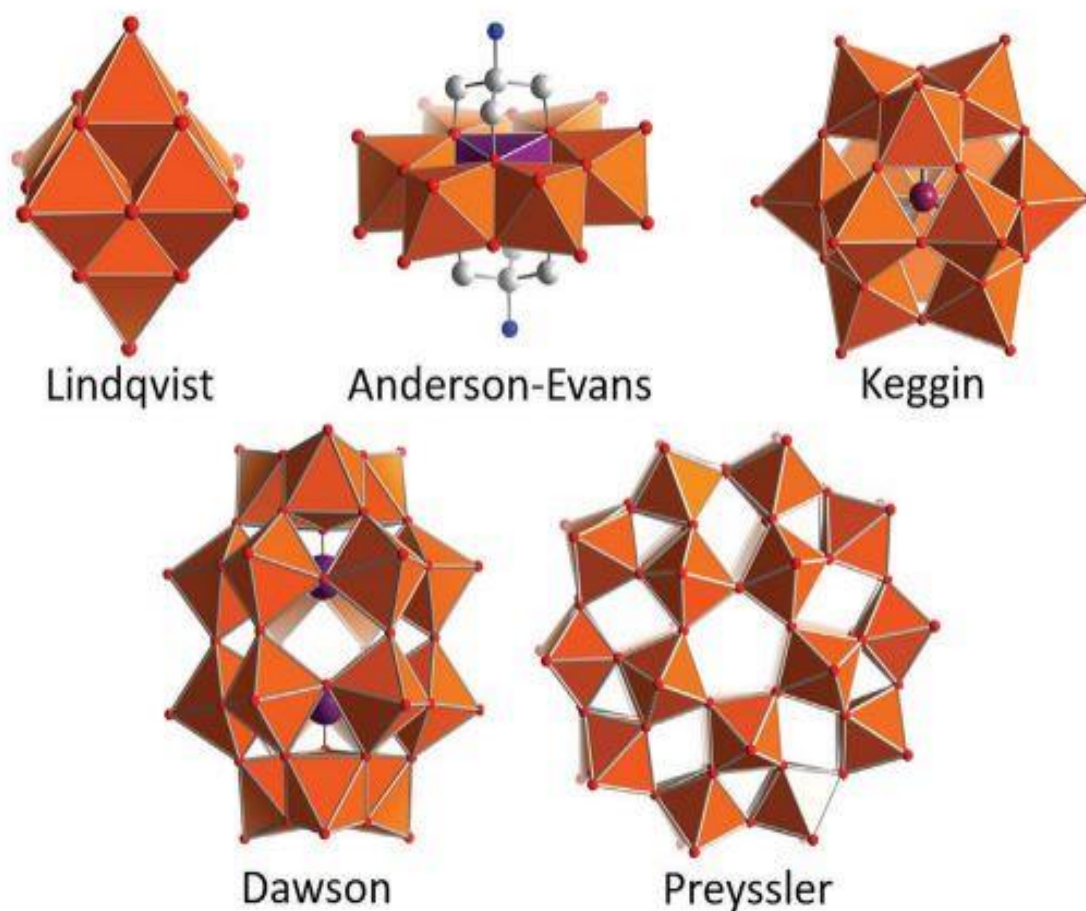


Figure 1.10 Structures of POM-Types. ^[72] Figure was reproduced with permission from reference (51)

In hexametalates, with the chemical formula $[M_6O_{19}]^{n-}$ adopt a Lindqvist structure; six octahedra are arranged in an octahedral pattern. Each octahedron shares four edges with four of its surrounding octahedra. Each octahedron represents a metal ion with its coordination sphere, as was stated above. The Lindqvist structure can really be viewed as a piece of a cubic closed packed metal oxide due to the extremely compact nature of this arrangement.

The Anderson structure is made up of heteropolyoxometalates. Around the core heteroatom, a planar hexagon made up of six edge-sharing octahedra is constructed. The Keggin ion, with the generic formula $[\text{XM}_{12}\text{O}_{40}]^{n-}$, is the most prevalent structure containing tetrahedrally coordinated heteroatoms. Around a center tetrahedron, there are four trimetallic groups organized. On each Keggin ion, a trimetallic group is removed, and the remaining pieces are associated. Lacunary structures are created by adding base while selectively removing one or more metal ions. They have available coordination sites that are accessible to atoms of other metals or non-metals. This method is frequently employed to change the composition and characteristics of POMs.^[73]

POM structures come in a wide variety, although the Keggin, Dawson, Lindqvist, Anderson, sandwich, and Preyssler structures are the most common. The most studied structures are the Lindqvist, Keggin and Dawson ones.^[74] New classes of hybrid species have also been produced as a result of more recent covalent functionalization of conventional POM structures.^[61] The most typical species of heteropolyanions are Keggin and Dawson structures.^[75] The phosphomolybdate with the formula $[\text{PMo}_{12}\text{O}_{40}]^{3-}$ was discovered by Berzelius in 1826,^[76] and the related anion $[\text{PW}_{12}\text{O}_{40}]^{3-}$ X-ray crystallographic structure was first characterized by Keggin in 1933.^[77] The Keggin heteropolyanions containing W and Mo have received the most attention throughout the past 20 years. The standard formula for them is $[\text{XM}_{12}\text{O}_{40}]^{3-/4-}$, where X is a heteroatom and M is an addenda atom. By substituting a transition metal (addenda) ion for W(VI) or Mo (VI) ions, modified POMs with distinct electrochemical and catalytic behavior may be created. $[\text{X}_2\text{M}_{18}\text{O}_{62}]^{n-}$ is the Wells-Dawson structure was initially proposed by Wells in 1945, and in 1953, Dawson used single-crystal X-ray diffraction to validate the locations of the W atoms in $[\text{P}_2\text{W}_{18}\text{O}_{62}]^{6-}$. High-valent transition metal ions from groups 5 or

6 are exclusively present in one form of isopolyanion. There have been claimed to be more than 30 isopolyanions so far, with the octamolybdate and Lindqvist being the most extensively researched.^[78]

1.6.1.1 Lindqvist-type for POMs

Applying the synthetic approach described by Klemperer and coworkers, the structure of Lindqvist, hexamolybdate ion $[\text{Mo}_6\text{O}_{19}]^{2-}$ can be synthesized, that has strong chemical and thermal stability and is simple to manufacture.^[79] Six MoO_6 octahedra that have their edges shared are arranged compactly to form its structure. Octahedral symmetry characterizes the overall structure. Due to their intriguing qualities, such redox activities and the capacity to receive electrons, these units are appealing for usage as building blocks (electron-relay) in numerous energy-related applications.

There are several nitrogen-containing groups that can replace the moderately active terminal metal-oxo groups in the Lindqvist structure, including imido, diazoalkyl, and diazenido.^[80] The organoimido Lindqvist derivatives, which Kang and Zubieta first described,^[81] are the class of POM derivatives that has undergone its most development. In the past ten years, interest in the chemistry of POM organoimido derivatization has grown because the resulting derivatives have fascinating qualities.^[23] The covalent bonding formation enhances the assembly's long-term stability, allowing for tighter control of interactions between various components, and results in improved POM diffusion in materials.^[63] These organo-imido ligands can be replaced for the hexamolybdate cluster whole or partly to produce organoimido POM derivatives.^[80] Many of these derivatives have recently reported with structural characterization and syntheses.^[23]

1.6.1.2 Organo-imido-hexamolybdate

POMs are thought to be suitable for photo/electrochromic materials since they display a redox reaction triggered by a light or electric stimulation while keeping the topological structure. POMs serve as the building blocks for the construction of dynamic assemblies due to their reversible photo/electrochromism. One of the least negatively charged POMs is the divalent Lindqvist-type hexamolybdate cluster $[\text{Mo}_6\text{O}_{19}]^{2-}$, making it the ideal component for creating inventive assembly structures. The functionalization is accomplished either by covalently altering organic species or by exchanging the counterions via ionic self-assembly processes. Maatta reported employing phosphinimines as the imido-releasing reagents in the formation of monosubstituted organoimido hexamolybdate derivatives.^[80] Proust and his associates stated that the molybdyl in the hexamolybdate ion behaves fairly similarly to the carbonyl of aldehydes, ketones, or esters two years after they replicated this reaction under nitrogen gas using anhydrous acetonitrile rather than pyridine. Similar to reactions combining primary amines and aldehydes or ketones, it can undergo Schiff base reactions, which include the nucleophilic addition of an amine to the carbonyl followed by the elimination of water molecules.^[80] Consequently, the chemistry of POM derivatives may sometimes be included into organic synthesis processes.

Other hexamolybdate organoimido compounds were reported by Errington in the interim.^[82] These were produced via the high-temperature reaction of hexamolybdate ions with alkyl and aryl isocyanates in acetonitrile. For the reaction to be successful, the water that is produced must be removed from the reaction mixture. The most widely used coupling reagents in organic chemistry, such as DCP (*N,N'*-diisopropylcarbodiimide) and DCC (*N,N'*-dicyclohexylcarbodiimide) (Fig. 1.11), were then employed by Peng and Wei in a unique DCC-dehydrating synthesis approach to synthesize arylimido derivatives of POMs.^[83]

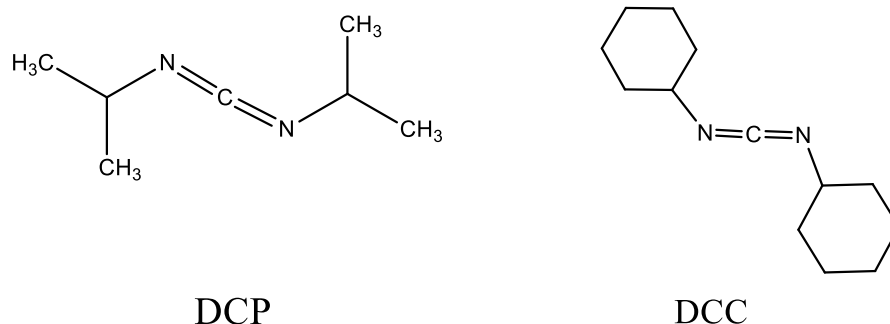
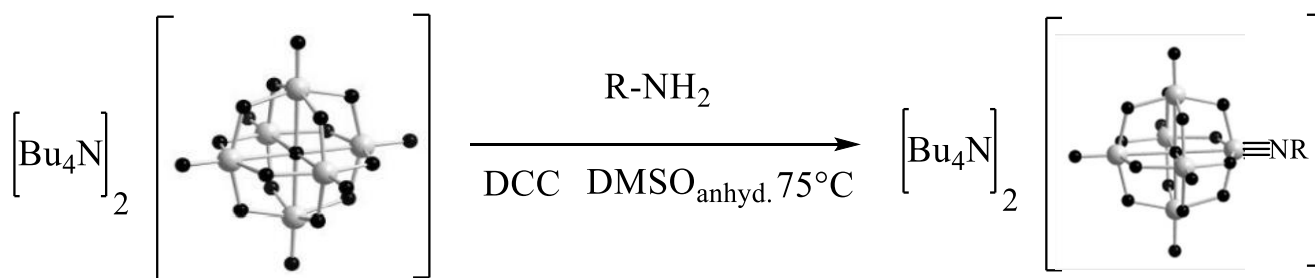


Figure 1.11 Structure of some coupling reagents

They have also looked into other dehydrating agents, such as magnesium sulfate (MgSO_4), calcium chloride (CaCl_2), zeolite, phosphorus pentoxide (P_2O_5), and calcium hydride, all of which had fewer activating effects than DCC.^[23] That implies that DCC does more than just function as a dehydrating agent; it also activates the terminal $\text{Mo}\equiv\text{O}$ bond, boosting the Molybdenum atom's electrophilicity. However, By-products might be produced by side reactions between the molybdate ions and the initial products if too much DCC is added. Although, due to the weak nucleophilicity or basicity, it is exceedingly difficult to synthesize using the DCC-dehydrating technique, by synthesize hexamolybdate organoimido derivatives (Scheme 1.2) from aromatic amines containing electron-withdrawing substituents such as nitro, fluoro, and chloro groups.^[84]



Scheme 1.1 Synthesis of organoimido Lindqvist derivatives.

Additionally, di-substituted compounds have already been investigated as possible components for POM-based hybrids. Maatta^[23] originally produced these compounds by combining two equivalents of 2,6-diisopropylphenyl isocyanate were added to $(n\text{-Bu}_4\text{N})_2[\text{Mo}_6\text{O}_{19}]$ in refluxing pyridine for eight days. However, this procedure is ineffective and time-consuming, and the crude products comprised a mixture of hexamolybdates with greater and lower substitution levels. Using $(n\text{-Bu}_4\text{N})_2 [\text{Mo}_8\text{O}_{26}]$ with DCC and 4-iodo-2,6- iisopropylaniline or 4-ethynyl-2,6-dimethylaniline (Fig. 1.12) at the ratio of 1: 2: 2 in refluxing dry acetonitrile for 6 to 12 hours, the Peng and Wei team reported the synthesis of difunctionalized arylimido derivatives of hexamolybdate.

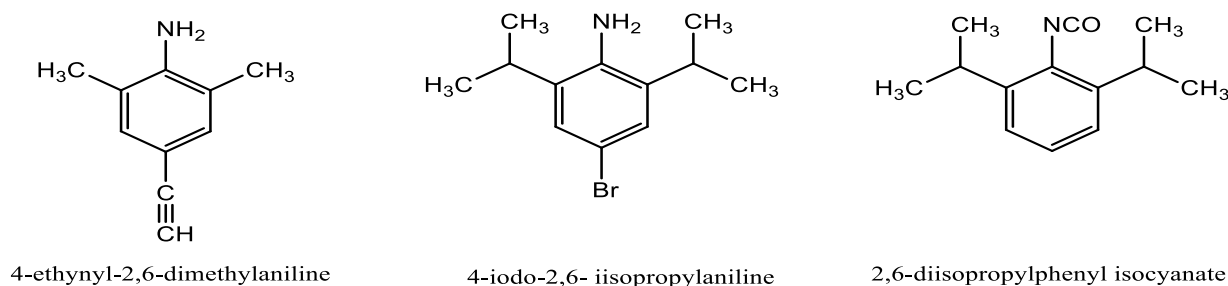
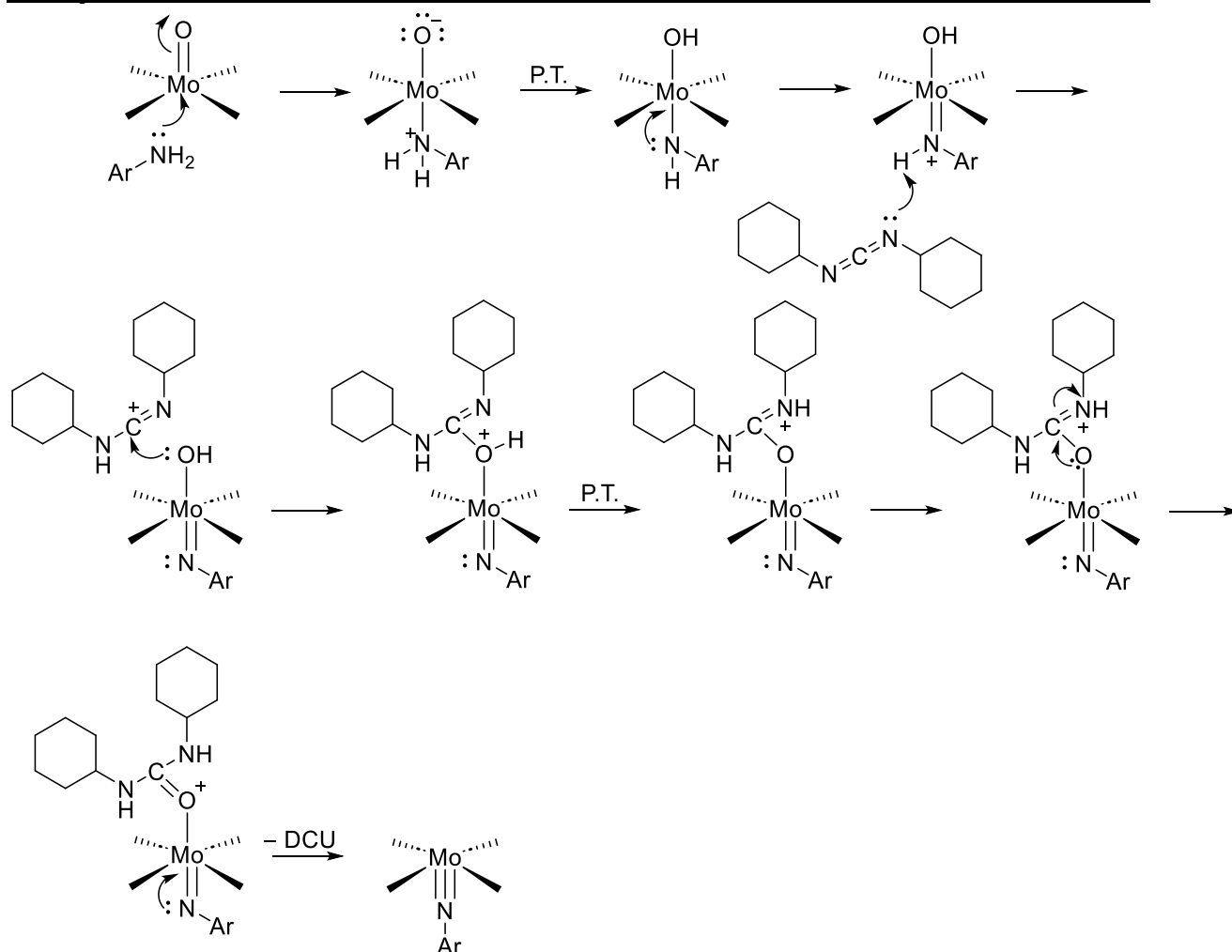


Figure 1.12 The donors that were used by Peng and Wei's team, Maatta.^[23]

The mechanism of above reaction was studied previously, shown in (scheme 1.2).

[60]



Scheme 1.2 Proposed mechanism for reaction **hexamolybdate** with primary amine.^[60]

In general, organoimido derivatives of POMs frequently exhibit d-p π electronic connections by extending the organic electrons in the imido-aryl unit to the inorganic structure, this drastically modifies the matching parent POMs' redox properties and electrical structure. Substantial charge transfer bands (missing in the isolated clusters and organic groups) and shifting electrode potentials in these derivatives demonstrate strong electronic coupling. The incorporation of organic ligands offers significant promise for the controlled synthesis of organic-inorganic

hybrids utilizing established typical organic methods such as coordination, carbon-carbon couplings, addition polymerization, and esterification.^[85]

Organoimido substituted POMs have been used as the building blocks for new nanostructured organic-inorganic hybrid materials employing a variety of organic synthesis techniques, such as Pd-catalyzed carbon-carbon coupling and esterification.^[85,86] POMs-based materials can be synthesized using both direct functionalization and post-functionalization, nonetheless, when the target's complexity increases, post-functionalization is preferred for such functionalization.^[23,63]

1.6.2 POMs in DSSCs

As mentioned earlier, low efficiency and electron recombination are the main problems that prevent future advancements in DSSC efficiency.^[87] Therefore, reducing these unfavourable electron recombination may greatly improve the efficiency of DSSCs. On the other hand, the low efficiency has motivated researchers to find new strategies to enhance efficiency in general, which could be solved via enhancing the charge separation and expanding the absorption of the dye sensitizer into the visible region (Vis).^[88,89] The Introduction of donor- π -acceptor (D- π -A) dyes into the active layers in solar cells could represent one particular solution to this issue, where a stronger donor such as anthracene, acridine, and other N-doped polyaromatic hydrocarbons could strongly cover the broad UV-Vis bands and the acceptor can efficiently increase the charge separation reaction.^[90-97] Hybrid organic-inorganic materials based on POMs appear to represent promising candidates as dyes for DSSCs due to their rapid electron transfer, tunable electrical and optical properties, and good redox stability upon cycling.^[61,64,98,99] In recent years, many novel donor- π -POM hybrid materials have been reported and their

structural, photonic, electrochemical, catalytic and magnetic properties explored.^[61,100] Among other POM derivatives, organoimido derivatives of hexamolybdate^[83,85] have attracted considerable attention due to the strong d- π interaction between the organic donor part (π -orbitals). The hexamolybdate cluster (d-orbitals) leading to changes in the position of the absorption band (red-shifted to the UV-Vis region) compared to that of parent POM, which may indicate synergistic properties.^[27,101–107] Thus, the organic–inorganic hybrid materials based on organoimido derivatives of hexamolybdate might be a good candidate for applications in DSSCs.^[108,109] In the past decade, Su and co-workers systematically studied the electronic and optical properties of a number of the POM-based organoimido derivatives of hexamolybdate and investigated their performance as DSSC dyes by means of quantum chemical DFT methods.^[109,110] In the past decade, we have experimentally explored the effects of Lindqvist POM-based organoimido additives on the photovoltages of the p-DSSCs.^[111] The incorporation of POMs as co-adsorbents produces substantial increases in V_{OC} in NiO p-DSSCs by up to 140% compared to poorly matched dyes and redox mediators.

1.7 A review of the dyes in DSSCs

The semiconductor used in DSSCs has a wide gap and is able to partially absorb UV light, resulting in an extremely poor efficiency.^[112] In order to fully utilize the sun's energy, a photosensitizer must be attached. This will allow the sun's absorption range to be expanded to include both visible light and IR light, significantly enhancing the power conversion efficiency (PCE) of DSSCs. The PCE of DSSCs depends heavily on dyes, which are also the heart and soul of the entire system. The dyes of DSSCs must adhere to the following requirements:^[113]

- Functional groups like carbonyl C=O, sulfonic, or phosphate groups [PO

$4]^{3-}$ should be present in dyes such that they can be safely adsorbed on the semiconductor oxide surface.

- The potential of the dyes oxidation states has to be high enough to allow the redox electrolyte to take the electrons.
- The energy levels of the dye's excited state and the CB of the semiconductor oxide should coincide.
- High stability and a greater molar extinction coefficient are required for dyes.

Several research teams have created and produced a variety of novel dyes for DSSCs in the advances of recent decades. The DSSCs use both natural and artificial dyes; artificial dyes are further divided into metal-organic complex and metal-free organic dyes.^[114]

The pure of the organic dyes and the complex of metal organic dyes, which have experienced significant advancements, make up the majority of the organic dyes.^[115-118] The standard dye at the time was tris(2,2-bipyridyl-4,4-carboxylate) ruthenium(II), the function of the carboxylate being the attachment by chemisorption of the chromophore to the oxide substrate. Progress thereafter, until the announcement in 1991 ^[119,120] of the sensitized electrochemical photovoltaic device with a conversion efficiency at that time of 7.1% under solar illumination, was incremental, a synergy of structure, substrate roughness and morphology, dye photophysics^[121] and electrolyte redox chemistry. That evolution has continued progressively since then, with certified efficiency now over 10%.^[122] Metal-organic dyes, such as cis-[Ru(2,2'-bipyridyl-4,4'-dicarboxylic acid)₂(NCS)₂] coded (N3) and (Bu₄N)₂[Ru(2,2'-bipyridyl-4,4'-dicarboxylic acid)₂(NCS)₂] coded (N719) (Fig. 1.13)

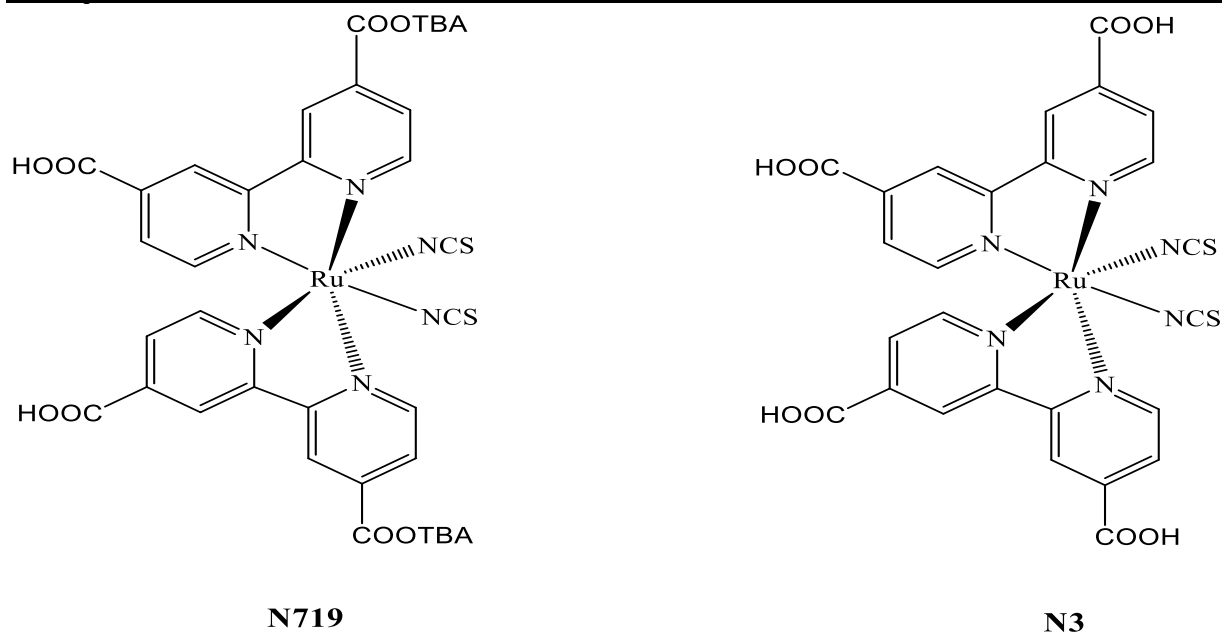


Figure 1.13 Structure of N3 and N719

In recent years, inorganic dyes such as Potassium Ferrocyanide (Fig. 1.13) have highly drawn the interest since they are less expensive, simpler to synthesize, and more stable against light and heat than organic dyes. In recent investigations, inorganic dyes mostly consist of polyoxometalates (POM), quantum dots, and precious metal nanoparticles.^[123,124]

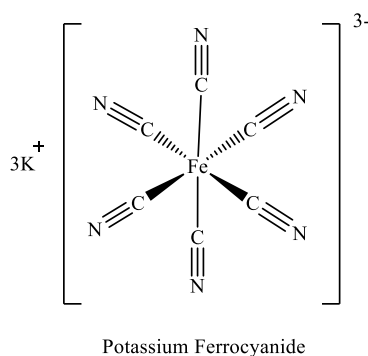


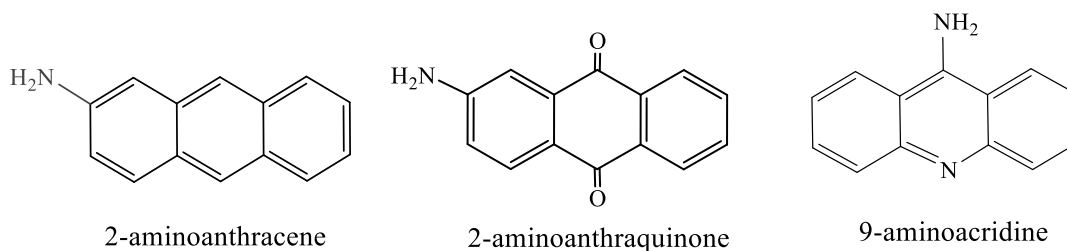
Figure 1.14 Some of Inorganic dye

Their semiconductor-like property is one of the most crucial characteristics of POMs.^[125] POMs are inorganic semiconductors because they have an energy band

structure that is comparable to that of metal oxides. A good match between their LUMO and HOMO energy levels and the energy levels of semiconductors may be achieved by changing their structures and compositions. Therefore this control is possible. POMs may be an ideal type of inorganic dye. POMs are easy to prepare, have cheap preparation costs, and have strong structural, thermal, solubility, redox, and acid-base stabilities, all of which help to increase the stability of DSSCs. Strong adsorption on the surface of the semiconductor is enabled by the ease with which carboxyl groups, phosphate groups, etc. may modify the surface of POMs.^[64]

1.8 Aims of the study

In this study, novel dye-sensitizer complexes combining quinone, acridine, anthracene with Lindqvist POM-based organoimido-substituted hexamolybdates would be exploring as follows: -



Part I: -

- 1- Theoretical design and investigation of new hybrid compounds (organo-imido-hexamolybdate) using computational methods for photonic applications / as DSSCs
- 2- Examine the use of the designed systems as sensitizers in DSSCs by means of DFT/TDDFT methods.

Part II: -

Based on results from Part I, promising systems with interesting properties as sensitizers in DSSCs will be: -

- 1- Synthesis using DCC protocol with strong donors such as (quinone, anthracene, and acridine) derivatives.
- 2- Characterization of the synthesized compounds using FT-IR, UV-Vis, and ¹H NMR spectroscopies.
- 3- Study enhanced optoelectronic properties for these systems.

Chapter Two
Experimental
Part

2.1 Materials

All chemicals, reagents and solvents were provided from the commercial sources and summarized in (Table 2.1)

Table 2.1 Chemicals and their commercial sources

Chemicals	Molecular formula	M.Wt.g/mol	Purity %	Supplied Companies
2-Aminoanthraquinon	$C_{14}H_9NO_2$	223.23	98	Macklin, China
Tetrabutylammonium bromide	$C_{16}H_{36}NBr$	322.37	99	Macklin, China
<i>N, N</i>-Dicyclohexyl carbodiimide	$C_{13}H_{22}N_2$	206.33	99	Macklin, China
2-aminoanthracene	$C_{14}H_{11}N$	193.25	98	Macklin, China
2,6-Diaminoanthraquinon	$C_{14}H_{10}N_2O_2$	238.25	96	Macklin, China
Acridine-9-amine	$C_{13}H_{10}N_2$	194.23	98	Macklin, China
Dimethyl Sulfoxide anhydrous	C_2H_6OS	78.13	99	Sigma-Aldrich, Germany
Acetone	C_3H_6O	58.08	99	Techno PharmChem, India
Diethyl ether	$C_4H_{10}O$	74.12	99	Romil, UK
Hydrochloric acid	HCl	36.46	35	HiMedia, India

Chapter Two

Experimental Part

Acetonitrile	C_2H_3N	41.05	99	Supelco, Germany
Ethanol (abs.)	CH_3CH_2OH	46	99	Honey Well, USA

2.2 Instrumentation

Table 2.2 Instrumentation used and their details

No.	Instrumentation	Details	Location
1	FT-IR spectroscopy	Spectra were recorded using a (SHIMADZU FTIR-8400S, Japan) infrared spectrophotometer.	University of Kerbala, College of Science, Department of Chemistry
2	UV-vis spectroscopy	Measurements were performed by using a spectrophotometer (UV-1800, Kyoto, Japan).	University of Kerbala, College of Science, Department of Chemistry
3	NMR spectroscopy	1D and 2D NMR spectra were recorded at 298 K (\pm 1 K) using Bruker Advance III, 400 MHz instruments, Nuclear Magnetic Resonance Facility, Mark Wainwright Analytical Centre.	The University of New South Wales UNSW, Sydney, Australia. NMR.

2.3 Methods

All organic syntheses were performed using conventional Schlenk methods in a nitrogen or argon environment. Organoimido hexamolybdate derivatives were made

utilizing a method from the literature that was modified^[126] using typical Schlenk methods in an environment of dry nitrogen or argon.^[23] Melting points for all compounds are above 350 °C and over the apparatus limits.

2.4 Synthesis of Lindqvist-POM and its derivatives

2.4.1 Synthesis of $[(\text{C}_4\text{H}_9)_4\text{N}]_2[\text{Mo}_6\text{O}_{19}]$ (A)

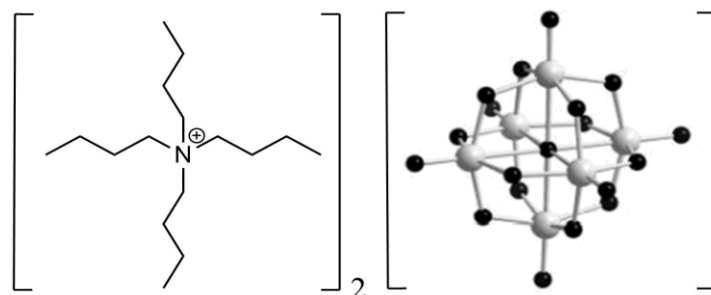
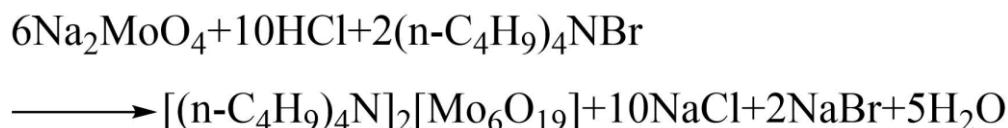


Figure 2.1 Structure of Compound (A)



Equation 2.1 synthesis of Compound (A)

Compound A was prepared using method that has already been published.^[127] Distil water (20 mL) was added to $\text{Na}_2\text{MoO}_4 \cdot 2\text{H}_2\text{O}$ (5.0 g, 20.01 mmol) and the mixture was acidified with 6M HCl. Then, a solution of tetrabutylammonium bromide (2.42 g, 7.5 mmol) in water (4 mL) and was added to the first solution and heated to 75 °C for 45 minutes to give a slurry which was developed to yellow solid. The crude was filtered and washed with water (3×40 mL). This precipitate was left to dry at the ambient temperature to yield yellow crystals were obtained by recrystallizing by using hot acetone and then washing with diethyl ether (2×20 mL). The final product was being vacuum-dried over 24 hours. ^[23]FTIR (cm^{-1}): 2962 cm^{-1} (m); 2874 cm^{-1} (m); 1465 cm^{-1} (m); 1381 cm^{-1} (m); 1176 cm^{-1} (vw); 1060 cm^{-1} (vw); 952 cm^{-1} (vs); 879 cm^{-1} (m); 786 cm^{-1} (vs); 740 cm^{-1} (m). UV-Vis: $\lambda_{\text{max}} = 326\text{nm}$

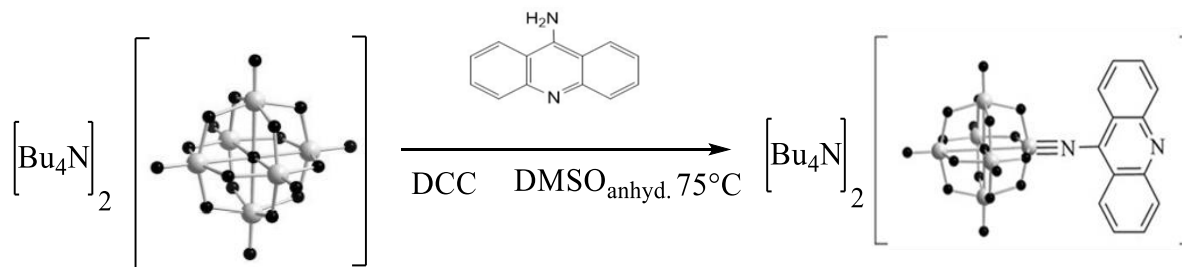
2.4.2 Synthesis of $[(C_4H_9)_4N]_2 [Mo_6O_{18}N_2C_{13}H_8]$ (1)

Figure 2.2 Synthesis of Compound (1)

A mixture of $[n-Bu_4N]_2[Mo_6O_{19}]$, (1.773 g, 1.3 mmol), Acridine-9-amine (0.194 g, 1 mmol), and 1,3-dicyclohexylcarbodiimide DCC (0.268 g, 1.3 mmol) in dry dimethyl sulfoxide DMSO (10 mL) was heated at 75 °C for 8 hours. After that time, the solid was filtered into a flask containing on ethanol (100 mL) and diethyl ether (100 mL) after cooling to ambient temperature. A precipitate of reddish orange was produced, it is obtained by filtration, and repeatedly washed with ethanol (10 mL) and ether (10 mL). After that recrystallization work with hot acetonitrile and being cleaned with diethyl ether and ethanol, the resultant solid produced a red solid. The final product was vacuum dried for 24 hours.^[23,126] FTIR (cm^{-1}): 2962.66 cm^{-1} (m); 2872.01 cm^{-1} (m); 1467.83 cm^{-1} (m); 1379.10 cm^{-1} (m); 950.91 cm^{-1} (vs); 785.63 cm^{-1} (vs); 740.67 cm^{-1} (vw). UV-Vis: $\lambda_{max} = 470nm$. 1H NMR: δ_H (400 MHz, CD_3CN) 8.50 (d, 2H, H_a), 7.99 (t, 2H, H_b), 7.80 (d, 2H, H_d), 7.55 (t, 2H, H_c), 3.19 (t, 16H, H_h), 1.50 (quintet, 16H, H_g), 1.23 (sex, 16H, H_f), 0.80 (t, 24H, H_e).

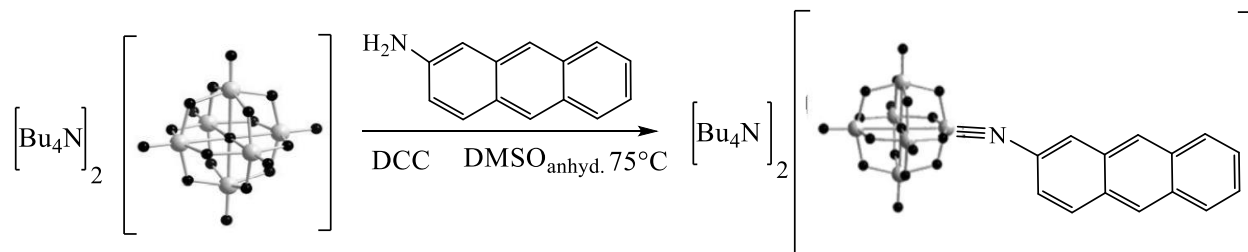
2.4.3 Synthesis of $[(C_4H_9)_4N]_2[Mo_6O_{18}NC_{14}H_9]$ (5)

Figure 2.3 Synthesis of Compound (5)

A mixture of $[n\text{-Bu}_4\text{N}]_2[\text{Mo}_6\text{O}_{19}]$, (1.773 g, 1.3 mmol), 2-Aminoanthracene (0.1932 g, 1 mmol), and 1,3-dicyclohexylcarbodiimide DCC (0.268 g, 1.3 mmol) in dry DMSO (10 mL) was heated at 75 °C for 8 hours. After that time, the solid was filtered into a flask containing on ethanol (100 mL) and diethyl ether (100 mL) after cooling to ambient temperature. A precipitate of brown was produced, it is obtained by filtration, and repeatedly washed with ethanol (10 mL) and ether (10 mL). After that recrystallization work with hot acetonitrile and being cleaned with diethyl ether and ethanol, the resultant solid produced a crimson solid. The final product was vacuum dried for 24 hours. ^[23,126]FTIR (cm^{-1}): 2962.79 cm^{-1} (m); 2874.03 cm^{-1} (m); 1465.95 cm^{-1} (m); 1381.08 cm^{-1} (w); 1311.64 cm^{-1} (vw); 949.01 cm^{-1} (s); 783.13 cm^{-1} (s). UV-Vis: $\lambda_{\text{max}} = 408\text{nm}$

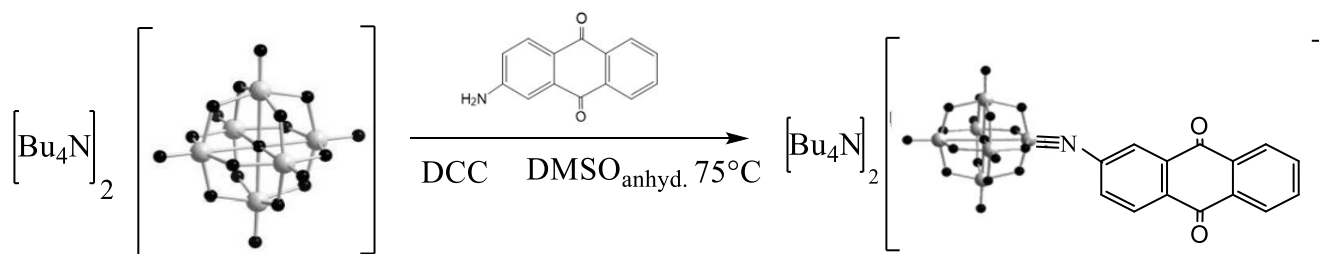
2.4.4 Synthesis of $[(C_4H_9)_4N]_2[Mo_6O_{20}NC_{14}H_7]$ (6)

Figure 2.4 Synthesis of Compound (6)

A mixture of $[n-Bu_4N]_2[Mo_6O_{19}]$, (1.773 g, 1.3 mmol), 2-Aminoanthraquinone (0.223 g, 1 mmol), and 1,3-dicyclohexylcarbodiimide DCC (0.268 g, 1.3 mmol) in dry DMSO (10 mL) was heated at 75 °C for 8 hours. After that time, the solid was filtered into a flask containing on ethanol (100 mL) and diethyl ether (100 mL) after cooling to ambient temperature. A precipitate of orange was produced, it is obtained by filtration, and repeatedly washed with ethanol (10 mL) and ether (10 mL). After that recrystallization work with hot acetonitrile and being cleaned with diethyl ether and ethanol, the resultant solid produced a red solid. The finished product was vacuum dried for 24 hours.^[23,126] FTIR (cm^{-1}): 2962.66 cm^{-1} (m); 2873.94 cm^{-1} (m); 1469.76 cm^{-1} (m); 1379.10 cm^{-1} (m); 950.91 cm^{-1} (vs); 788.89 cm^{-1} (vs); 740.67 cm^{-1} (m). UV-Vis: $\lambda_{max} = 326nm$. 1H NMR: δ_H (400 MHz, CD_3CN) 7.62 (d, 3H, H_a), 7.22 (t, 2H, H_b), 6.50 (d, 1H, H_c), 5.25 (s, 1H, H_d), 3.19 (t, 16H, H_h), 1.50 (quintet, 16H, H_g), 1.23 (sex, 16H, H_f), 0.80 (t, 24H, H_e).

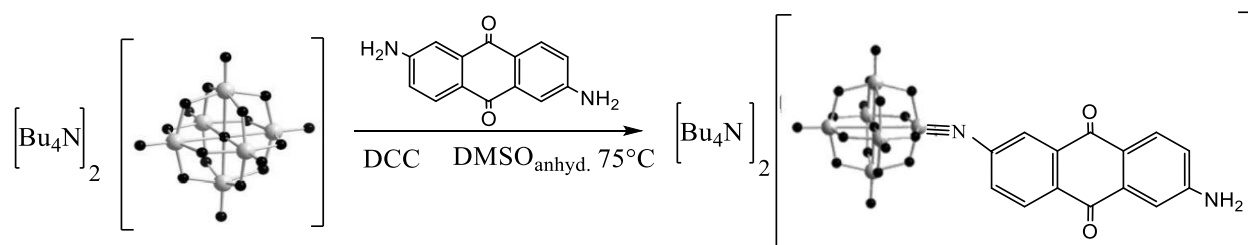
2.4.5 Synthesis of $[(C_4H_9)_4N]_2[Mo_6O_{20}N_2C_{14}H_8]$ (7)

Figure 2.5 Synthesis of Compound (7)

A mixture of $[n\text{-Bu}_4\text{N}]_2[\text{Mo}_6\text{O}_{19}]$, (1.773 g, 1.3 mmol), 2,6-Diaminoanthraquinone (0.238 g, 1 mmol), and 1,3-dicyclohexylcarbodiimide DCC (0.268 g, 1.3 mmol) in dry DMSO (10 mL) was heated at 75 °C for 8 hours. After that time, the solid was filtered into a flask containing on ethanol (100 mL) and diethyl ether (100 mL) after cooling to ambient temperature. A precipitate of orange was produced, it is obtained by filtration, and repeatedly washed with ethanol (10 mL) and ether (10 mL). After that recrystallization work with hot acetonitrile and being cleaned with diethyl ether and ethanol, the resultant solid produced brown crystals. The final product was vacuum dried for 24 hours.^[23,126] FTIR (cm^{-1}): 2962.66 cm^{-1} (m); 2873.94 cm^{-1} (m); 1467.38 cm^{-1} (m); 1379.10 cm^{-1} (m); 950.91 cm^{-1} (vs); 785.03 cm^{-1} (vs); 738.74 cm^{-1} (m). UV-Vis: $\lambda_{\text{max}} = 328\text{nm}$. ^1H NMR: δ_{H} (400 MHz, CD_3CN) 7.62 (d, 3H, H_a), 7.22 (t, 2H, H_b), 6.50 (d, 1H, H_c), 5.25 (s, 1H, H_d), 3.19 (t, 16H, H_h), 1.50 (quintet, 16H, H_g), 1.23 (sex, 16H, H_f), 0.80 (t, 24H, H_e).

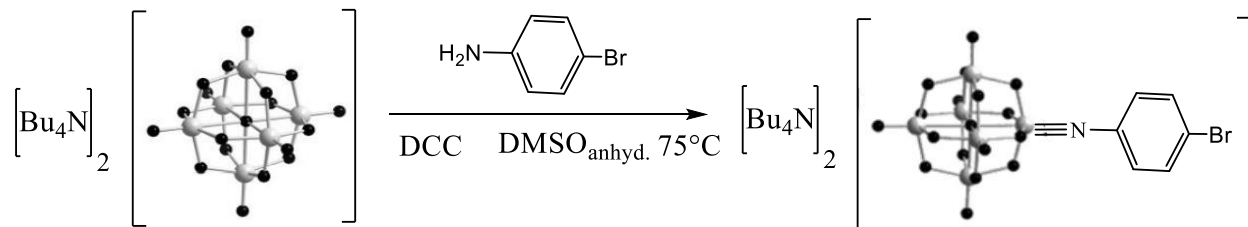
2.4.6 Synthesis of $[(C_4H_9)_4N]_2[Mo_6O_{18}NC_6H_4Br]$ (8)

Figure 2.6 Synthesis of Compound (8)

A mixture of $[n\text{-Bu}_4\text{N}]_2[\text{Mo}_6\text{O}_{19}]$, (1.773 g, 1.3 mmol), 4-Bromoaniline (0.172 g, 1 mmol), and 1,3-dicyclohexylcarbodiimide DCC (0.268 g, 1.3 mmol) in dry DMSO (10 mL) was heated at 75 °C for 8 hours. After that time, the solid was filtered into a flask containing on ethanol (100 mL) and diethyl ether (100 mL) after cooling to ambient temperature. A precipitate of reddish orange was produced, it is obtained by filtration, and repeatedly washed with ethanol (10 mL) and ether (10 mL). After that recrystallization work with hot acetonitrile and being cleaned with diethyl ether and ethanol, the resultant solid produced (orang crystals) a crimson solid. The final product was vacuum dried for 24 hours.^[23,126] FTIR (cm^{-1}): 2962.66 cm^{-1} (m); 2873.94 cm^{-1} (m); 1469.76 cm^{-1} (m); 1334.74 cm^{-1} (m); 948.98 cm^{-1} (vs); 781.17 cm^{-1} (vs); 738.74 cm^{-1} (m). UV-Vis: $\lambda_{\text{max}} = 341$

Chapter Three
Theoretical and
Computational Methods

3.1 Theoretical Background about quantum mechanics

Scientists have always been driven to develop a full theory that can be applied to the task of describing all physical occurrences. They discovered that classical physics could only be applied to a stunning number of actual issues, failing when things moved more quickly or shrunk dramatically. As one of the most reliable and potent theories now in use, quantum mechanics has therefore been widely used.

3.1.1 Quantum mechanics theories of calculations

The Schrodinger equation, which is the fundamental equation of all quantum mechanics, is the most used formula for representing quantum mechanics. Schrodinger's equation is provided in the straightforward case of non-time-dependent systems as follows:

$$\hat{H} \Psi = E \Psi \dots\dots (3.1)$$

Where E represents energy, H Hamilton factor, and Ψ wave function.^[128]

The following approximation techniques are the only ones that can be used to solve the Schrodinger equation for the molecular system.

- 1-Ab initio techniques of computation
- 2-Semi-empirical techniques
- 3-The DFT approach

3.1.2 Approximation via Born-Oppenheimer

The system's nucleus and electrons' positions affect the wavefunctions. However, a nucleus moves considerably more slowly than an electron since it is so much heavier than an electron (by around 1900 times). In this situation, they can be seen as frozen, with their kinetic energy set to zero, but they nevertheless add to the system's potential energy, which is called Born-Oppenheimer approximation. This is no longer reliant on anything other than the electrons' kinetic energy (T_e), the electron-nuclear attraction (V_{ne}) and electron-electron repulsion (V_{ee}). Through the thorough and accurate solution of the Schrodinger equation, which results in the acquisition of wave functions describing these systems, Schrodinger's equation is able to solve many small systems, including the hydrogen atom system and atoms with similar systems. This integrated treatment of the electron structure of the hydrogen atom and similar atoms was made possible. But other than the hydrogen atom, no other atom system can easily do this (one electron-nucleus system). The forces of the contending electrons, which create energy that is inversely proportional to the distance between electrons, will emerge for atoms with more than one electron revolving around the nucleus. As a result, solving all of the differential equations with this many variables becomes extremely challenging, if not impossible. This forces researchers to develop approximations that can be utilized to accurately answer the Schrodinger equation for these kinds of systems. Different theories, such the theory of perturbation and the theory of variance, can be employed to give an effective and integrated mechanism to solve the Schrodinger equation for complex systems.^[129]

3.1.3 Hartree-Fock (HF)

A clever trick to come to approximate solutions of Schrödinger equation (differential equation), called the Hartree-Fock method, is to take (Equ. 3.2) and add/subtract a constant term:

$$\hat{H} = -\sum_{i=1}^n \frac{1}{2} \nabla_i^2 - \sum_{i=1}^n \sum_{A=1}^N \frac{Z_A}{r_{iA}} + \sum_{i=1}^n V_{ri} + \underbrace{\sum_{i=1}^n \left(\sum_{j>i}^n \frac{1}{r_{ij}} - V_{ri} \right)} \dots \dots (3.2)$$

The physical reasoning behind it is the following: with a carefully selected potential $V(r_i)$ the term H_{pert} can become sufficiently small so that it can be neglected, although neither $\sum_{j>i} \frac{1}{r_{ij}}$ nor $\sum_{i=1}^n V(r_i)$ are separately small. When the function $V(r_i)$ has been determined, the Hamiltonian will be a sum of one-particle terms:

$$\hat{H} = \sum_{i=1}^n \hat{F}(i) \dots \dots (3.3)$$

Where

$$\hat{F}(i) = -\frac{1}{2} \nabla_i^2 - \sum_{A=1}^N \frac{Z_A}{r_{iA}} + V(r_i) \dots \dots (3.4)$$

Now the variables of the electrons are separated, the solution is obvious: $\Psi(r_1 \dots r_i)$ will be the product of the solutions of the one-electron eigenvalue equations $\hat{F}(i)\phi_k(i) = \epsilon_k \phi_k(i)$. The potential energy operator, $V(r_i)$, represents the averaged, repulsive energy that electron i feels, due to the presence of all other electrons. Electron i moves in the mean field created by all other electrons, an effective potential so to speak. By ‘replacing’ the inter-electronic repulsion term with a simple sum of one electron operators $V(r_i)$, the electrons can be treated as being separate and independent of each other. It is important to stress that this independent-electron

model is an approximation of reality, and the approximations are actually so severe, that quantitative results are rarely correct.

3.2 Density Functional Theory (DFT)

The Density Functional Theory (DFT) determines the electronic energy of the ground state by the electron density (ρ) and this implies the existence of a one-to-one correspondence between the electron density of a system and its energy.^[130] Incorporating the idea of molecular orbitals (MOs), the wave function approaches, like HF, offer helpful insights into the description of electronic configurations. But one drawback of wave function approaches is that we have to deal with a quantity that cannot be detected experimentally, forcing computational chemists to use intuitive approximations to explain the true state of the system under study. Frontier molecular orbitals analysis (FMOs) is one instance. In fact, chemists frequently characterize the behavior of molecules using just valence electrons, which is effective in many organic instances but insufficient for inorganic compounds where the contribution from inner electrons may be significant. The electron density notion provides a different approach of representing physical systems. The born interpretation of wavefunction derives from the fundamental rules of quantum physics that the chance of detecting a particle at a given point is related to the square of its wavefunction. The electron density may be used as a variable in contemporary quantum chemistry thanks to this assumption. Such a probability for an electron is actually determined by its electron density.^[131]

Many chemical processes, including those used to examine molecular levels, may be modeled using quantum mechanics. The Schrodinger's solution to the situation under investigation is approximated using a variety of methods. For the accurate and reliable calculation of many electronic systems, density functional theory (DFT)

approaches are at the highest level. Over the past two decades, DFT has evolved into the workhorse of computational physics and chemistry. Chemists and physicists may now research complicated and massive systems with high precision at low to moderate computing cost because to the ongoing development of high-quality exchange-correlation functional (XCFS). Despite the fact that DFT has a thorough understanding of a wide variety of typical systems. However, many chemicals continue to exist that have not yet been investigated.^[132] The most significant solids and thin film physical phenomenon, electronic-electronic stress, is studied using DFT. It works effectively for studying the microscopic characteristics of biological systems. Intensive state physics also uses DFT successfully. This theory is widely used since it operates by using miniaturization functions to identify the ground state and is straightforward and reliable in implementation. The Density Function Hypothesis Due to the tremendous capacity of the molecules, many processes were performed to determine their various characteristics.^[129]

3.2.1 Concept of Basis Set

The usage of a basis set (BS) is one of the most used approximations in approach to describe atomic orbitals. A set of functions known as a BS is utilized in quantum chemistry techniques like HF or DFT to approximate any wavefunction. It is important to keep in mind that if a BS is full, meaning it includes an unlimited number of functions, then expanding a wavefunction with it would not be an approximation. In practical computations, however, this is not possible, and the electrical wavefunction is approximated by a limited number of BS functions. A number of variables affect how accurate a BS is; for example, the representation will be worse the smaller the BS. Its performance is also influenced by the kind of basic functions. These elements are very significant.^[131]

A basis set is a collection of linearly coupled functions used to simulate molecular orbitals. Because the equations describing the molecular orbitals are otherwise highly challenging to solve, basis functions, which may be thought of as representing the atomic orbitals of the atoms, are added in quantum chemical computations. Using the base set is an approximation that causes error reduction. Reliable computational chemistry requires an understanding of how to manage and reduce error by using computational chemistry and an appropriate base set for the prepared compounds.

3.3 DSSCs Theoretical background

Based on the theoretical principles^[90], the efficiency of the DSSCs can be enhanced by optimizing the parameter of light-harvesting efficiency (LHE), hole-injecting efficiency (HJE), dye regeneration efficiency (DRE), and reducing charge recombination efficiency (CRE). The performance of the DSSCs can be estimated from the photon to current conversion efficiency (η) which depends on the short circuit current (J_{SC}), open circuit voltage (V_{OC}), incoming solar light falling on cell [P_{in}], and fill factor [FF], as shown in (Equ. 3.5):

$$\eta (\%) = \frac{J_{SC} \times V_{OC} \times FF}{P_{in}} \dots \dots \dots (3.5)$$

The LHE can be calculated from the oscillator strength (f) of the dye corresponding to λ_{max} following (Equ. 3.6):^[133,134]

$$\text{LHE} = 1 - 10^{-f} \dots \dots \dots (3.6)$$

The free energy of the HJE (ΔG_{inj}) can be determined from (Equ. 3.7):^[133,135]

$$\Delta G_{inj} = (E^{dye} - E_{00}) - E_{CB} \dots \dots \dots (3.7)$$

Where E^{dye} is the oxidation potential energy of the dye in the ground state, E_{00} is the electronic vertical transition energy corresponding to the λ_{max} , while E_{CB} is the

reduction potential of the conduction band of TiO₂ ($E_{CB} = -4.00$ eV). Based on Marcus' theory,^[136] reorganization energies for both electron (λ_e) and hole (λ_h) were computed according to the following:^[90]

$$\lambda_i = [E_0^\pm - E_\pm^\pm] + [E_\pm^0 - E_0] \dots \dots \dots (3.8)$$

Where E_0^\pm is calculated the cation/anion using the optimized structure of the neutral molecule, E_\pm^\pm is the cation/anion energy calculated with the optimized cation or anion structure, E_\pm^0 is neutral molecule energy calculated at the cationic or anionic state, and the E_0 is the energy of the neutral molecule at ground state. Finally, V_{oc} which explains the overall strength of voltage in any optical material, can be approximated in eV by the energy difference between E_{LUMO} and E_{CB} in theoretically^[133,135]:

$$V_{OC} = E_{LUMO} - E_{CB} \dots \dots \dots (3.9)$$

3.4 Computational details

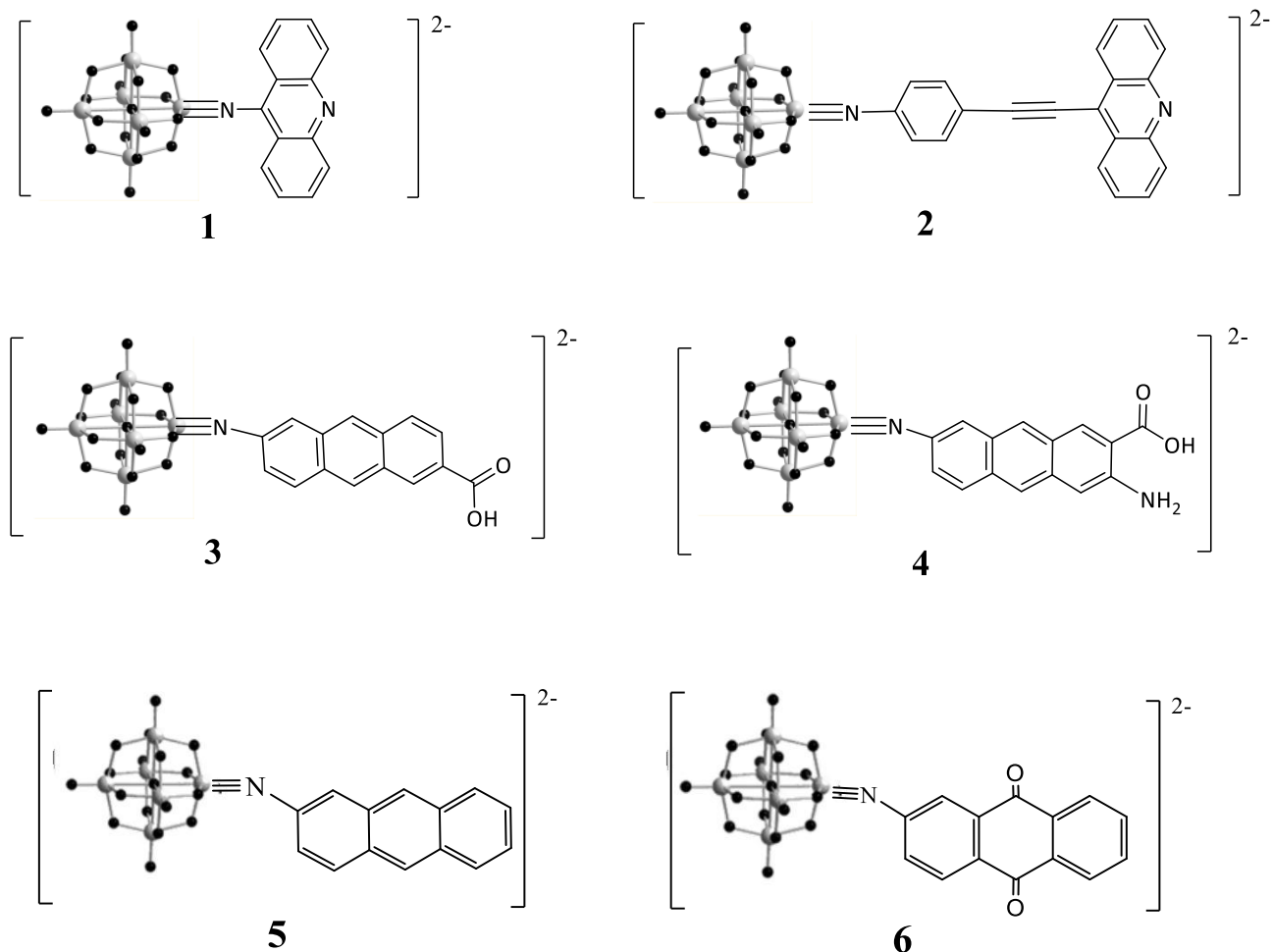
All computations in this work were done remotely using the High Performance Computing Cluster (HPC) at UEA, which is sponsored by the Research and Specialist Computing Support service, and the Gaussian16 suite.^[137] For geometry optimizations of the ground states and positive and negative ions were performed using the range-separated hybrid functional ω B97XD^[138] (uses Grimme's D2 dispersion model) with the 6-311+G(d)^[139,140] basis set for C, H, N, O. On the other hand, LANL2TZ^[141,142] was implemented for Mo atoms. These geometry optimizations were firstly carried out in the gas phase, and afterward single point energy at the same level of theory with SMD solvation model by Truhlar and coworkers^[143] in acetonitrile were performed. The electronic absorption was calculated using the same level of theory mentioned above in acetonitrile, where

50:50 mix of singlet/triplet of 100 lowest energy transitions were calculated. Significant transitions were only considered. To better understand the charge transfer mechanism of the studied chromophores and HOMO-LUMO analysis was also performed. Using the Multiwfn program,^[144] Guido's charge-transfer lengths (r) were calculated in accordance with the method outlined by Guido et. al.^[145]

Chapter Four

Results & Discussion

Lindqvist POMs may be derivatized by substituting or derivatizing the terminal oxygens of hexamolybdate with a variety of nitrogen-containing ligands, such as organoimido $[\text{NR}]^{2-}$ species, producing hybrid materials with promising and complementary characteristics.^[61,146] The goal of this research is the development of novel organoimido hexamolybdate derivatives (Fig. 4.1) for use as optoelectronic materials. This chapter discusses the design, investigation and synthesis of novel series of organoimido Lindqvist derivatives with a variety of organic donors as dyes



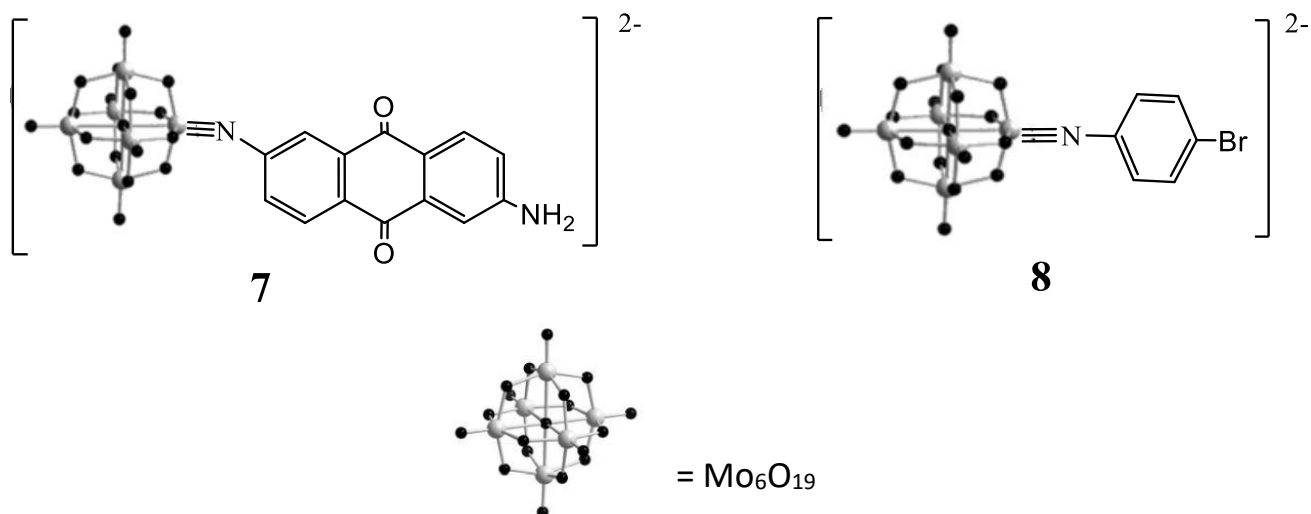


Figure 4.1 Structures of Lindqvist-POMs derivatives.

Part I:-

4.1 Theoretical design & Investigation

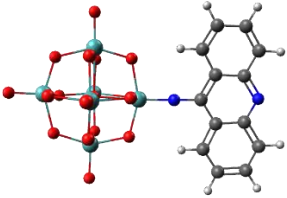
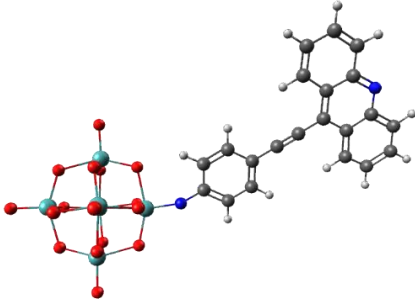
4.1.1 Molecular Geometric Structure

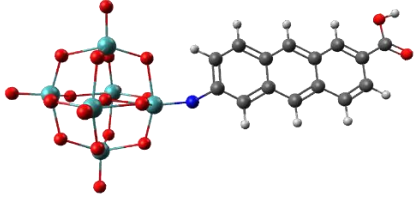
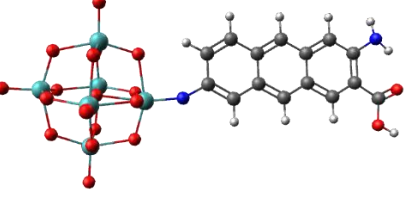
The Chemical reactivity and chemical properties are affected by the change in molecular structure. Therefore, the effect of replacing the organic donors (R-NH₂) with the oxo groups (M=O) of hexamolybdate have been studied. For geometry optimizations of the ground states and positive and negative ions were performed using the range-separated hybrid functional ω B97XD^[138] (uses Grimme's D2 dispersion model) with the 6-311+G(d)^[139,140] basis set for C, H, N, O. On the other hand, LANL2TZ^[141,142] was implemented for Mo atoms. Geometric structures of the as-studied molecules of as obtained by calculations are presented in (Table 4.1) Selections of the most important structural parameters of all molecules are listed in (Table 4.2), and the full details of geometric.

In this work all dyes **1-8** have been explored using DFT studies. However only dyes **1-4** were successfully optimized at hence been further studied (Table 4.1), based on the

Lindqvist POM conjugated acridine, anthracene, with anchoring groups, pyridine, and carboxylate, respectively, for TiO₂ electrode were carefully selected in order to investigate the properties of DSSCs via the DFT/TDDFT method. Dye **1** and dye **2** are the POM-based acridine derivatives, where in the latter a π -spacer was introduced to investigate the effect of π -bridge length. On the other hand, dye **3** and **4** are POM-based anthracene derivatives that are without and with an amino group, respectively. The amino group was introduced in order to red-shift the maximum absorption in the UV-vis spectra. The resultant bond lengths and angles are in good agreement with typical imido species. Compared to species **2-4**, species **1** show more linear Mo \equiv N-C bonding, which could be attributed to the steric hindrance of the side-phenyl rings of the acridine. The optimized structures of dyes **1-4** from the calculations at the ω B97XD/6-311+G (d)/LANL2TZ level of theory with SMD/acetonitrile.

Table 4.1 Optimized structures of derivatives **1** to **4**.

1		Acridine-imido-hexamolybdate
2		Acridine-9-Phenylactylene-imido-hexamolybdate

3		Aminoanthracene-imido-hexamolybdate
4		2-amino-3-carboxylantracene-imido-hexamolybdate

Gray = C, cyan = Mo, white = H, blue = N, and red = O

Table 4.2 Calculated geometrical parameters (distances (Å) and angles (°)) for compounds **1-4**.

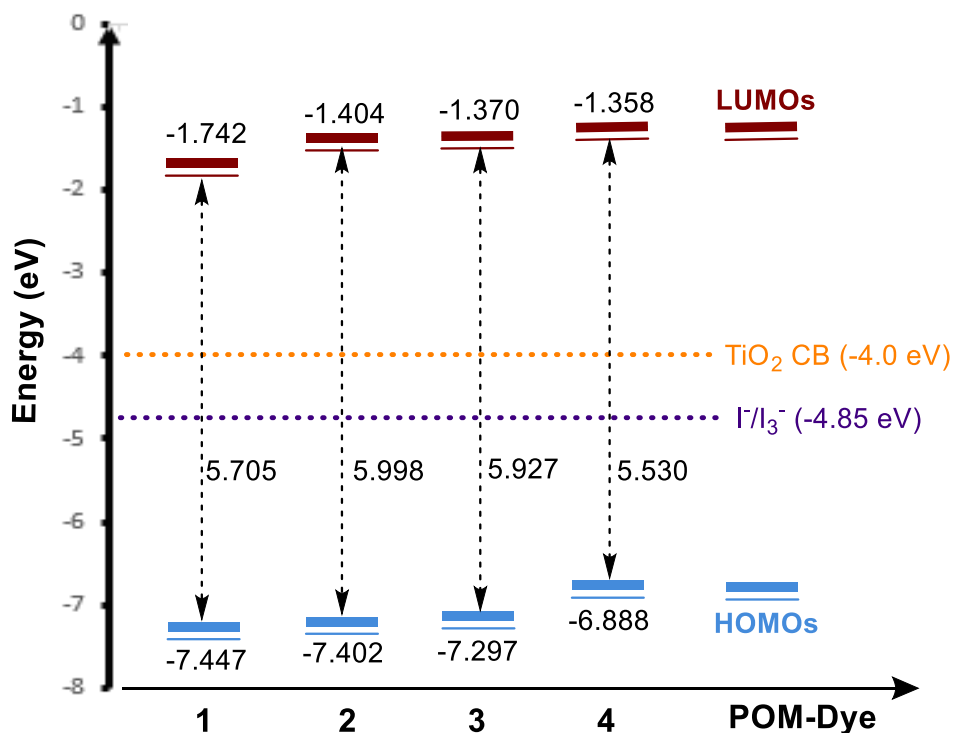
Geometric Parameters	1	2	3	4
Mo≡N-C	177.0	154.8	154.9	155.5
Mo≡N	1.790	1.767	1.765	1.761
N-C	1.342	1.356	1.395	1.363
Mo_{imido}-O_c^a	2.222	2.193	2.194	2.196
Mo-O_c^a	2.402	2.396	2.396	2.396
Mo=O^b	1.712	1.694	1.694	1.694

a Central oxygen. b Average of Mo=O lengths in calculated structures

4.1.3 Electronic Structure of derivatives 1 to 4.

Generally, based on the n-type DSSCs principle, the HOMO energy level of the dyes must be lower (more negative) than the redox couple of I^-/I_3^- of -4.80 eV to enable fast and effective dye regeneration while also improving charge-hole separation, while the LUMO energy should be greater than -4.00 eV, which is the conduction band of TiO_2 to generate charges. (Scheme 4.1) displays the HOMO and LUMO energy levels for dyes **1-4**. It can clearly be seen from that the HOMO energy levels of dyes **1-4** are more

negative than the redox of I^-/I_3^- and the LUMO energy levels are higher than the conduction band of TiO_2 , suggesting these dyes to match the requirements of n-type DSSCs. The HOMO levels decrease in the order $4 > 3 > 2 > 1$, and the LUMO levels also decrease in the order $4 > 3 > 2 > 1$. System **1** has the lowest HOMO and LUMO levels with a HOMO-LUMO energy gap of 5.705 eV, while in system **2**, in which the π -spacer was introduced, both the HOMO and LUMO levels are raised compared to system **1**, but with a larger energy gap of 5.998 eV (with differences of 0.045 eV for the HOMO and 0.338 eV for the LUMO levels). However, comparing system **3** with its analogue **4** where the amino group (donor group) is introduced, both the LUMO and HOMO energies increased, with the smallest with SMD/acetonitrile for solvation effects.



Scheme 4.1 Calculated HOMO and LUMO energy levels for dyes 1–4.

4.1.4 Electronic Absorption Spectra and Molecular Orbitals

TDDFT was employed to investigate the optical properties, such as the absorption wavelength and coefficient of the studied systems, at the ω B97XD/6-311+G(d)/LANL2TZ level of theory with SMD/acetonitrile for solvation effects. The UV–visible absorption spectra of the dyes **1-4** show that the absorption band ranging between 390 nm and 495 nm (Fig. 4-2 to 4-5). These bands are a result of the donor segment's confined (high energy) aromatic π - π^* transition and organic donor to POM intramolecular charge transfer (ICT) electronic transitions [147,148]

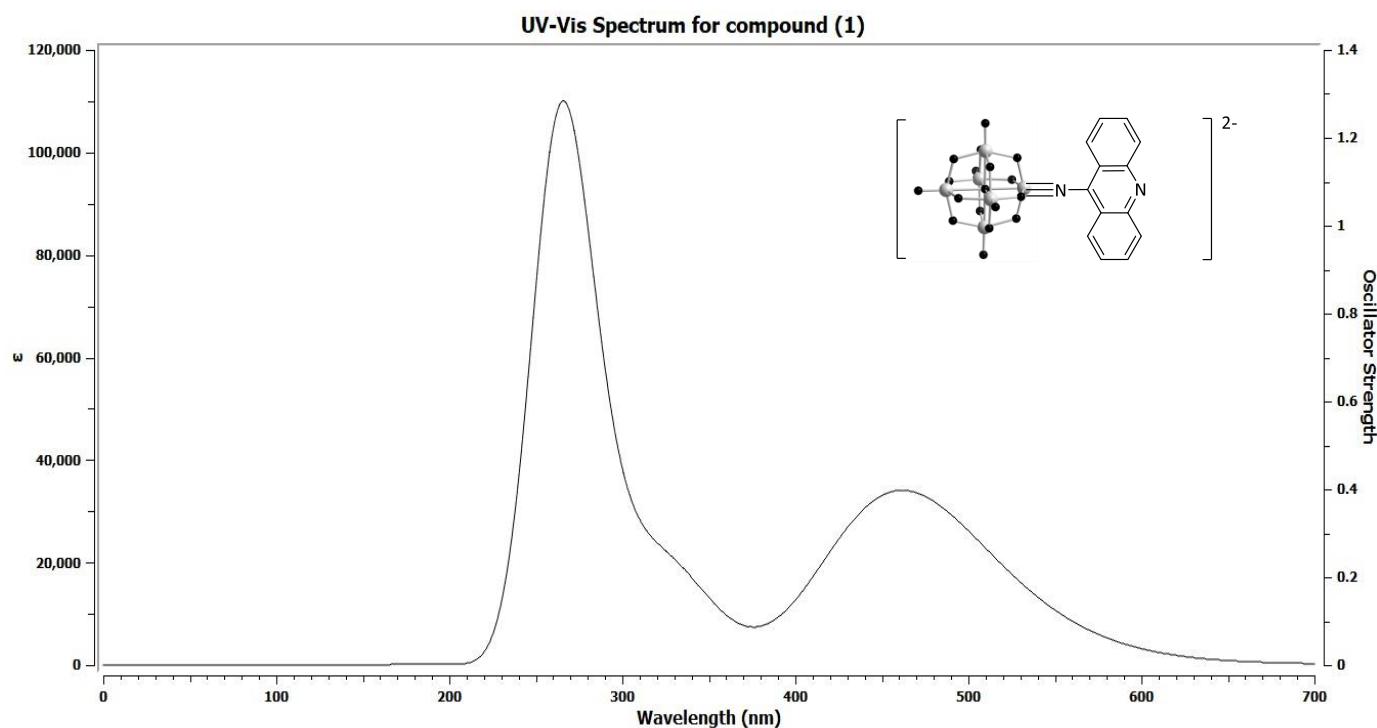


Figure 4.2 Uv-vis Computational Calculations for Compound (1)

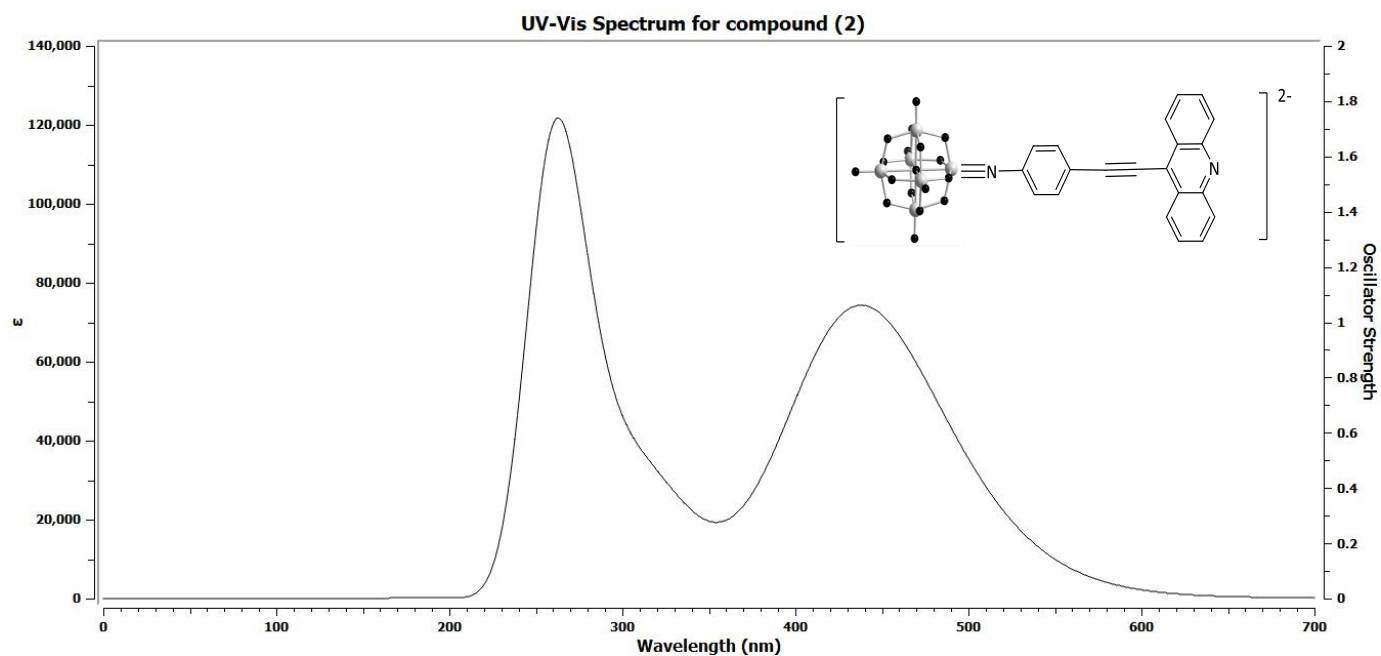


Figure 4.3 Uv-vis Computational Calculations for Compound (2)

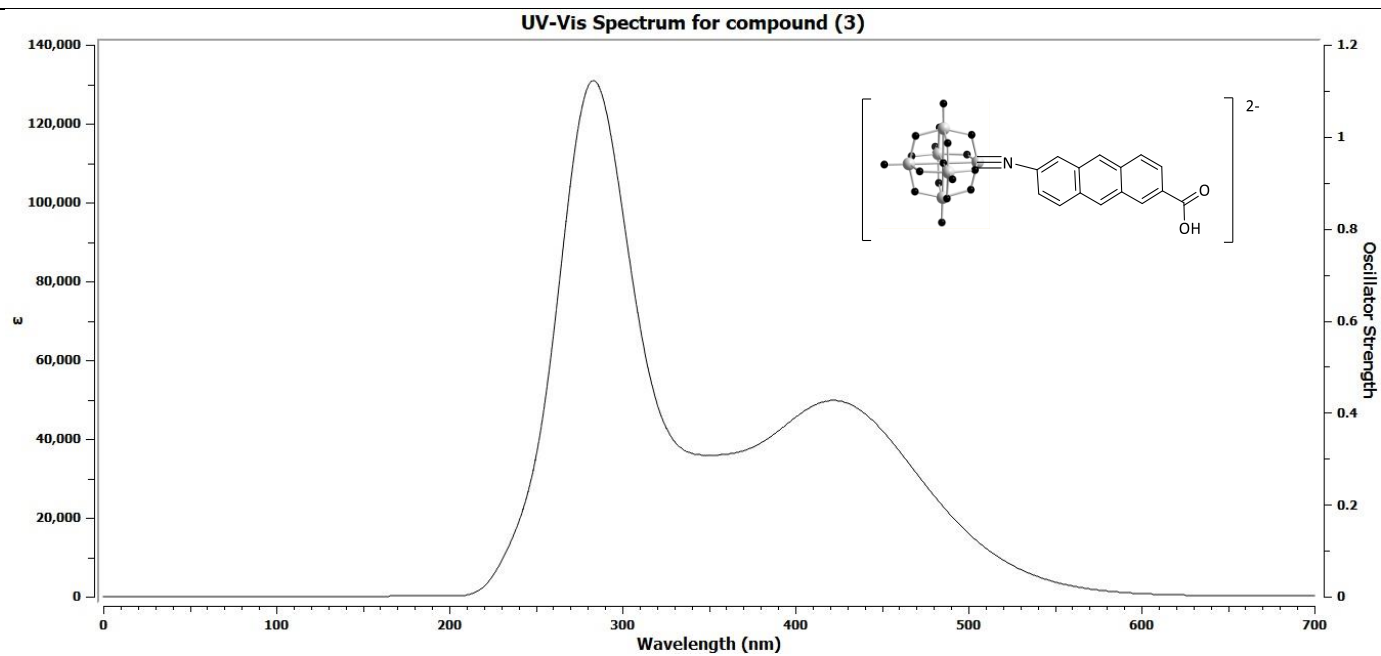


Figure 4.4 Uv-vis Computational Calculations for Compound (3)

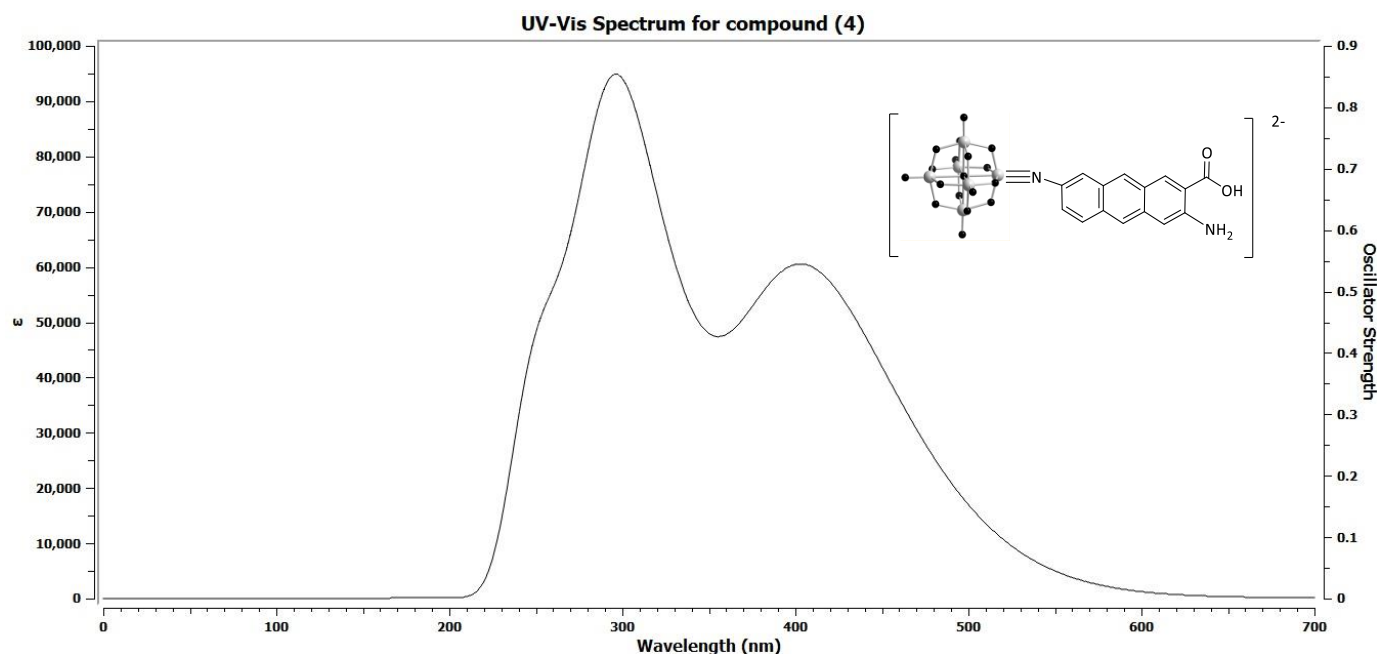


Figure 4.5 Uv-vis Computational Calculations for Compound (4)

Table 4.3 presents the computed maximum absorption wavelength (λ_{\max}), oscillator strength (f_{os}), electronic transition energy (E_{\max}), and the percentage molecular orbital contribution in the excitation. For all systems, the low-energy absorption band is produced by a single excited state. Based on λ_{\max} , all systems **1-4** have absorption bands in visible range from 420 nm to \sim 494 nm, with relatively high oscillator strengths despite system **4**, where **1** (POM-acridine system) has the largest maximum absorption wavelength λ_{\max} of 494 nm with $f_{\text{os}} = 0.8657$ and $\Delta r = 3.66 \text{ \AA}$. The computed absorption spectrum for **1** is in good agreement with the preliminary experimental results (see Part II (4.2.4)). Interestingly, introducing π -linker in system **2** is blue shifted by 54 nm in λ_{\max} and an increase in f_{os} by a factor of ≈ 2.1 and Δr by a factor of ~ 2 compared to system **1**. This is consistent with our previous published work.^[103,149,150] The blue shift could be attributed to the greater HOMO-LUMO gap for species **2** due to the increase in the charge separation between donor and acceptor, resulting in raising the energies of the POM-based orbitals (LUMOs), upon π -spacer enlargement. For POM-anthracene systems, a slight red shift of 23 nm in λ_{\max} for **4** was noted upon the

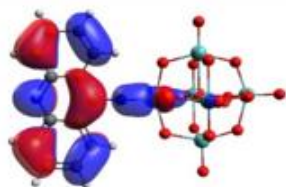
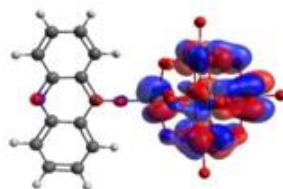
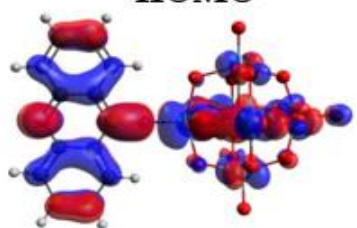
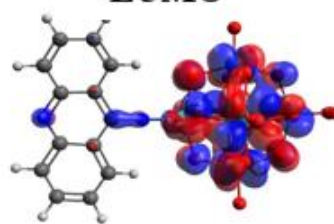
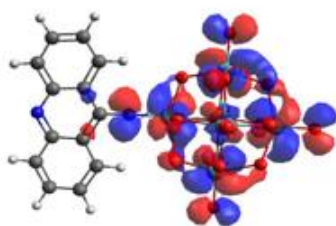
introduction of amino group compared to **3**, which is consistent with the smaller HOMO-LUMO gap due to the donating effect of $-NH_2$ group, leading to an increase in the energies of the aryl-based orbitals (HOMO)

Table 4.3 Calculated maximum absorption wavelength (λ_{max}), oscillator strength (f_{os}), electronic transition energy (E_{max}), and the percentage MO contribution.

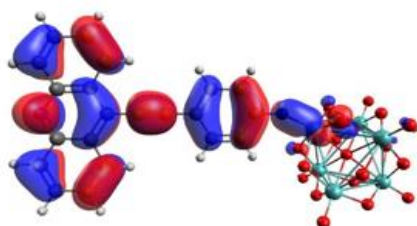
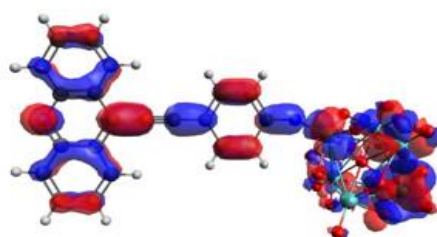
Compound	n	λ_{max} (nm)	E_{max} (eV)	f_{os}	E_{HOMO}	E_{LUMO}	$E_{HOMO-LUMO}$ gap (eV)	Δr Å	Transition	Contribution %
1	2	494	2.508	0.865	-7.447	-1.742	5.705	3.644	HOMO→LUMO	9
									HOMO→LUMO+1	77
									HOMO→LUMO+2	3
									HOMO→LUMO+7	5
2	3	440	2.8195	1.791	-7.402	-1.404	5.998	6.924	HOMO→LUMO	50
									HOMO→LUMO+1	21
									HOMO→LUMO+2	6
									HOMO→LUMO+4	7
									HOMO → LUMO+7	4

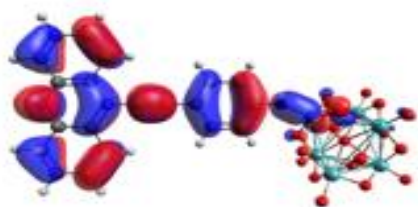
3	5	428	2.8935	1.1336	-7.297	-1.37	5.927	6.087	HOMO → LUMO	10
									HOMO → LUMO+1	7
									HOMO → LUMO+3	52
									HOMO → LUMO+5	11
									HOMO → LUMO+7	17
									HOMO → LUMO+8	8
4	4	451	2.7492	0.5068	-6.888	-1.358	5.53	6.733	HOMO-1 → LUMO	3
									HOMO-1 → LUMO+2	30
									HOMO-1 → LUMO+4	20
									HOMO-1 → LUMO+5	4
									HOMO → LUMO+6	24
									HOMO → LUMO+7	7

(1)

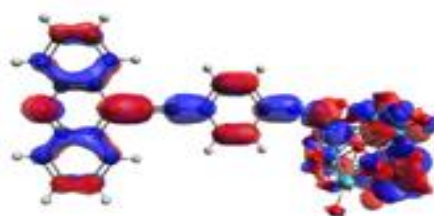
**HOMO****LUMO****LUMO+1****LUMO+2****LUMO+7**

(2)

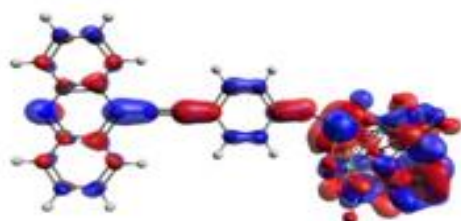
**HOMO****LUMO**



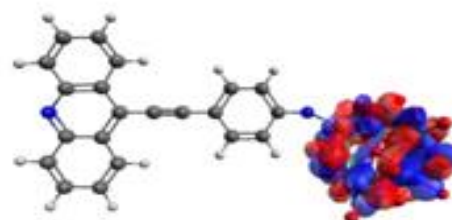
HOMO



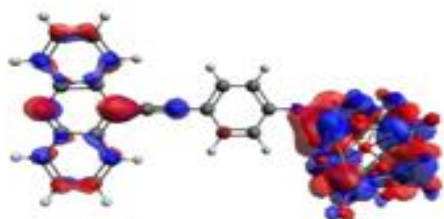
LUMO



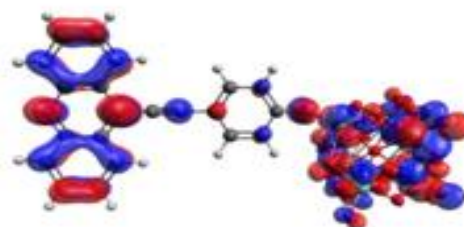
LUMO+1



LUMO+2

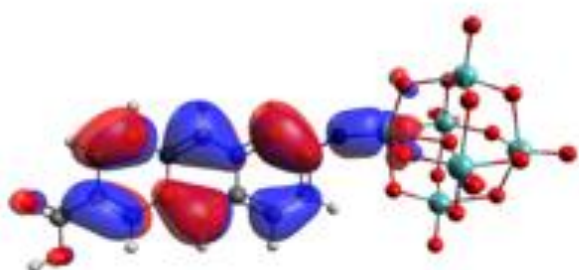


LUMO+4



LUMO+7

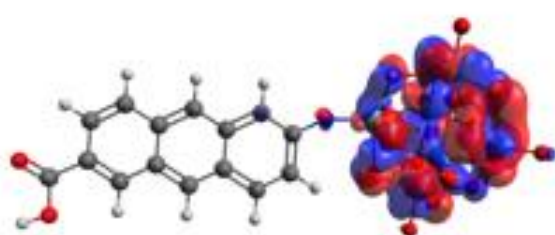
(3)



HOMO



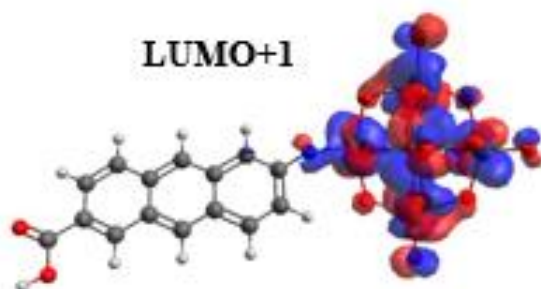
LUMO



LUMO+1



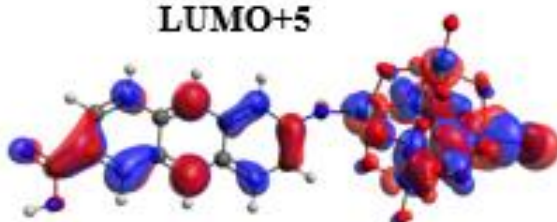
LUMO+3



LUMO+5



LUMO+7



LUMO+8

(4)

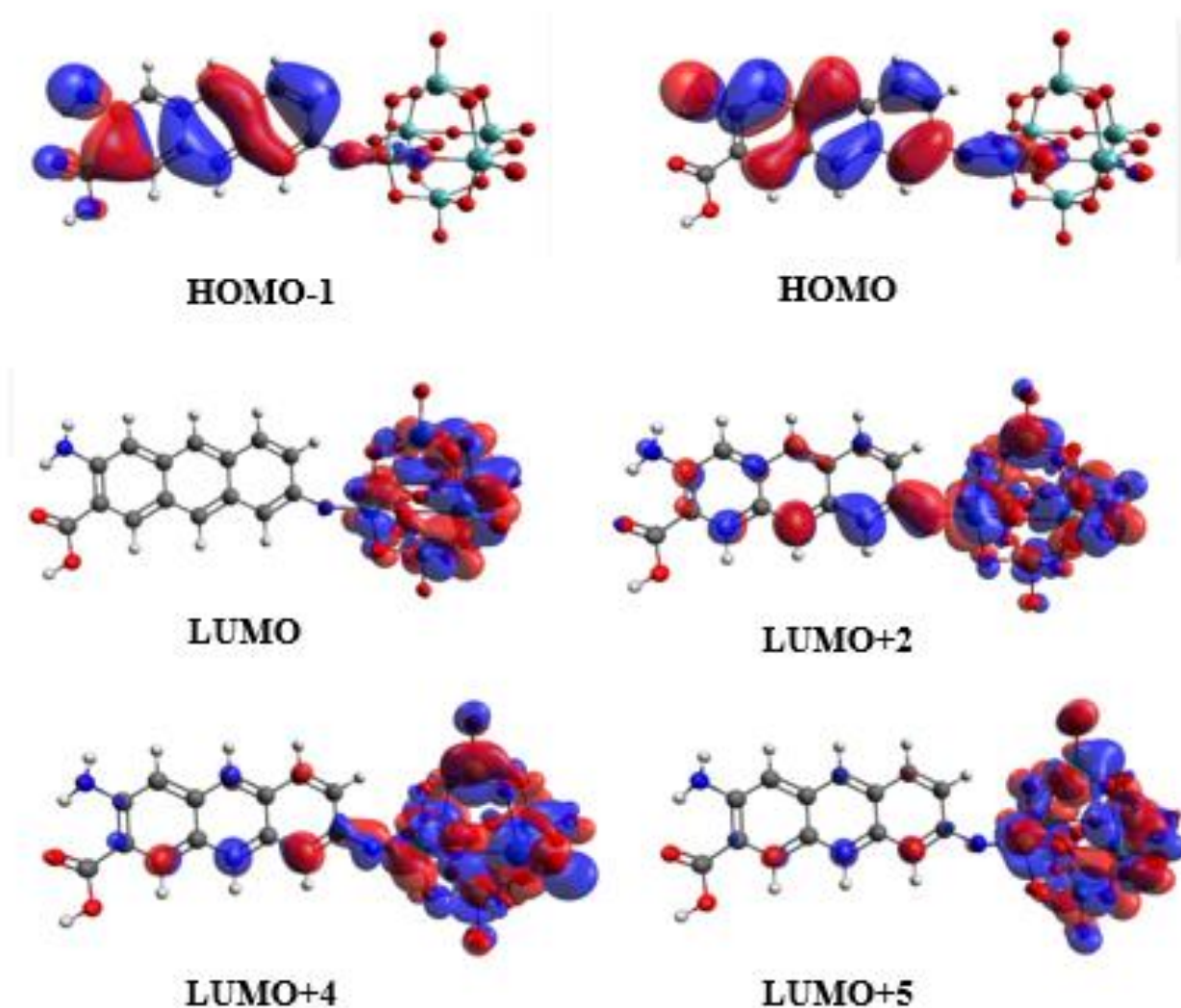


Figure 4.6 Representation showing the changes in **HOMO** and **LUMO** energies caused by varying the electron donor strength for compounds **1-4**.

To further investigate the intermolecular charge transfer (ICT) characteristics of the studied systems, analysis of the molecular orbitals (MOs) was performed. The electron densities for HOMOs and LUMOs involved in the transitions in system **1-4**. For all systems, both HOMO and HOMO-1 donor orbitals spread from the acridine/anthracene donors, including anchoring groups, to the imido bond. LUMOs are significantly

localized on the POM acceptor with some imido group and organic donor character. Upon excitation, the electron density and the corresponding $\Delta\rho$ is transferred from the donor acridine/anthracene part to the POM acceptor cluster, as shown in (Fig. 4.7). This clearly indicates that the strong charge transfer is due to an electronic transition from the donor (acridine and anthracene) to the POM cluster, which is further supported by the large Δr for all dyes.

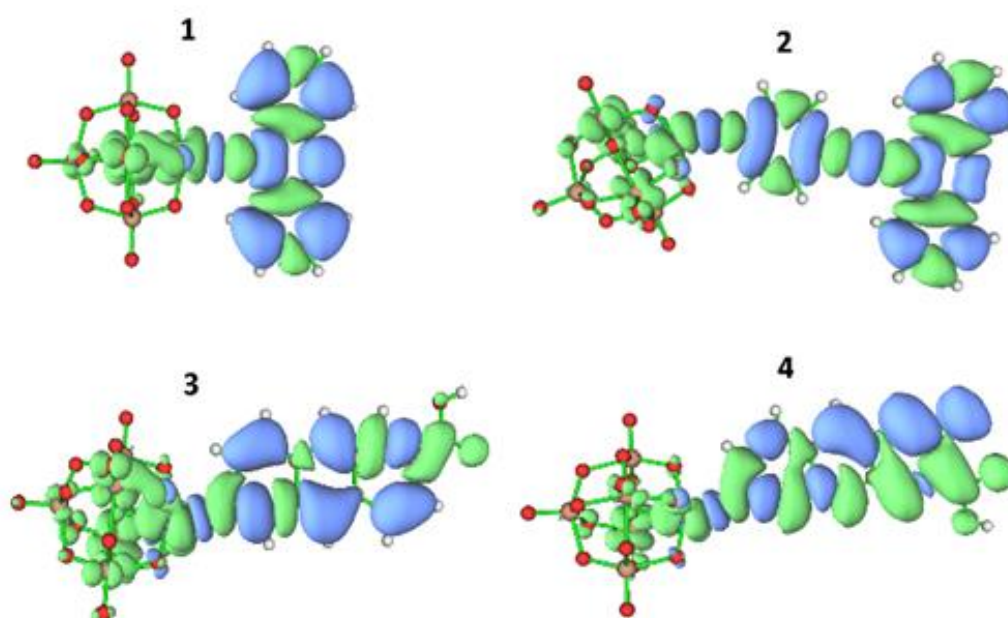


Figure 4.7 Excitation-induced charge density difference ($\Delta\rho$) for compounds **1-4** in their main excited states (isovalue = 0.0002 au; green and blue corresponds to positive and negative $\Delta\rho$, respectively. Upon excitation, transfer of the induced electron occurs from blue to green).

4.1.5 Photovoltaic Performance

Based on n-type DSSCs principles, high LHE, Φ_{inj} , and DRE with low CRE are important in terms of enhancing J_{sc} and ultimately lead to an increase in η of the DSSCs. Moreover, it is well-known that small reorganization energies, λ_h and λ_e , are crucial to increase the charge transfer rate. Therefore, ΔG_{inj} , LHE, V_{oc} , λ_h and λ_e of dyes **1-4** are computed, as presented in (Table 4.4). It can be observed from table

(Table 4.4) that the LHEs for dyes **1-4** range from 0.6887 to 0.9838, which are relatively high compared to other imido hexamolybdate-based dyes described in the literature. ^[109,110,151] The result indicates that dye **2** has a relatively high LHE and hence high η performance.

Table 4.4 Calculated photovoltaic parameters

No.	E^{dye^*} eV	E_{max} eV	ΔG_{in} eV	LHE	V_{oc} eV	λ_h eV	λ_e eV
1	3.153	2.508	-0.846	0.863	2.25	-0.50	-0.97
2	2.959	2.819	-1.040	0.983	2.59	-0.66	-1.21
3	2.624	2.893	-1.375	0.926	2.63	-0.53	-1.40
4	2.388	2.749	-1.611	0.688	2.64	-0.38	-1.25

ΔG_{inj} , λ_h and λ_e values are negative, which is advantageous for dye regeneration and electron injection. The ΔG_{inj} of dyes **1-4** show more negative values (in the order of **4** < **3** < **2** < **1**) compared to other dyes that have been reported in the literature. ^[36] The negative values of ΔG_{inj} means that the energy levels of the excited states of dyes lie above the E_{CB} of TiO_2 leading to high electron injection efficiency from the excited dye to the conduction band of TiO_2 . ^[152] The dyes examined are relevant as n-type materials for DSSCs since the values of λ_e (reorganization energy for electron transport) are significantly smaller than the λ_h (reorganization energy for hole transport) values. ^[153] Dye **3** shows the smallest λ_e indicating **3** has the highest yield with regard to electron injection. It was also found that all dyes **1-4** showed relatively high V_{OC} , in the order **4** > **3** > **2** > **1**. Dye **4** has an essentially similar V_{OC} (~2.64 eV) to dye **3**, while the LHE for **4** is smaller than dyes **1**, **2**, and **3** as discussed above. Therefore, by considering LHE, V_{OC} , ΔG_{inj} , λ_h , λ_e and absorption spectrum

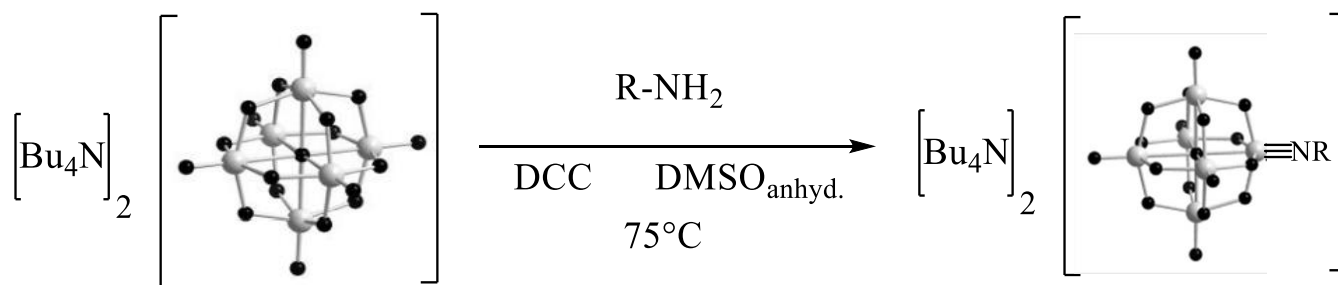
parameters, we expect that dyes **2** and **3** will have higher η and better performance in DSSC than the others, where **2** is the most promising candidate in this regard.

Part II:-

4.2 Experimental Results and Discussion

4.2.1 General Synthesis

Five Lindqvist-derived dyes were synthesized using a method previously described in the literature^[127] using DCC-mediated coupling of $[n\text{-Bu}_4\text{N}]_2[\text{Mo}_6\text{O}_{19}]$ (**A**) with amines to produce a novel series of organoimido hexamolybdate derivatives B–F illustrated in (Fig. 4.1) The Procedures for the reaction of hexamolybdate with organic compounds as described in (Fig. 2-2 and 2-6) was used with DCC and anhydrous DMSO as a solvent. The reaction was carried out by linking hexamolybdate with nitrogen atoms in the donor (forming an imido bond) after withdrawing a water molecule with the aid of DCC. The reaction was carried out in the Schlenk line technique using inert conditions using nitrogen gas (Scheme 4.2). Purification (recrystallization) and characterization of all products were performed using FTIR, ^1H NMR and UV-Vis.



Scheme 4.2 Synthesis of novel **organo-imido Lindqvist POMs**.

4.2.2 Characterization of the synthesized compounds using FT-IR spectrum

4.2.2.1 Compound (A)

Hexamolybdate was synthesized as (Equ. 2.1) in chapter two. Identity was confirmed by its FT-IR spectrum and ^1H NMR spectrum. The yield was yellow crystals, (Fig. 4.8) shows FT-IR spectrum of compound (A) that showed a good evidence that the reactions occurred successfully through appearing a strong band at the range 952 cm^{-1} and 786 cm^{-1} attributed to the Mo=O and Mo-O bonds.^[154] Bands at 2982 and 2874 cm^{-1} are attributed to C-H stretching for CH_2 and CH_3 groups of the tetrabutylammonium cation ion (counter ion).

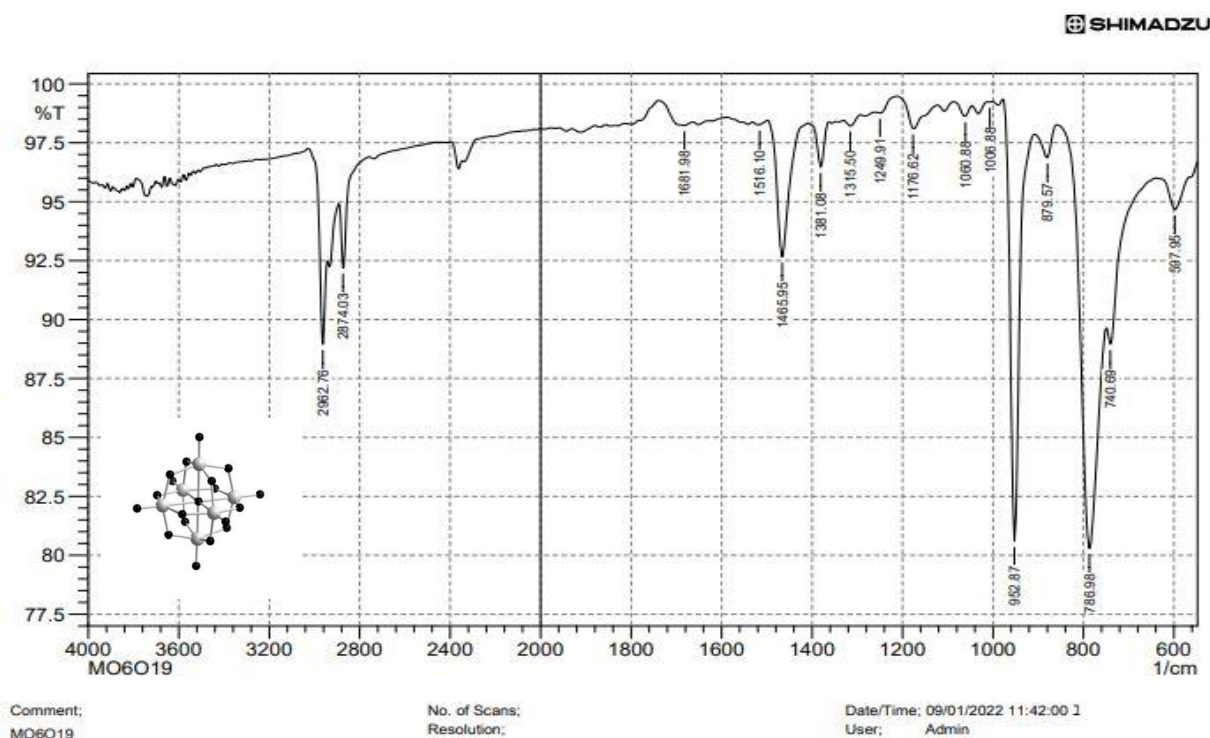


Figure 4.8 FT-IR spectrum of compound (A).

4.2.2.2 Characterization of the synthesized compounds

The FTIR spectra of the compounds (**1**, **5**, **6**, **7**, and **8**) are shown in (Fig. 4-10, 12, 14, 16, 18) compared to the donor spectra (Fig. 4-9, 11, 13, 15,17) showed a difference in the positions of the peaks, which is a preliminary indicator for the formation of functional group for dyes. In the donor spectra, we observe sharp absorption in the range (3300–3450 cm^{-1}) due to the stretching vibrations of the N-H (primary amine) bond.^[155] While we notice its disappearance in the spectra of the dyes, we deduce the formation of the imido bond (Mo=N-C). The appearance of two Strong peaks in range (950, 790 cm^{-1}) these two peaks indicate the formation of bonds (Mo=O) and (Mo-O).^[154] Bands at 2982 and 2874 cm^{-1} are attributed to C-H stretching of CH_2 and CH_3 groups of the tetrabutylammonium cation ion (counter ion).

4.2.2.2.1 Compound (1)

Compound **1** was identified by FT-IR spectrum ν , cm^{-1} : (Fig. 4.10) of compound **1** showed the strong band at 950 cm^{-1} due to (Mo=O)str, additionally the appearance of the following characteristic bands at 2962 ($\nu\text{C-H}$, benzene), 1467($\nu\text{C=C}$, benzene), 785 (Mo-O)str, Compared with (Fig. 4.9) of the donor (Acrdine), the disappearance of the sharp peak 3336 (N-H)str, This indicates the appearance of a tertiary amine in compound **1**. Bands at 2982 and 2874 cm^{-1} are attributed to (C-H)str for CH_2 and CH_3 groups of the tetrabutyle ammonium cation ion (counter ion).

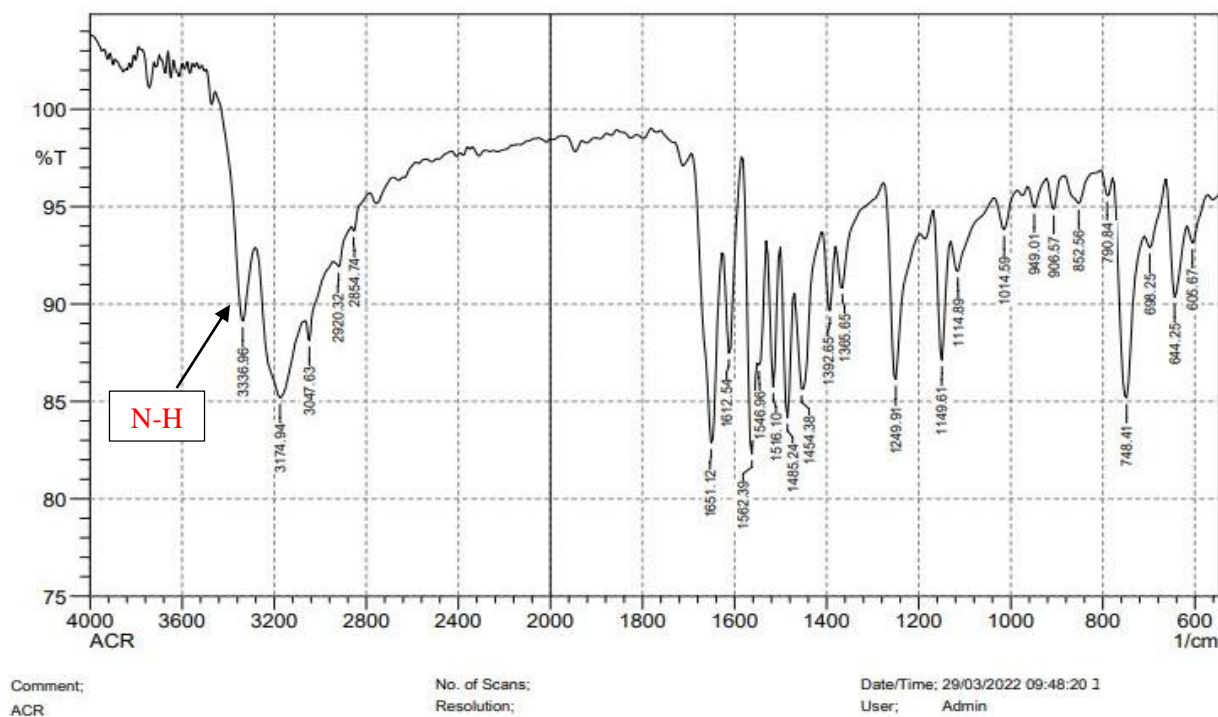


Figure 4.9 FTIR spectrum for 9-aminoacridine (donor)

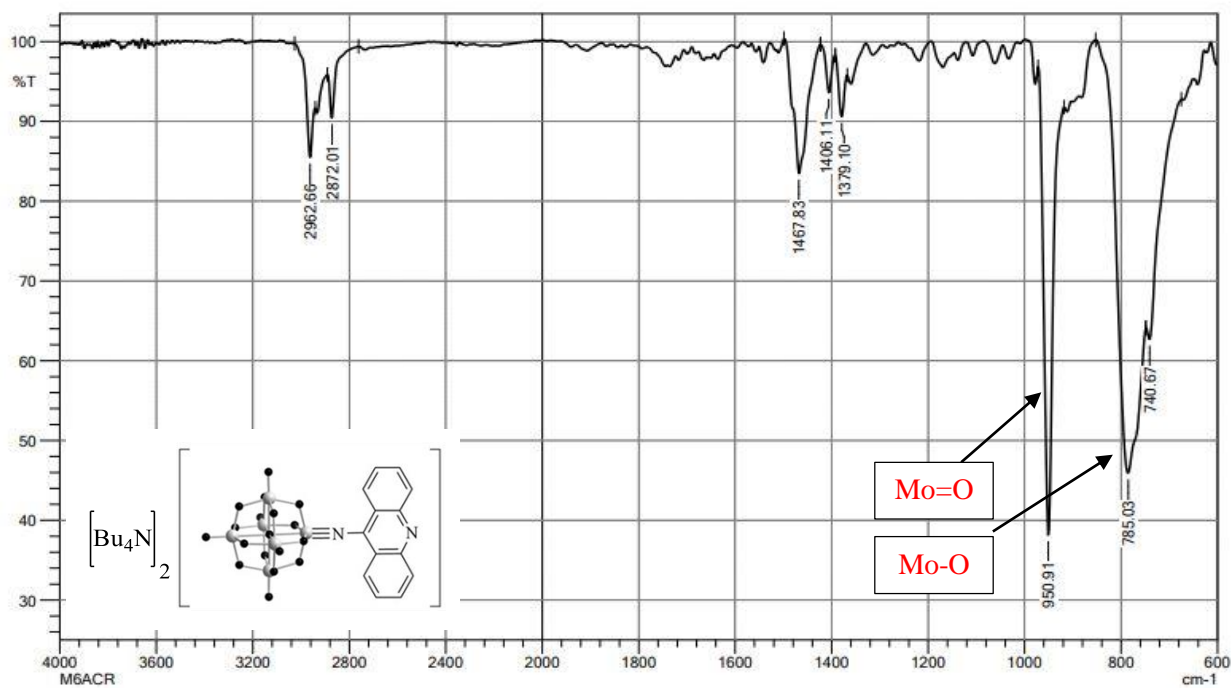


Figure 4.10 FTIR spectrum for compound 1

4.2.2.2.2 Compound (5)

Compound **5** was recognized by FT-IR spectra ν , cm^{-1} : In contrast to the donor (2-aminoanthracene) in (Fig. 4.11), compound **5** exhibits a strong band at 949 cm^{-1} in (Fig. 4.12) due to $(\text{Mo}=\text{O})_{\text{str}}$, as well as the characteristic bands at 2962 (C-H, benzene), 1465 (C=C, benzene), and 783 (Mo-O)str. The disappearance of the sharp peak 3313 (N-H) str, which indicates the formation of an imido bond ($\text{Mo}=\text{N}-\text{C}$). Bands at 2982 and 2874 cm^{-1} are attributed to (C-H)str for CH_2 and CH_3 groups of the tetrabutyle ammonium cation ion (counter ion).

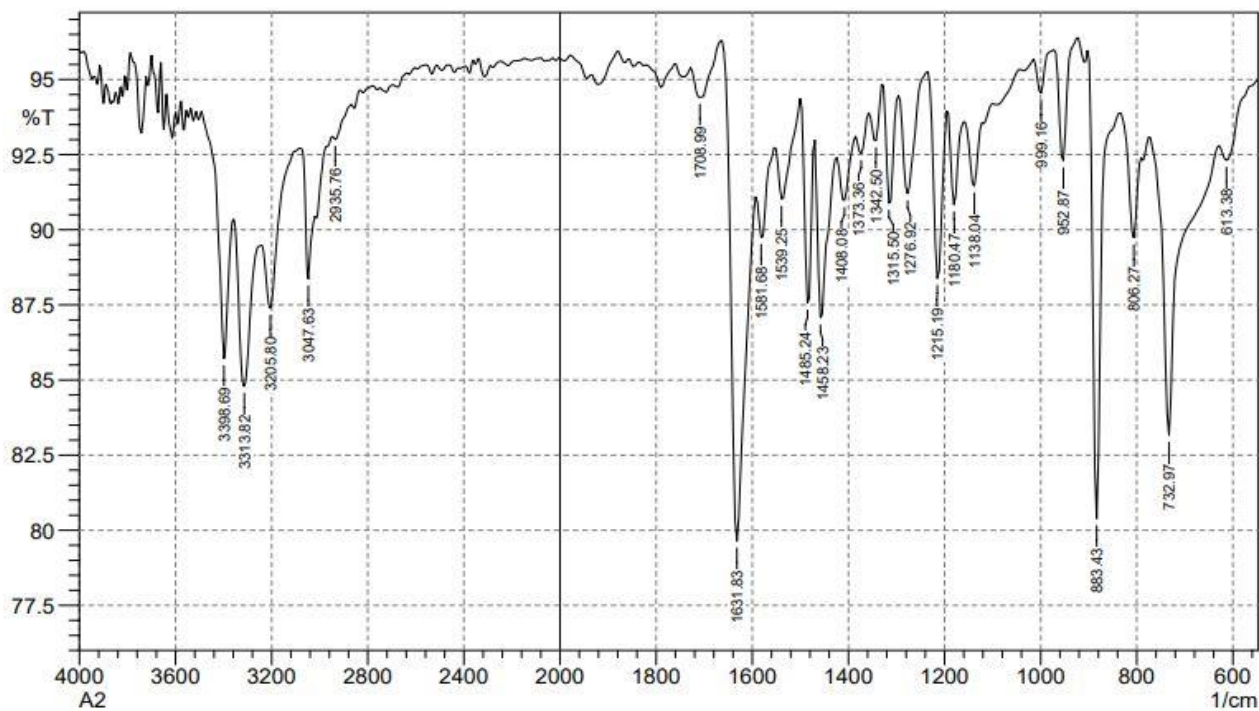


Figure 4.11 FTIR spectrum for the compound 2-aminoanthracene (donor)

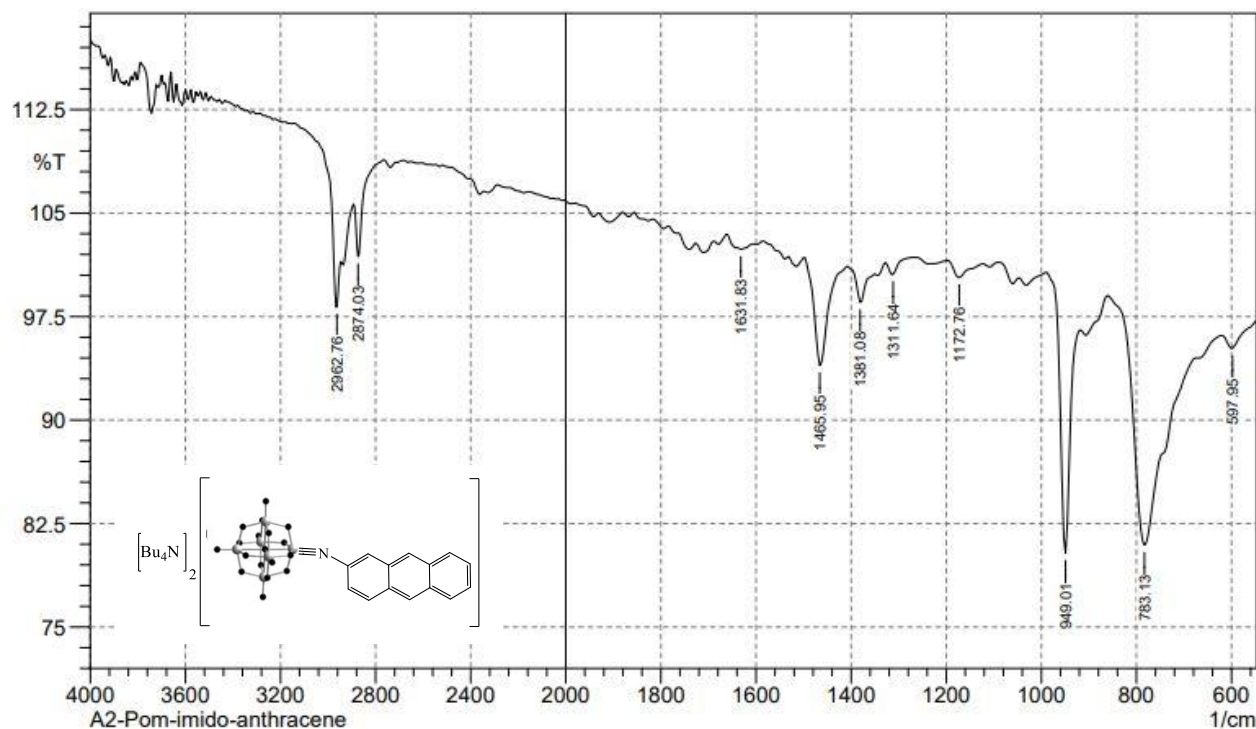


Figure 4.12 FTIR spectrum for compound 5

4.2.2.2.3 Compound (6)

It was determined via FT-IR spectrum ν , cm^{-1} : In contrast with the results (Fig. 4.13) of the donor (2-aminoanthraquinone), compound **6** showed the strong band at 950 cm^{-1} due to $(\text{Mo}=\text{O})_{\text{str}}$, as well as the appearance of the following characteristic bands at $2962 \text{ (C-H, benzene)}$, $1469 \text{ (C=C, benzene)}$, and $788 \text{ (Mo-O)_{str}}$. The disappearance of the sharp peak 3344 (N-H) str , which indicates the formation of an imido bond $(\text{Mo}=\text{N}-\text{C})$. This indicates the appearance of a tertiary amine in compound **6**. Bands at 2982 and 2874 cm^{-1} are attributed to $(\text{C-H})_{\text{str}}$ for CH_2 and CH_3 groups of the tetrabutyle ammonium cation ion (counter ion).

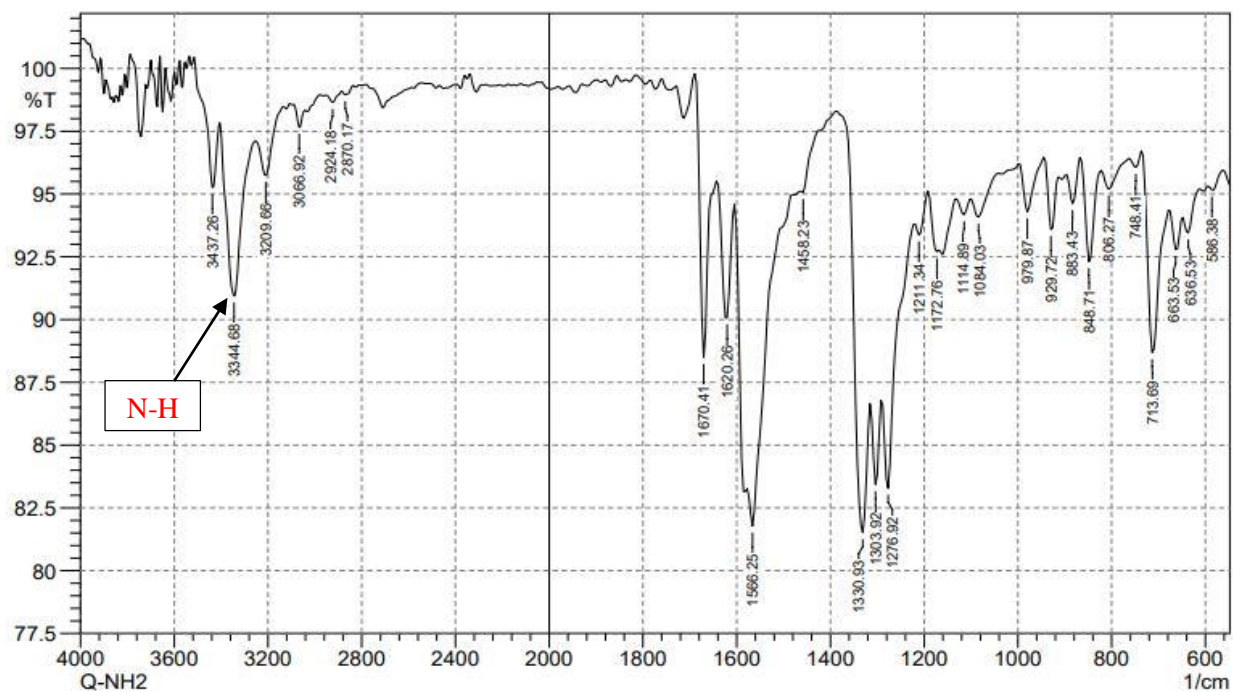


Figure 4.13 FTIR spectrum for the compound 2-aminoanthraquinone (donor)

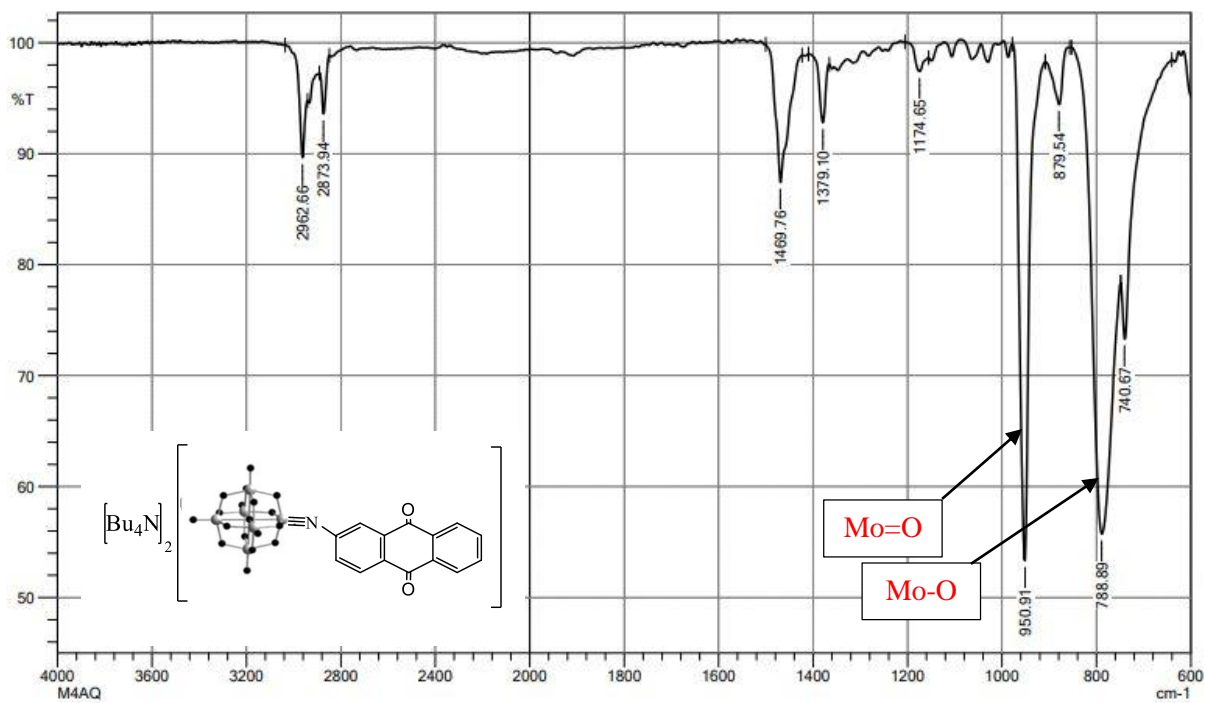


Figure 4.14 FTIR spectrum for compound 6

4.2.2.2.4 Compound (7)

It was recognized by FT-IR spectra ν , cm^{-1} : In contrast to the donor (2,6-Diaminoanthraquinone) in (Fig. 4.15), compound **7** exhibits a strong band at 950 cm^{-1} in (Fig. 4.16) due to $(\text{Mo}=\text{O})_{\text{str}}$, as well as the characteristic bands at 2962 (C-H, benzene), 1467 (C=C, benzene), and 785 $(\text{Mo}-\text{O})_{\text{str}}$. The disappearance of the sharp peak 3329 (N-H) str, which indicates the formation of an imido bond $(\text{Mo}\equiv\text{N}-\text{C})$. Bands at 2982 and 2874 cm^{-1} are attributed to (C-H)str for CH_2 and CH_3 groups of the tetrabutylammonium cation ion (counter ion).

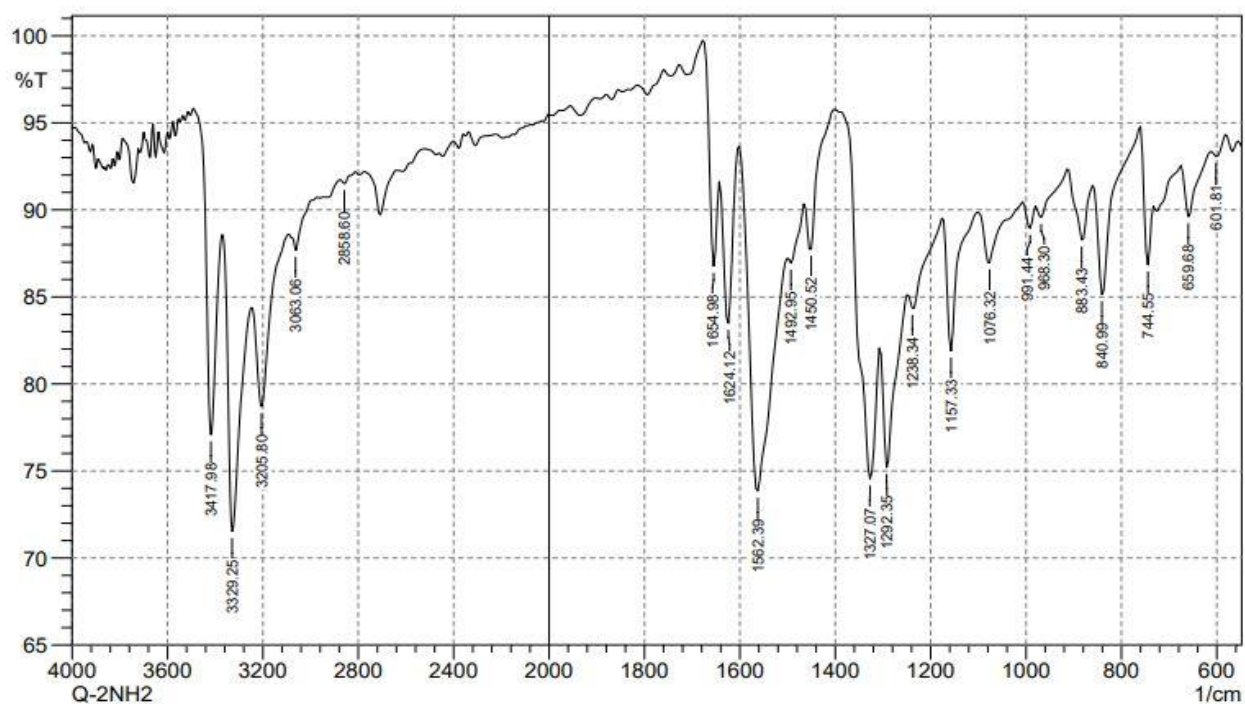


Figure 4.15 FTIR spectrum for the compound **2, 6-Diaminoanthraquinone** (donor)

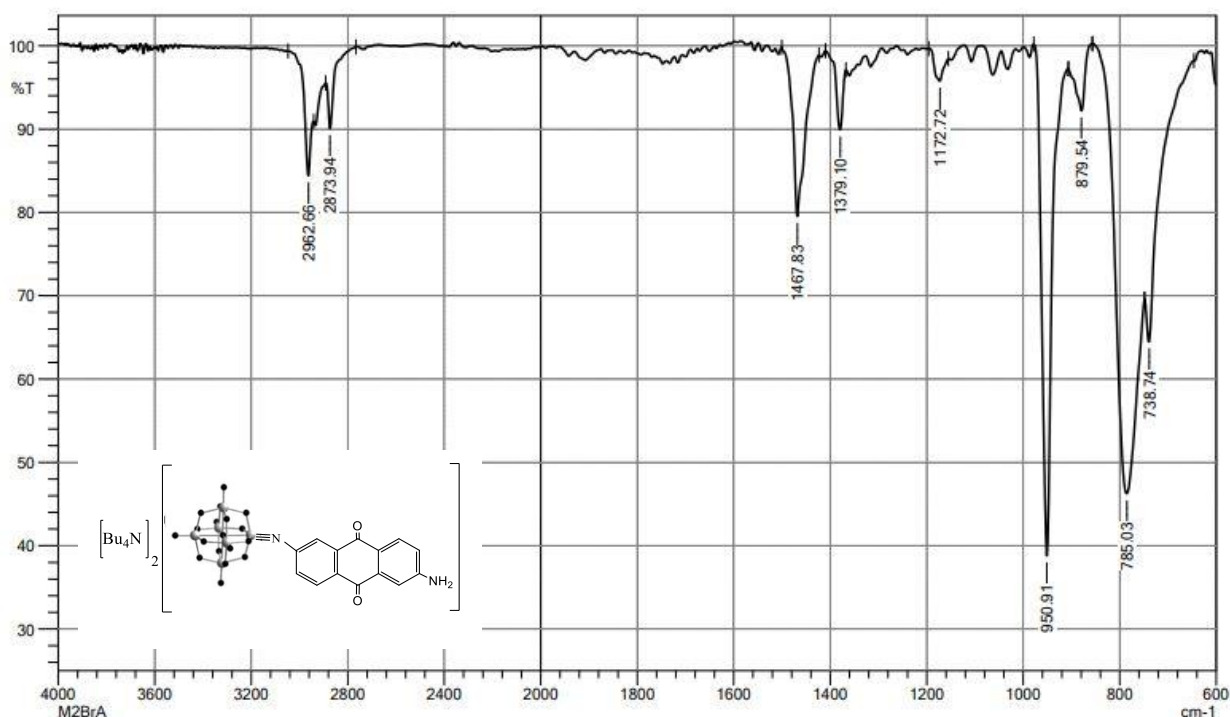


Figure 4.16 FTIR spectrum for compound 7

4.2.2.2.5 Compound (8)

It was recognized by FT-IR spectra ν , cm^{-1} : In contrast to the donor (4-bromoaniline) in (Fig. 4.17), compound **8** exhibits a strong band at 948 cm^{-1} in (Fig. 4.18) due to $(\text{Mo}=\text{O})_{\text{str}}$, as well as the characteristic bands at 2962 (C-H, benzene), 1469 (C=C, benzene), and 781 $(\text{Mo}-\text{O})_{\text{str}}$. The disappearance of the sharp peak 3379 (N-H) str, which indicates the formation of an imido bond $(\text{Mo}=\text{N}-\text{C})$. Bands at 2982 and 2874 cm^{-1} are attributed to $(\text{C}-\text{H})_{\text{str}}$ for CH_2 and CH_3 groups of the tetrabutylammonium cation ion (counter ion).

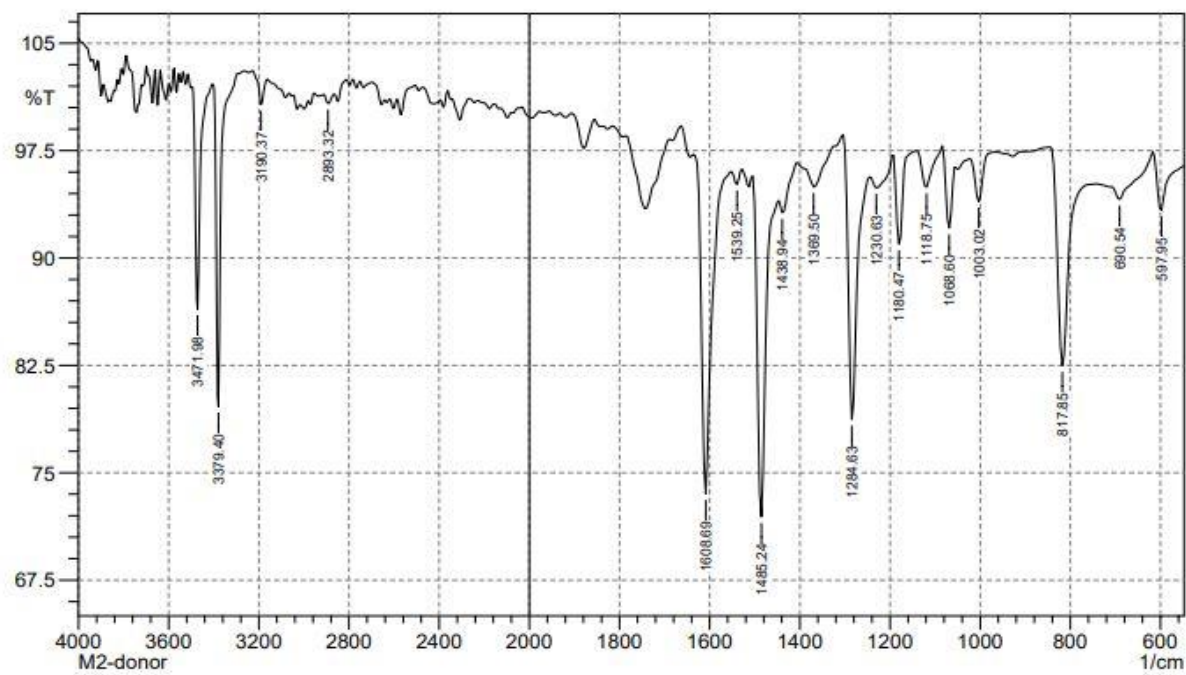


Figure 4.17 FTIR spectrum for the compound **4-bromoaniline** (donor)

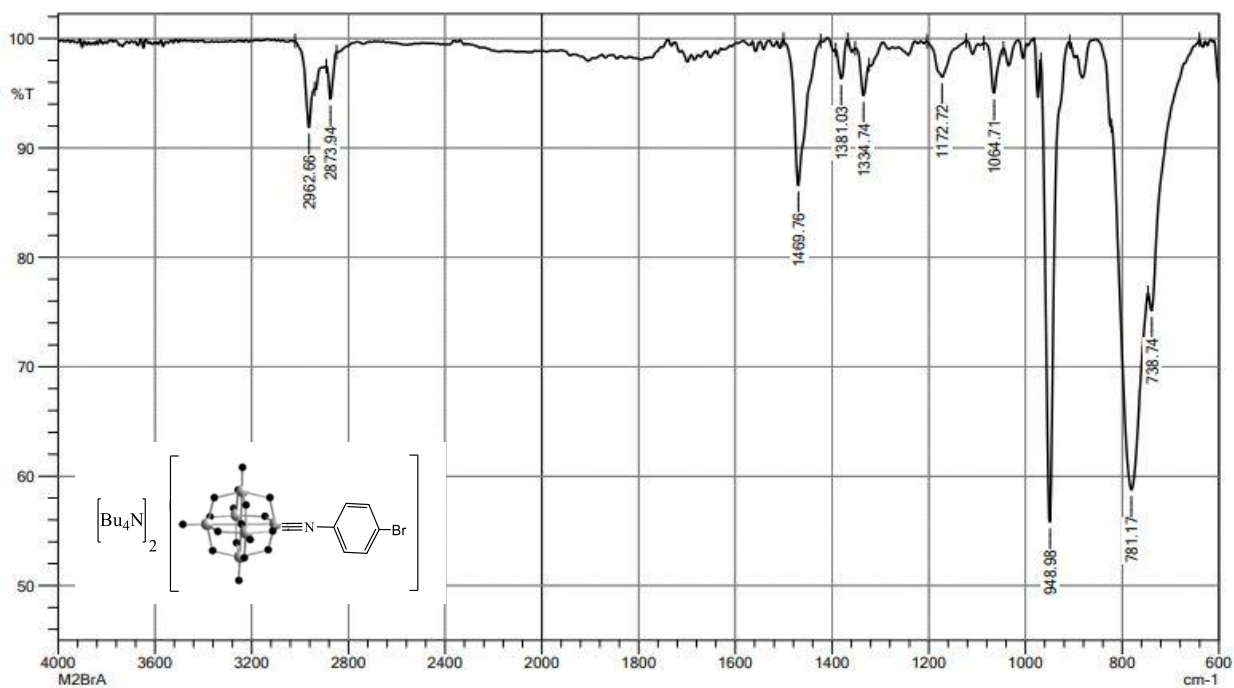


Figure 4.18 FTIR spectrum for compound **8**

4.2.3 (^1H NMR) characterization

^1H NMR for compounds **1**, **6** and **7** are presented below. Initially, by looking at the ^1H NMR spectrum (Fig. 4.19), four sharp peaks (e, f, g, h) are observed at high-field, attributed to the counter tetrabutylammonium cation. It also showed both protons (a and d) exhibit a pair of doublets and (c and b) exhibit a pair of triplets with higher chemical shifts after imido bond formation compared to the ^1H NMR of the corresponding free amine (Fig. 4.20) indicating the formation of targeted compounds.

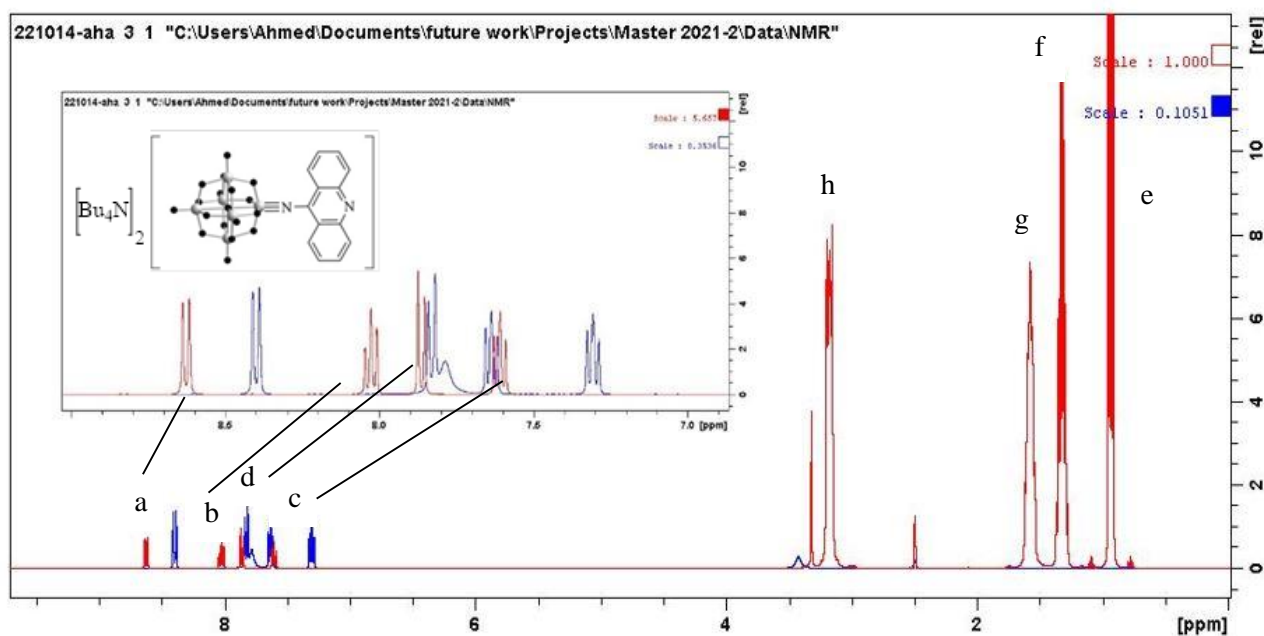


Figure 4.19 ^1H NMR for compound **1**

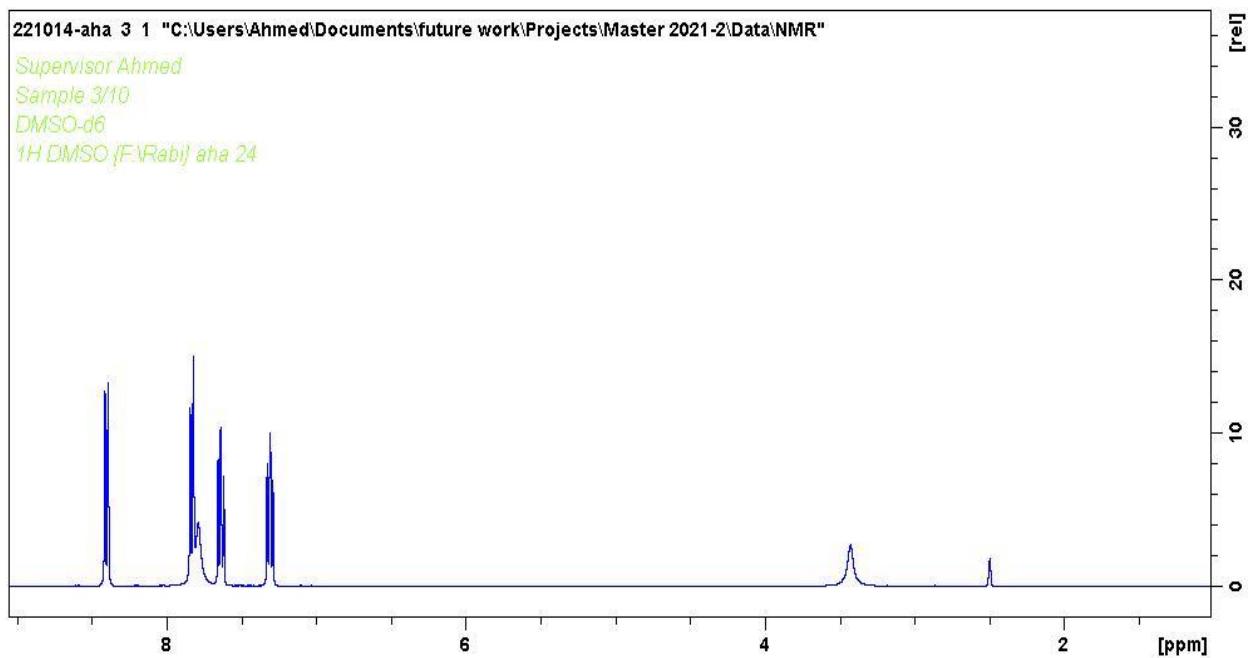


Figure 4.20 ^1H NMR for 9-aminoacridine (donor)

^1H NMR of compound **6** shown in (Fig. 4.21), which showed both protons (a and c) exhibit a pair of doublets, (b) exhibit a pair of triplets, (d) exhibit a proton of singlet with slightly higher chemical shifts after imido bond formation compared to the ^1H NMR of the corresponding free amine.

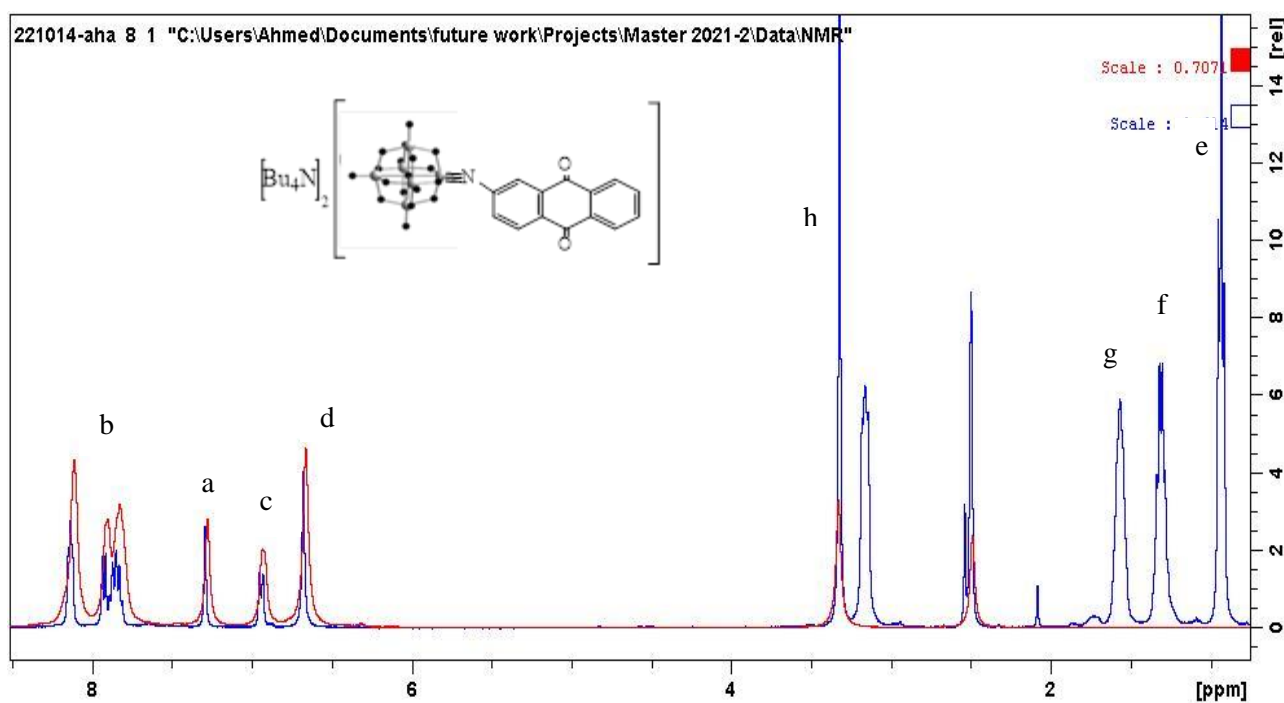


Figure 4.21 ^1H NMR for compound **6**

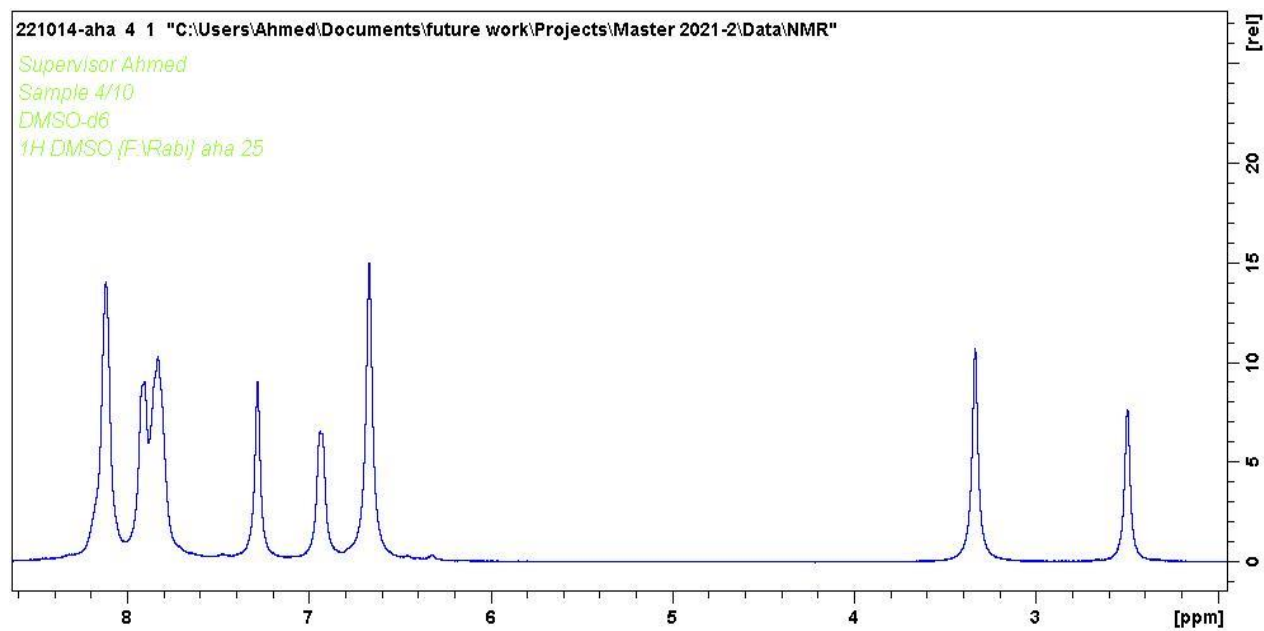


Figure 4.22 ^1H NMR for 2-aminoanthraquinone(donor)

In compound **7**, ^1H NMR (Fig. 2.23) showed both protons (a and d) exhibit a pair of doublets and (c and b) exhibit a pair of triplets with lower chemical shifts after imido bond formation in opposite trend to dye **1**. This could be attributed to the strongly electron donating nature of the aryleminoquinone part.

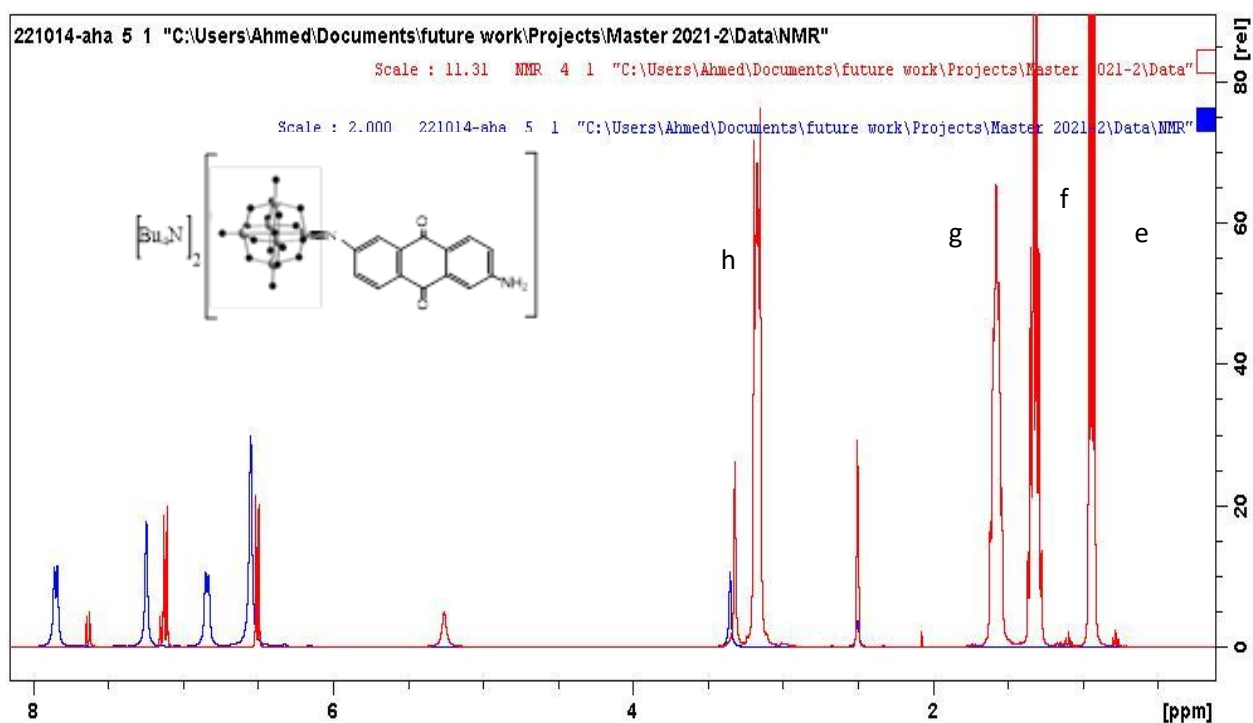


Figure 4.23 ^1H NMR for compound **7**

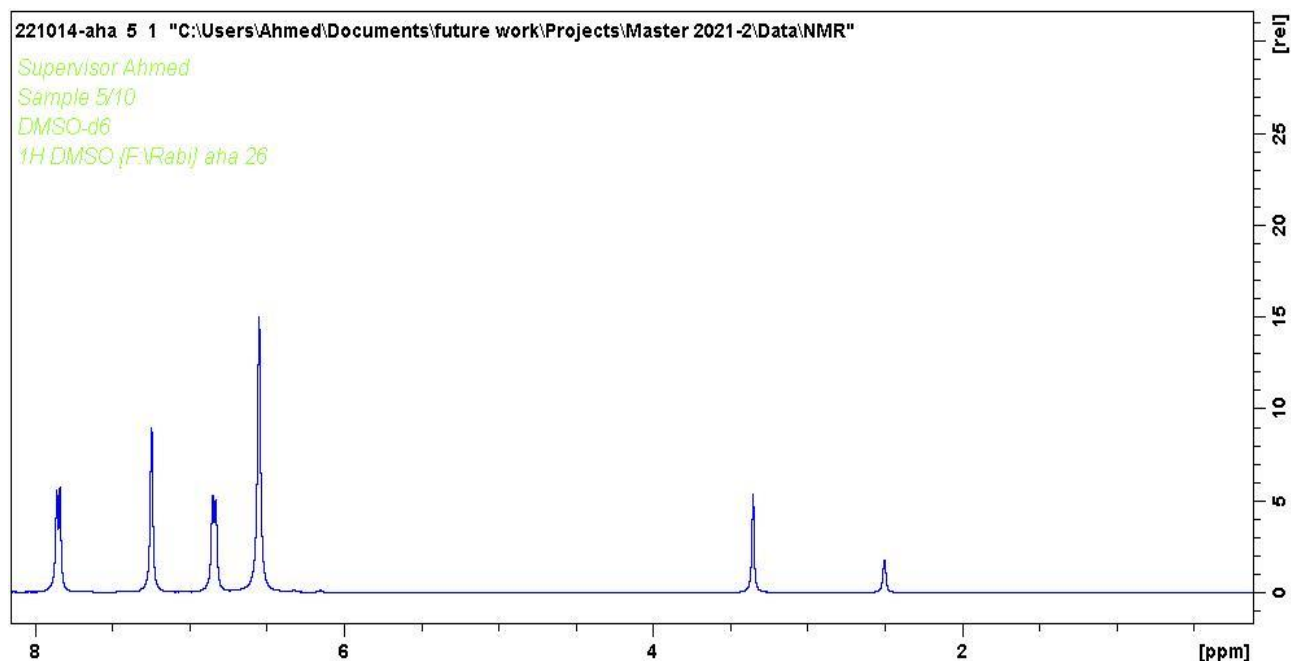


Figure 4.24 ^1H NMR for 2,6-Diaminoanthraquinone (donor)

Finally, we attempted synthesis of compound **5** and **8** as a precursor for a variety of coupling reactions. Surprisingly, however, we found that in our hands, this was unsuccessful. A colour change from yellow to brown and Orange was observed, but yields were low and the product contained lots of unreacted hexamolybdate (**A**) and also more highly substituted imido derivatives as monitored by ^1H NMR characterization. This may be due to hydrolysis that may occur during the reaction.

4.2.4 Electronic Spectroscopy

In acetonitrile at room temperature, the electronic spectra of compounds **1**, **6** and **7** were examined; the findings are shown in (Table 4.5). Compound **1** displayed a strong visible/near-UV absorption band brought on by a ligand-to-POM interaction charge-transfer process (LPCT). Additionally, compound **6** and **7** they exhibit UV absorption

bands brought on by the overlapping of O-to-Mo charge transfer (CT) in the Mo₆ acceptor unit and intra-ligand ($\pi \rightarrow \pi^*$) activities in the attached organic group, which is in line with earlier literature.^[156]

Table 4.5 UV-vis absorption data for compounds **1**, **6** and **7** in acetonitrile at room temperature

Compound	λ_{\max} (nm)	E_{\max} (eV)	Assignment
1	470	2.64	LPCT
6	326	3.80	O \rightarrow Mo and $\pi \rightarrow \pi^*$
7	328	3.78	O \rightarrow Mo and $\pi \rightarrow \pi^*$

According to the donor-based HOMO and acceptor-based LUMO energies, the energy of the LPCT band typically falls as the donor strength rises. According to the electrochemical studies, the HOMO energy in these derivatives is predicted to rise as the electron donor strength rises, but the LUMO energy is predicted to be about constant in most of these chromophores.

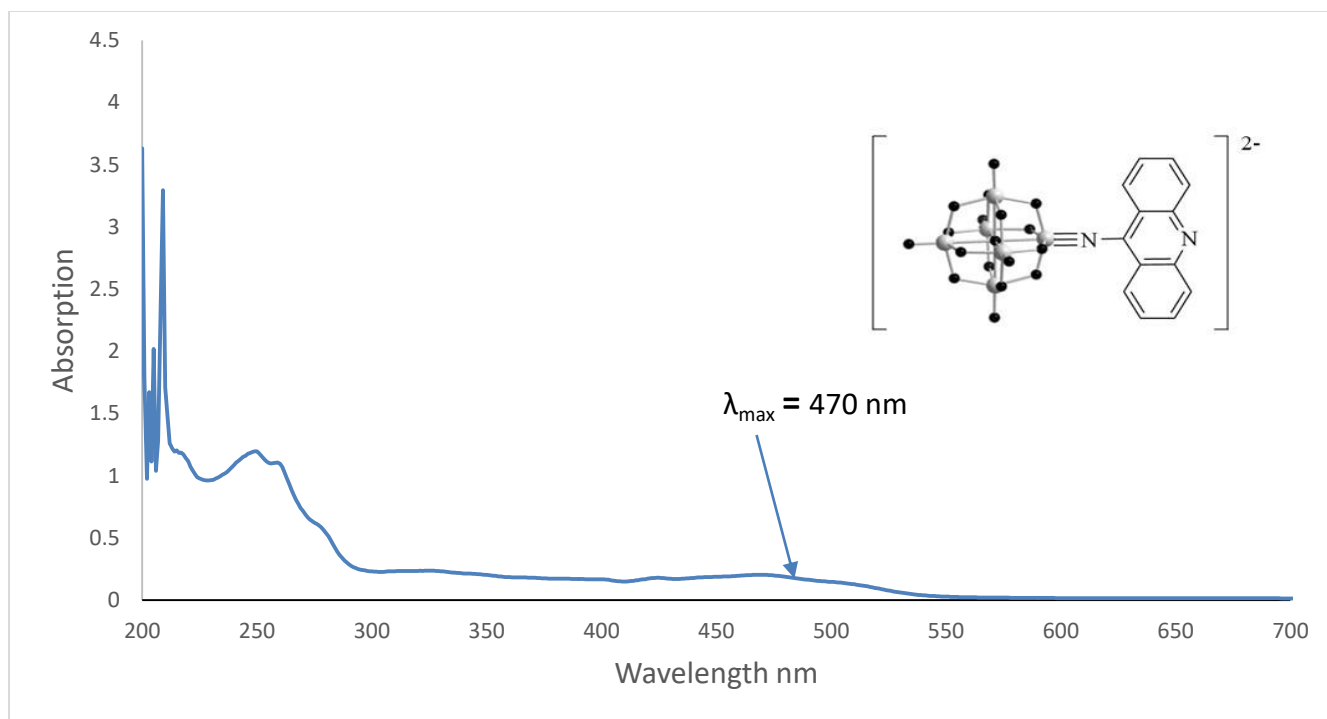


Figure 4.25 UV-Vis spectra of compound **1** in acetonitrile

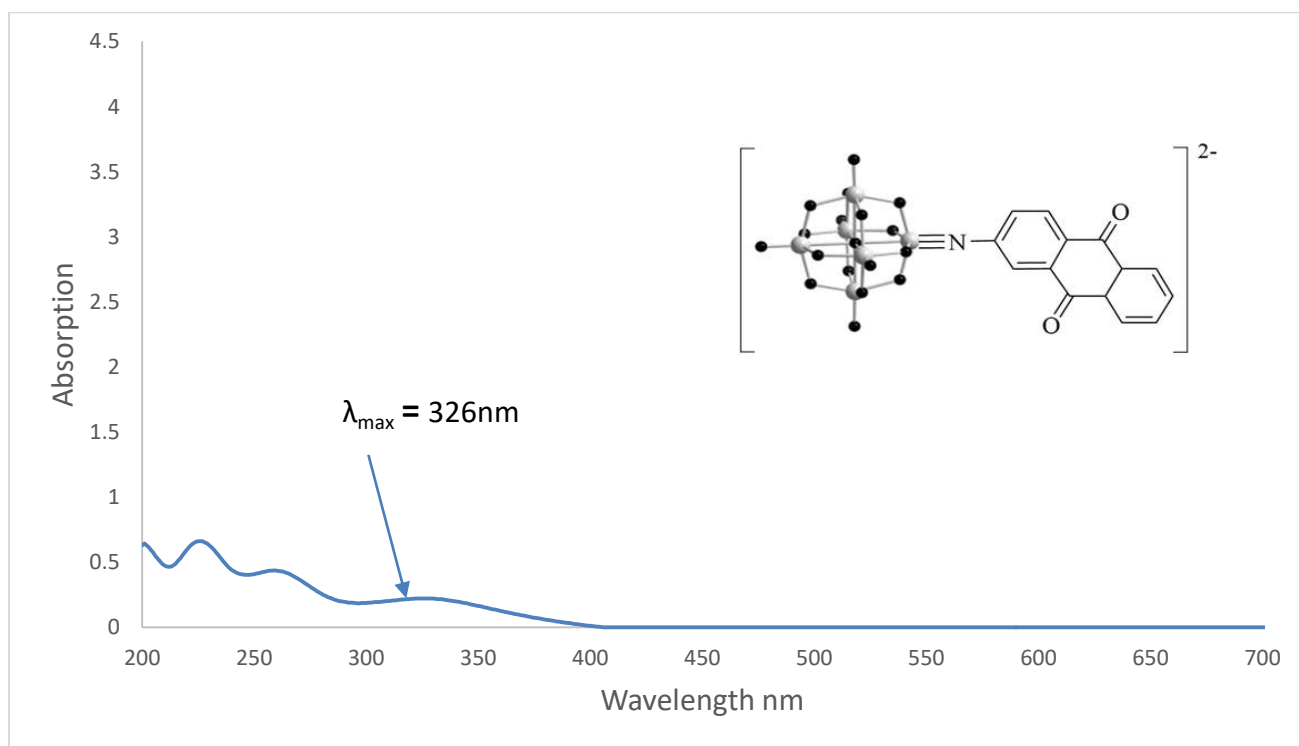


Figure 4.26 UV-Vis spectra of compound **6** in acetonitrile

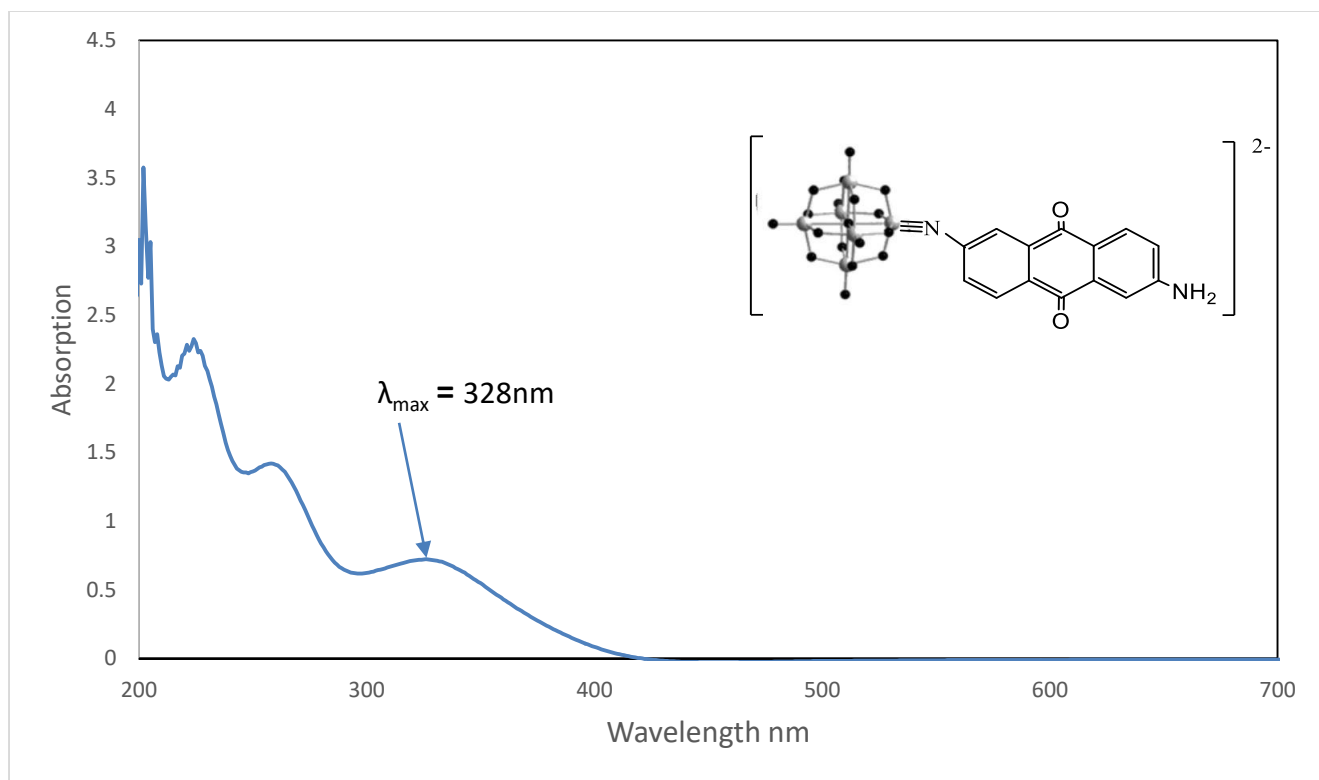


Figure 4.27 UV-Vis spectra of compound 7 in acetonitrile

Conclusions

A series of new organic-inorganic hybrid hexamolybdates based on acridine and anthracene donors were first designed and investigated using DFT and TDDFT calculations. The electronic properties, absorption spectra, and charge-transfer characters of the excited states were systematically computed. All designed dyes are suitable for n-type DSSC as their LUMO energy levels are higher than the conduction band of TiO_2 , whilst the LUMO energy level is lower than the redox couple of I^-/I_3^- . The UV-Vis spectra of dyes **1–4** exhibit strong absorption bands in the visible spectra region, which are attributed to the strong charge transfer from acridine/anthracene to the POM cluster. The LHEs of dyes **1–4** are in the range of 0.6887 to 0.9838 and are higher than those of other reported dyes. They also show remarkable reorganization energies for electron-transport (λ_e) in the range -0.97 to -1.4, together with the high open-circuit voltage (V_{OC}). The results indicate that dyes **2** and **3** would be expected to show high DSSC performance. Compounds **1,5,6,7** and **8** have been experimentally synthesized and investigated the photonic properties of these. All the new compounds have been fully characterised using FT-IR, UV-Vis, and ^1H NMR. UV-vis studies show that as the electron donor strength or π -conjugated bridge increases the LPCT band red-shifts. The anthraquinone derivatives showed lower stability and lower λ_{max} value (probably due to hydrolysis) and could be highly affected by ambient conditions compared to acridine and anthracene derivatives, However, the latter showed high stability and high λ_{max} value (red-shifts) . All FT-IR readings showed the formation of dyes and the success of the reaction with the formation (organo-imido-hexamolybdate).

Future works

Based on the promising results, future work will include:-

- 1- Explorer the synthesis of dyes **1-4** at fully characterize them.
- 2- Investigate the integration of these dyes into the DSSCs at study their performance.
- 3- Investigate the possibility at increasing the donor character of the organic part to further enhance their performance in DSSCs via tailing their structures.
- 4- Alteration of the POM types (Keggin, Anderson, etc.) and hence studying the acceptor strength on the performance in DSSCs.

References

- [1] F. J. Duarte, In *Organic Lasers and Organic Photonics*, IOP Publishing, **2018**, pp. 12-1-12–17.
- [2] T. Fuhrmann, J. Salbeck, *MRS Bull.* **2003**, *28*, 354.
- [3] IEA, *World Energy Statistic 2017*, **2017**, p. 95.
- [4] O. Shevarevskiy, *Pure Appl. Chem.* **2008**, *80*, 2079.
- [5] N. S. Lewis, *Toward Cost-Effective Solar Energy Use*, Science, **2007**.
- [6] N. S. Lewis, *Science (80-.)*. **2016**, *351*, 353.
- [7] T. R. Cook, D. K. Dogutan, S. Y. Reece, Y. Surendranath, T. S. Teets, D. G. Nocera, *Solar Energy Supply and Storage for the Legacy and Nonlegacy Worlds*, Vol. 110, **2010**, pp. 6474–6502.
- [8] J. Y. Kim, J.-W. Lee, H. S. Jung, H. Shin, N.-G. Park, *Chem. Rev.* **2020**, *120*, 7867.
- [9] C. Chen, S. Zheng, H. Song, *Chem. Soc. Rev.* **2021**, *50*, 7250.
- [10] M. Faraji, M. Yousefi, S. Yousefzadeh, M. Zirak, N. Naseri, T. H. Jeon, W. Choi, A. Z. Moshfegh, *Energy Environ. Sci.* **2019**, *12*, 59.
- [11] K. Sivula, R. van de Krol, *Nat. Rev. Mater.* **2016**, *1*, 15010.
- [12] X. Zhang, W. Song, J. Tu, J. Wang, M. Wang, S. Jiao, *Adv. Sci.* **2021**, *8*.
- [13] W. C. Tan, L. H. Saw, H. S. Thiam, J. Xuan, Z. Cai, M. C. Yew, *Renew. Sustain. Energy Rev.* **2018**, *96*, 181.
- [14] J. Lv, J. Xie, A. G. A. Mohamed, X. Zhang, Y. Wang, *Chem. Soc. Rev.* **2022**, *51*, 1511.

References

- [15] O. Ostroverkhova, *Chem. Rev.* **2016**, *116*, 13279.
- [16] M. Gouda, M. Berghot, A. Shoeip, K. Elattar, A. E. G. Khalil, *Turkish J. Chem.* **2010**, *34*, 651.
- [17] Q. ul Ain, R. A. Shehzad, U. Yaqoob, A. Sharif, Z. Sajid, S. Rafiq, S. Iqbal, M. Khalid, J. Iqbal, *Comput. Theor. Chem.* **2021**, 1200.
- [18] R. Mosurkal, L. Hoke, S. A. Fossey, L. A. Samuelson, J. Kumar, D. Waller, R. A. Gaudiana, *J. Macromol. Sci. Part A Pure Appl. Chem.* **2006**, *43*, 1907.
- [19] K. Prabakaran, R. Manivannan, H. Oh, C. Parthiban, Y. A. Son, *Dye. Pigment.* **2021**, 192.
- [20] M. Pope, C. E. Swenberg, *Electronic processes in organic crystals and polymers*, Oxford University Press, **1999**.
- [21] A. Köhler, H. Bässler, *Electronic Processes in Organic Semiconductors: An Introduction*, Wiley, **2015**.
- [22] L. R. Dalton, P. Günter, M. Jazbinsek, O.-P. Kwon, P. A. Sullivan, In *Organic Electro-Optics and Photonics*, Cambridge University Press, **2015**, pp. 1–10.
- [23] A. Hadi, A. Al-Yasari, *Synthesis, Non-Linear Optical and Electrochemical Properties of Novel Organo-Imido Polyoxometalate Derivatives*, University of East Anglia., **2016**.
- [24] S. Günes, N. S. Sariciftci, *Inorganica Chim. Acta* **2008**, *361*, 581.
- [25] G. Kickelbick, *Hybrid Mater.* **2014**, *1*.
- [26] H. Zhang, M. Fallahi, *Opt. Commun.* **2005**, *248*, 415.

References

- [27] A. Al-Yasari, N. Van Steerteghem, H. Kearns, H. El Moll, K. Faulds, J. A. Wright, B. S. Brunschwig, K. Clays, J. Fielden, *Inorg. Chem.* **2017**, *56*, 10181.
- [28] S. S. Mukrimaa, Nurdyansyah, E. F. Fahyuni, A. YULIA CITRA, N. D. Schulz, T. Taniredja, E. M. Faridli, S. Harmianto, *Functional Hybrid Materials*, Vol. 6, Wiley-VCH, **2016**.
- [29] S. A. Alshehri, A. Al-Yasari, F. Marken, J. Fielden, *Macromolecules* **2020**, *53*, 11120.
- [30] S. Li, H. Wan, J. Lin, J. Min, *Mater. Des.* **2023**, *230*, 111993.
- [31] K. Yavir, Ł. Marcinkowski, R. Marcinkowska, J. Namieśnik, A. Kloskowski, *Anal. Chim. Acta* **2019**, *1054*, 1.
- [32] G. Kickelbick, *Hybrid Materials*, **2007**.
- [33] N. Zhou, M. G. Kim, S. Loser, J. Smith, H. Yoshida, X. Guo, C. Song, H. Jin, Z. Chen, S. M. Yoon, A. J. Freeman, R. P. H. Chang, A. Facchetti, T. J. Marks, *Proc. Natl. Acad. Sci. U. S. A.* **2015**, *112*, 7897.
- [34] J. Kim, Z. Hong, G. Li, T. Song, J. Chey, Y. S. Lee, J. You, C.-C. Chen, D. K. Sadana, Y. Yang, *Nat. Commun.* **2015**, *6*, 6391.
- [35] A. Polman, M. Knight, E. C. Garnett, B. Ehrler, W. C. Sinke, *Science (80-.)*. **2016**, *352*, aad4424.
- [36] J. Kim, Z. Hong, G. Li, T. Song, J. Chey, Y. S. Lee, J. You, C.-C. Chen, D. K. Sadana, Y. Yang, *Nat. Commun.* **2015**, *6*, 6391.
- [37] B. Kumar, D. Garg, K. Swamy, P. Kumar, In *Sustainable and Clean Energy Production Technologies* (Eds.: Pal, D. B.; Jha, J. M.), Springer Nature

References

- Singapore, Singapore, **2022**, pp. 269–288.
- [38] A. A. Chand, P. P. Lal, K. A. Prasad, N. M. Kumar, In *Solar Energy Advancements in Agriculture and Food Production Systems* (Eds.: Gorjian, S.; Campana, P. E.), Academic Press, **2022**, pp. 391–423.
- [39] E. K. Solak, E. Irmak, *RSC Adv.* **2023**, *13*, 12244.
- [40] Z. I. Alferov, V. M. Andreev, V. D. Rumyantsev, *Semiconductors* **2004**, *38*, 899.
- [41] S. F. Abdulhussein, Synthesis and theoretical study of new imidazole derivatives dyes and their application in dye sensitized solar cells, University of Kerbala, **2022**.
- [42] J. H. Kim, D. Hansora, P. Sharma, J. W. Jang, J. S. Lee, *Toward practical solar hydrogen production-an artificial photosynthetic leaf-to-farm challenge*, Vol. 48, **2019**, pp. 1908–1971.
- [43] X. X. Li, T. Ji, J. Y. Gao, W. C. Chen, Y. Yuan, H. Y. Sha, R. Faller, G. G. Shan, K. Z. Shao, X. L. Wang, Z. M. Su, *Chem. Sci.* **2022**.
- [44] S. Shalini, R. Balasundaraprabhu, T. S. Kumar, N. Prabavathy, S. Senthilarasu, S. Prasanna, *Int. J. Energy Res.* **2016**, *40*, 1303.
- [45] C. Cavallo, F. Di Pascasio, A. Latini, M. Bonomo, D. Dini, *J. Nanomater.* **2017**, *2017*, 1.
- [46] F. Odobel, Y. Pellegrin, E. A. Gibson, A. Hagfeldt, A. L. Smeigh, L. Hammarström, *Coord. Chem. Rev.* **2012**, *256*, 2414.
- [47] A. Nattestad, A. J. Mozer, M. K. R. Fischer, Y.-B. Cheng, A. Mishra, P. Bäuerle,

References

- U. Bach, *Nat. Mater.* **2010**, *9*, 31.
- [48] F. Teng, K. Hu, W. Ouyang, X. Fang, *Adv. Mater.* **2018**, *30*.
- [49] C. Shi, S. Dai, K. Wang, X. Pan, L. Zeng, L. Hu, F. Kong, L. Guo, *Electrochim. Acta* **2005**, *50*, 2597.
- [50] G. Kickelbick, *Hybrid materials: synthesis, characterization, and applications*, John Wiley & Sons, **2007**.
- [51] L. A. Kosyachenko, *Solar Cells: Dye-Sensitized Devices*, BoD–Books on Demand, **2011**.
- [52] A. Carella, F. Borbone, R. Centore, *Front. Chem.* **2018**, *6*.
- [53] A. Hagfeldt, G. Boschloo, L. Sun, L. Kloo, H. Pettersson, *Chem. Rev.* **2010**, *110*, 6595.
- [54] Y. Ooyama, Y. Harima, *ChemPhysChem* **2012**, *13*, 4032.
- [55] M. M. Al Mogren, N. M. Ahmed, A. A. Hasanein, *J. Saudi Chem. Soc.* **2020**, *24*, 303.
- [56] P. Semalti, S. N. Sharma, *J. Nanosci. Nanotechnol.* **2020**, *20*, 3647.
- [57] J. V. S. Krishna, M. Mrinalini, S. Prasanthkumar, L. Giribabu, In *Dye-Sensitized Solar Cells*, Elsevier, **2019**, pp. 231–284.
- [58] D. Devadiga, M. Selvakumar, P. Shetty, M. S. Santosh, *J. Electron. Mater.* **2021**, *50*, 3187.
- [59] M. R. Horn, A. Singh, S. Alomari, S. Goberna-Ferrón, R. Benages-Vilau, N. Chodankar, N. Motta, K. Ostrikov, J. Macleod, P. Sonar, P. Gomez-Romero,

References

- D. Dubal, *Energy Environ. Sci.* **2021**, *14*, 1652.
- [60] C. Lv, J. Hu, H. Zhou, Z. Li, R. N. N. Khan, Y. Wei, *Chem. - A Eur. J.* **2012**, *18*, 8681.
- [61] J. J. Walsh, A. M. Bond, R. J. Forster, T. E. Keyes, *Coord. Chem. Rev.* **2016**, *306*, 217.
- [62] D. Wang, L. Liu, J. Jiang, L. Chen, J. Zhao, *Nanoscale* **2020**, *12*, 5705.
- [63] A. Proust, B. Matt, R. Villanneau, G. Guillemot, P. Gouzerh, G. Izzet, *Chem. Soc. Rev.* **2012**, *41*, 7605.
- [64] L. Chen, W.-L. Chen, X.-L. Wang, Y.-G. Li, Z.-M. Su, E.-B. Wang, *Chem. Soc. Rev.* **2019**, *48*, 260.
- [65] N. I. Gumerova, A. Rompel, *Nat. Rev. Chem.* **2018**, *2*, 0112.
- [66] T. Ueda, *ChemElectroChem* **2018**, *5*, 823.
- [67] M. Nyman, P. C. Burns, *Chem. Soc. Rev.* **2012**, *41*, 7354.
- [68] M. FRIGO, Synthesis of polyoxometalates and conjugation with peptides for cancer cell targeting, University of Padova, **2021**.
- [69] J. Zhang, Y. Huang, G. Li, Y. Wei, *Coord. Chem. Rev.* **2019**, *378*, 395.
- [70] S. Passadis, T. Kabanos, Y.-F. Song, H. Miras, *Inorganics* **2018**, *6*, 71.
- [71] O. S. Panteleieva, A. V Shtemenko, G. A. Senchyk, V. V Ponomarova, B. Galmés, A. Frontera, E. B. Rusanov, K. V Domasevitch, *Inorganica Chim. Acta* **2022**, *537*, 120945.
- [72] J. Kruse, M. Langer, I. Romanenko, I. Trentin, D. Hernández-Castillo, L.

References

- González, F. H. Schacher, C. Streb, *Adv. Funct. Mater.* **2022**, 32.
- [73] Bernold Hasenknopf, *Polyoxometalates: introduction to a class of inorganic compounds and their biomedical applications*, Bioscience, **2005**.
- [74] D.-L. Long, E. Burkholder, L. Cronin, *Chem. Soc. Rev.* **2007**, 36, 105.
- [75] S. Herrmann, C. Ritchie, C. Streb, *Dalt. Trans.* **2015**, 44, 7092.
- [76] J. J. Berzelius, *Beitrag zur näheren Kenntniss des Molybdän's*, Vol. 82, **1826**, pp. 331–350.
- [77] J. F. KEGGIN, *Nature* **1933**, 131, 908.
- [78] S. A. Cheng, T. F. Otero, *Synth. Met.* **2002**, 129, 53.
- [79] N. H. Hur, W. G. Klemperer, R. C. Wang, M. Fournier, P. Alvin, *Inorg. Synth* **1990**, 27, 77.
- [80] J. Zhang, F. Xiao, J. Hao, Y. Wei, *Dalt. Trans.* **2012**, 41, 3599.
- [81] H. Kang, J. Zubieta, *J. Chem. Soc. Chem. Commun.* **1988**, 1192.
- [82] B. Krebs, R. Klein, M. T. Pope, A. Müller, *Polyoxometalates: from platonic solids to anti-retroviral activity*, Kluwer Academic Publishers Dordrecht, **1994**.
- [83] Y. Wei, B. Xu, C. L. Barnes, Z. Peng, *J. Am. Chem. Soc.* **2001**, 123, 4083.
- [84] P. Wu, Q. Li, N. Ge, Y. Wei, Y. Wang, P. Wang, H. Guo, *Eur. J. Inorg. Chem.* **2004**, 2004, 2819.
- [85] J. Zhang, F. Xiao, J. Hao, Y. Wei, *Dalt. Trans.* **2012**, 41, 3599.

References

- [86] J. Kang, B. Xu, Z. Peng, X. Zhu, Y. Wei, D. R. Powell, *Angew. Chemie* **2005**, *117*, 7062.
- [87] S. Y. Huang, G. Schlichthörl, A. J. Nozik, M. Grätzel, A. J. Frank, *J. Phys. Chem. B* **1997**, *101*, 2576.
- [88] Z. Ning, Y. Fu, H. Tian, *Energy Environ. Sci.* **2010**, *3*, 1170.
- [89] N. Robertson, *Angew. Chemie Int. Ed.* **2006**, *45*, 2338.
- [90] K. Sharma, V. Sharma, S. S. Sharma, *Nanoscale Res. Lett. 2018 131* **2018**, *13*, 1.
- [91] G. Boschloo, *Front. Chem.* **2019**, *7*.
- [92] J. Gong, K. Sumathy, Q. Qiao, Z. Zhou, *Renew. Sustain. Energy Rev.* **2017**, *68*, 234.
- [93] M. Karuppusamy, V. S. K. Choutipalli, D. Vijay, V. Subramanian, *J. Chem. Sci.* **2020**, *132*, 20.
- [94] G. Marotta, M. A. Reddy, S. P. Singh, A. Islam, L. Han, F. De Angelis, M. Pastore, M. Chandrasekharam, *ACS Appl. Mater. Interfaces* **2013**, *5*, 9635.
- [95] Y.-H. Chen, V. S. Nguyen, H.-H. Chou, Y. S. Tingare, T.-C. Wei, C.-Y. Yeh, *ACS Appl. Energy Mater.* **2020**, *3*, 5479.
- [96] V. V. Divya, C. H. Suresh, *New J. Chem.* **2021**, *45*, 11585.
- [97] V. V. Divya, C. H. Suresh, *New J. Chem.* **2020**, *44*, 7200.
- [98] A. Proust, B. Matt, R. Villanneau, G. Guillemot, P. Gouzerh, G. Izzet, *Chem. Soc. Rev.* **2012**, *41*, 7605.

References

- [99] J. S. Li, X. J. Sang, W. L. Chen, L. C. Zhang, Z. M. Zhu, T. Y. Ma, Z. M. Su, E. B. Wang, *ACS Appl. Mater. Interfaces* **2015**, *7*, 13714.
- [100] C. Costa-Coquelard, S. Sorgues, L. Ruhlmann, *J. Phys. Chem. A* **2010**, *114*, 6394.
- [101] B. Matt, J. Fize, J. Moussa, H. Amouri, A. Pereira, V. Artero, G. Izzet, A. Proust, *Energy Environ. Sci.* **2013**, *6*, 1504.
- [102] K. J. Elliott, A. Harriman, L. Le Pleux, Y. Pellegrin, E. Blart, C. R. Mayer, F. Odobel, *Phys. Chem. Chem. Phys.* **2009**, *11*, 8767.
- [103] A. Al-Yasari, H. El Moll, R. Purdy, K. B. Vincent, P. Spence, J. P. Malval, J. Fielden, *Phys. Chem. Chem. Phys.* **2021**, *23*, 11807.
- [104] M. Lu, B. Xie, J. Kang, F.-C. Chen, Yang, Z. Peng, *Chem. Mater.* **2005**, *17*, 402.
- [105] Y. Zhu, L. Wang, J. Hao, Z. Xiao, Y. Wei, Y. Wang, *Cryst. Growth Des.* **2009**, *9*, 3509.
- [106] Y. Zhu, Z. Xiao, N. Ge, N. Wang, Y. Wei, Y. Wang, *Cryst. Growth Des.* **2006**, *6*, 1620.
- [107] J. Hao, L. Ruhlmann, Y. Zhu, Q. Li, Y. Wei, *Inorg. Chem.* **2007**, *46*, 4960.
- [108] A. Al-Yasari, J. Fielden, *Rev. Adv. Sci. Eng.* **2014**, *3*, 304.
- [109] T. Zhang, W. Guan, S. Wen, T. Ma, L. Yan, Z. Su, *J. Phys. Chem. C* **2014**, *118*, 29623.

References

- [110] J. Wang, S. Cong, S. Wen, L. Yan, Z. Su, *J. Phys. Chem. C* **2013**, *117*, 2245.
- [111] H. El Moll, F. A. Black, C. J. Wood, A. Al-Yasari, A. Reddy Marri, I. V. Sazanovich, E. A. Gibson, J. Fielden, *Phys. Chem. Chem. Phys.* **2017**, *19*, 18831.
- [112] C. Chen, W. Ma, J. Zhao, *Chem. Soc. Rev.* **2010**, *39*, 4206.
- [113] M. Wright, A. Uddin, *Sol. Energy Mater. Sol. Cells* **2012**, *107*, 87.
- [114] A. M. Ammar, H. S. H. Mohamed, M. M. K. Yousef, G. M. Abdel-Hafez, A. S. Hassanien, A. S. G. Khalil, *J. Nanomater.* **2019**, *2019*, 1.
- [115] S. Ito, S. M. Zakeeruddin, R. Humphry-Baker, P. Liska, R. Charvet, P. Comte, M. K. Nazeeruddin, P. Péchy, M. Takata, H. Miura, S. Uchida, M. Grätzel, *Adv. Mater.* **2006**, *18*, 1202.
- [116] C. Teng, X. Yang, C. Yang, S. Li, M. Cheng, A. Hagfeldt, L. Sun, *J. Phys. Chem. C* **2010**, *114*, 9101.
- [117] Z. Ning, Q. Zhang, W. Wu, H. Pei, B. Liu, H. Tian, *J. Org. Chem.* **2008**, *73*, 3791.
- [118] J. T. Lin, P.-C. Chen, Y.-S. Yen, Y.-C. Hsu, H.-H. Chou, M.-C. P. Yeh, *Org. Lett.* **2009**, *11*, 97.
- [119] B. O'Regan, M. Grätzel, *Nature* **1991**, *353*, 737.
- [120] M. Grätzel, *Nature* **2001**, *414*, 338.
- [121] R. Amadelli, R. Argazzi, C. A. Bignozzi, F. Scandola, *J. Am. Chem. Soc*

References

- 1990, *112*, 7029.
- [122] M. Grätzel, *J. Photochem. Photobiol. C Photochem. Rev.* **2003**, *4*, 145.
- [123] Y.-Q. Zhang, D.-K. Ma, Y.-G. Zhang, W. Chen, S.-M. Huang, *Nano Energy* **2013**, *2*, 545.
- [124] A. Renaud, F. Grasset, B. Dierre, T. Uchikoshi, N. Ohashi, T. Takei, A. Planchat, L. Cario, S. Jobic, F. Odobel, S. Cordier, *ChemistrySelect* **2016**, *1*, 2284.
- [125] R. Carlisle Chambers and Craig L. Hil, *Am. Chem. Soc.* **1991**, *30*, 2776.
- [126] I. Bar-Nahum, K. V. Narasimhulu, L. Weiner, R. Neumann, *Inorg. Chem.* **2005**, *44*, 4900.
- [127] W. G. Klemperer, **1990**, pp. 74–85.
- [128] T. J. Boesen, Foundation for a parallel time-dependent density functional theory simulator in a spherical harmonic basis using the exact exchange energy functional, University of Aarhus, **2011**.
- [129] B. Haitham Fadhil Abdul Hassan, A. RahmanTama Al-Tamimi Ahmed Hadi Al-Yasari, Synthesis and Density Functional Theory (DFT) study for Heterocyclic Derivatives Chemistry, University ofKerbala, **2019**.
- [130] R. Mary, L. Álvarez, BASIS FUNCTIONS IN COMPUTATIONAL CHEMISTRY : ANALYSIS OF THE SECOND PERIOD DIATOMIC HYDRIDES, University of Oviedo, **2021**.
- [131] T. P. FALBO, Emanuele, Using Theoretical Chemistry to understand

References

- the Properties of Polyoxometalates and their potential as energy storage materials, NEWCASTLE UNIVERSITY, **2021**.
- [132] W. C. Witt, B. G. del Rio, J. M. Dieterich, E. A. Carter, *J. Mater. Res.* **2018**, *33*, 777.
- [133] W. Sang-Aroon, S. Saekow, V. Amornkitbamrung, *J. Photochem. Photobiol. A Chem.* **2012**, *236*, 35.
- [134] V. V. Divya, C. H. Suresh, *New J. Chem.* **2021**, *45*, 11585.
- [135] R. Katoh, A. Furube, T. Yoshihara, K. Hara, G. Fujihashi, S. Takano, S. Murata, H. Arakawa, M. Tachiya, *J. Phys. Chem. B* **2004**, *108*, 4818.
- [136] R. A. Marcus, *Rev. Mod. Phys.* **1993**, *65*, 599.
- [137] M. J. Frisch, G. W. Trucks, H. B. Schlegel, G. E. Scuseria, M. a. Robb, J. R. Cheeseman, et. al, *G16_C01*, Wallingford CT, **2016**, p. Gaussian 16, Revision C.01, Gaussian, Inc., Wallin.
- [138] J. Da Chai, M. Head-Gordon, *Phys. Chem. Chem. Phys.* **2008**, *10*, 6615.
- [139] J. W. Ochterski, G. A. Petersson, J. A. Montgomery, *J. Chem. Phys.* **1998**, *104*, 2598.
- [140] A. D. McLean, G. S. Chandler, *J. Chem. Phys.* **2008**, *72*, 5639.
- [141] P. J. Hay, W. R. Wadt, *J. Chem. Phys.* **1998**, *82*, 270.
- [142] W. R. Wadt, P. J. Hay, *J. Chem. Phys.* **1998**, *82*, 284.
- [143] A. V. Marenich, C. J. Cramer, D. G. Truhlar, *J. Phys. Chem. B* **2009**.

References

- [144] T. Lu, F. Chen, *J. Comput. Chem.* **2012**, *33*, 580.
- [145] C. A. Guido, P. Cortona, B. Mennucci, C. Adamo, *J. Chem. Theory Comput.* **2013**, *9*, 3118.
- [146] M. Carraro, S. Gross, *Materials (Basel)*. **2014**, *7*, 3956.
- [147] S. Sambathkumar, S. Priyadharshini, M. Fleisch, D. W. Bahnemann, G. G. Kumar, S. Senthilarasu, R. Renganathan, *Mater. Lett.* **2019**, *242*, 28.
- [148] Q. Cui, Q. Yang, W. Wang, J. Yao, Z. Liu, X. Zuo, K. Zhu, G. Li, S. Jin, *J. Mater. Sci. Mater. Electron.* **2020**, *31*, 1797.
- [149] A. Al-Yasari, P. Spence, H. El Moll, N. Van Steerteghem, P. N. Horton, B. S. Brunshwig, K. Clays, J. Fielden, *Dalt. Trans.* **2018**, *47*, 10415.
- [150] A. H. S. AlSilaykhee, A. Al-Yasari, H. F. Alesary, *Int. J. Quantum Chem.* **2023**, *123*, e27086.
- [151] Y. Wei, T. Zhang, Z. Lang, L. Yan, Z. Su, *Dye. Pigment.* **2014**, *102*, 6.
- [152] J. B. Asbury, Y.-Q. Wang, E. Hao, H. N. Ghosh, T. Lian, *Res. Chem. Intermed.* **2001**, *27*, 393.
- [153] C. I. L. Alongamo, S. N. Tasheh, N. K. Nkungli, F. K. Bine, J. N. Ghogomu, *J. Chem.* **2022**, *2022*, 1.
- [154] P. Beato, Synthesis and characterization of realistic molybdenum oxide based model systems in heterogeneous catalysis, University of Berlin, **2005**.
- [155] A. B. D. Nandiyanto, R. Oktiani, R. Ragadhita, *Indones. J. Sci.*

References

Technol. **2019**, *4*, 97.

- [156] B. Xu, Y. Wei, C. L. Barnes, Z. Peng, *Angew. Chemie Int. Ed.* **2001**, *40*, 2290.

الخلاصة

في هذا العمل، تم تصميم وتحضير سلسلة من الصبغات الهجينة الجديدة عضوية-لاعضوية لبوليمرات أكاسيد الفلزات كنظام مانح - جسر - مستقبل حيث يمكن استخدامها كمحسس/أو محسس مساعد في الخلايا الشمسية المتحسسة للصبغة (DSSCs). في البداية، قمنا نظرياً، باستخدام مزيج من حسابات نظرية الكثافة الوظيفية (DFT) ونظرية الكثافة الوظيفية المعتمدة على الوقت (TDDFT)، ودرسنا بشكل منهجي كروموفورات جديدة يتم فيها توصيل مستقبل الإلكترون لمشتقات هكساموليبيدات نوع (Lindqvist) عبر مجموعات فنيل يميديو مع المانح للإلكترون العضوي مثل (أكردين-يميديو-هكساموليبيدات (1)، أكردين-9-فنيل استلين- يميديو-هكساموليبيدات (2)، امينوأنثراسين-يميديو-هكساموليبيدات (3)، -2-امينو-3-كاربوكسيل أنثراسين-يميديو-هكساموليبيدات (4)، أنثراسين- يميديو-هكساموليبيدات (5)، أنثراكوينون- يميديو-هكساموليبيدات (6)، اميدوانثراكوينون- يميديو-هكساموليبيدات (7)، بروموفنيل- يميديو-هكساموليبيدات (8)). تم تقييم مستويات الطاقة للمدارات الجزيئية الحدودية، وأطياف الامتصاص مع عوامل الانتقال الإلكترونية، والحدود الكهروضوئية للصبغات 1-4 بشكل منهجي. لقد وجد أن مستويات طاقة HOMO للصبغات 1-4 أكثر سلبية من الأكسدة والاختزال في I/I_3^- ومستويات طاقة LUMO أعلى من نطاق التوصيل لـ TiO_2 ، مما يشير إلى أن هذه الصبغات تتوافق مع متطلبات النوع n DSSCs. تتخفض مستويات HOMO بالترتيب $4 < 3 < 2 < 1$ ، وتتنخفض مستويات LUMO أيضاً بالترتيب $4 < 3 < 2 < 1$. استناداً إلى حسابات TD-DFT، تتمتع جميع الأنظمة 1-4 بنطاقات امتصاص في المنطقة المرئية تتراوح من 420 إلى 494 نانومتر تقريباً، مع قوة مذبذب عالية نسبياً على الرغم من النظام 4، حيث يتمتع 1 (نظام POM-acridine) بأكبر طول موجي لامتصاص أقصى λ_{max} من 494 نانومتر مع $f_{os} = 0.8657$ و $\Delta r = 3.66 \text{ \AA}$. تؤكد هذه النتائج مدى ملاءمة جميع الصبغات المدروسة لـ DSSCs من النوع n ويمكن إدخال الأصباغ التي تم فحصها كصبغة ماصة نشطة بالإضافة إلى صبغة رئيسية. أظهرت جميع الصبغات طاقة إعادة تنظيم ملحوظة لنقل الإلكترون (λ_e) وبالتالي زيادة معدل نقل الإلكترون. نظراً للامتصاص القوي في المنطقة المرئية، فضلاً عن كفاءة حصاد الضوء العالية (LHE)، وكفاءة تجديد الصبغة (DRE)، وكفاءة حقن الإلكترون (Φ_{inj})، تعد الصبغات 2 و3 من أكثر المرشحين الواعدين لمواد DSSC عالية الأداء. لقد حفرتنا نتائج DFT الواعدة على استكشاف التحضير التجريبي لهذه الصبغات. تم تشخيص جميع هذه الصبغات باستخدام أجهزة التحليل الطيفي FTIR، 1H NMR، و UV-Vis. يتوافق

طيف الامتصاص المحسوب لـ **1** بشكل جيد مع النتائج التجريبية الأولية. ومن المثير للاهتمام أن إدخال رابط π في النظام **2** يتحول إلى اللون الأزرق بمقدار 54 نانومتر في λ_{\max} وزيادة في f_{os} بعامل ≈ 2.1 و Δr بعامل ~ 2 مقارنة بالنظام **1**.



جامعة كربلاء
كلية العلوم
قسم الكيمياء

تحضير مواد هجينة عضوية-لاعضوية لبوليمرات اكاسيد الفلزات للتطبيقات الكهروضوئية

رسالة مقدمة الى مجلس كلية العلوم/جامعة كربلاء وهي جزء من متطلبات نيل درجة الماجستير في
الكيمياء

كتبت بواسطة

مريم خليل خليل
بكالوريوس علوم في الكيمياء (٢٠١٧) جامعة كربلاء

بإشراف

أ.م.د. احمد هادي اليساري

أ.د. عدنان ابراهيم محمد

